Numerical Modelling of River Ice in Complex River Systems

by

Julia Lynn Blackburn

A thesis submitted in partial fulfillment of the requirements for the degree of

Doctor of Philosophy

in

WATER RESOURCES ENGINEERING

Department of Civil and Environmental Engineering

University of Alberta

Abstract

Rivers in cold regions experience ice conditions for a significant part of the year. River ice can cause ice jam flooding, impact hydropower generation operations, and affect a river's ecological and morphological conditions. Many ice processes are highly dynamic and are affected by meteorological / hydrodynamic conditions, and river geomorphology. River ice can be very challenging to study due to the risks and costs associated with data collection in harsh winter conditions. One of the most economical and efficient approaches to study river ice processes and to evaluate the effects of ice on a river's regime is to use numerical model simulations. At present, most existing one-dimensional (1D) river ice models are based on an implicit finite difference solution to the Saint-Venant equations. As a result, highly dynamic events such as rapid ice jam formation or sudden ice jam release are difficult to model due to numerical instabilities that can arise if the flow approaches supercritical. Also, river ice models with network modelling capabilities reduce conservation of mass and energy principles to continuity of discharge and equality of water levels at the junctions, which may not be reasonable when the ice and flow conditions are rapidly changing. There is a need for a comprehensive 1D river ice process model that is capable of simulating the full ice regime in rivers with complex natural channel geometry where mixed flow regimes are anticipated. The ultimate goal of this research is to develop a robust public-domain comprehensive 1D river ice process model, capable of handling complex natural channel geometry and channel networks for the full spectrum of scenarios from simple known steady ice conditions to highly dynamic cases such as ice jam formation or release. In this study, a number of

developments were made to the University of Alberta's public-domain hydrodynamic and river ice process model, *River1D*, as steps towards realizing this ultimate long-term goal.

Firstly, the model was reformulated to accommodate natural channel geometry and enhanced to include previously excluded ice processes. Previous versions of the model allowed for a rectangular channel approximation only. The new natural channel geometry version of the model was then enhanced to include new ice processes: water supercooling, frazil accretion, frazil re-entrainment, anchor ice formation and release, border ice formation, under-cover transport of frazil, and ice cover formation based on leading edge stability criteria. The model was validated with freeze-up data from the Susitna River, Alaska.

Secondly, the model was modified to simulate flow in channel networks using a momentum based approach to simulate junctions that includes important physical effects at junctions but without the need to adjust model parameters or redefine junctions should a flow reversal occur. A series of steady and unsteady tests were used to assess this new approach. The results were compared to and agreed favourably with results simulated with a two-dimensional (2D) model. The unsteady test results demonstrated the model's capability of handling transient flow reversals. The model was then applied to a network of channels in the Mackenzie Delta for both open water and ice jam conditions. Model results agreed well with observed water level data. Modelled ice jam conditions indicated a flow reversal in the Peel Mackenzie Connector, which is consistent with observations in this channel during breakup.

Lastly, the model was enhanced to simulate ice jam profiles in multi-channel networks. The enhancements include provisions for handling junctions when solving the ice jam stability equation within a channel network. The model was compared to a series of idealized test cases from a previous study that sought to investigate the impacts of islands on ice jam profiles. Model results agreed very favourably with the results from the previous study. The model was then applied to the Hay River Delta. The model was validated for both open water and ice jam conditions.

Preface

Chapter 2 of this thesis has been published as Blackburn, J. and She, Y. 2019. A comprehensive public-domain river ice process model and its application to a complex natural river. Cold Regions Science and Technology. 163, 44-58. I was responsible for model development, model application, and writing the manuscript. Dr. She and Dr. Hicks were both involved with conceptualization. Dr. She provided supervision, and reviewing and editing of the manuscript.

Chapter 3 of this thesis has been published as Blackburn, J. and She. Y. 2021. One-dimensional channel network modelling and simulation of flow conditions during the 2008 ice breakup in the Mackenzie Delta, Canada. Cold Regions Science and Technology. 189 (2021) 103339. I was responsible for the model development, model application, and writing the manuscript. Dr. She was involved with conceptualization, supervision, and reviewing and editing of the manuscript.

Chapter 4 of this thesis has been submitted for publication to Cold Regions Science and Technology as Blackburn, J. and She. Y. 2022. The simulation of ice jam profiles in multi-channel systems using a one-dimensional network model. I was responsible for the model development, model application, and writing the manuscript. Dr. She was involved with conceptualization, supervision, and reviewing and editing of the manuscript.

Acknowledgements

Lastly, I would also like to thank my family and friends who supported me throughout this long and at times very stressful journey.

Table of Contents

List of Tables

List of Figures

List of Symbols

A	cross sectional area to the water surface
A_A	cross sectional area to the water surface at junction node A
$A_{A(\text{Element B})}$	portion of A_A contributing to the flow in Element B
$A_{A(\text{Element C})}$	portion of A_A contributing to the flow in Element C
A_{an}	cross sectional area of anchor ice
A_b	cross sectional area of border ice
$ADDF$	accumulated degree days of freezing
A_{fs}	cross sectional area of the frazil slush layer
A_i	cross sectional area of surface ice
A_{si}	cross sectional area of the solid ice layer
A_{ui}	cross sectional area of under-cover moving frazil layer
A_w	cross sectional area of water (under and through the ice)
a	border ice equation coefficient
a_s	site specific coefficient for the Stefan equation
B	channel width
B_b	border ice width from a given bank
B_o	width of open water between border ice at a cross section

B_{bl}	width of border ice at the left bank
B_{br}	width of border ice at the right bank
B_{btotal}	total width of border ice at a cross section
B_{wi}	width of the underside of the ice jam
$B_{wiA(Element\ B)}$	width of the underside of the ice jam at Node A in Element B
$B_{wiA(Element\ C)}$	width of the underside of the ice jam at Node A in Element C
B_{ws}	total width of the channel at the water surface for main channel excluding overbank flow
b	border ice equation coefficient
C_{an}	fraction of bed covered by anchor ice
C_i	surface ice concentration
C_f	volumetric concentration of suspended frazil
C_{fo}	frazil seeding concentration
C_p	specific heat of water
C_s	Chézy's coefficient
$D_{CM}, D_{TU}, D_{TD}, D_{BU}, D_{BD}$	water depths at model sections in parallel channels tests
D_{LD}, D_{MD}, D_{MU}	water depths at model sections in diverging junction tests
D_{TOP}, D_{BOTTOM}	water depth at outflow boundaries in parallel channels tests

D_w	mean hydraulic depth of water (A_w/T)
D_{wl}	local water depth at the edge of border ice
d	border ice equation coefficient
d_e	typical frazil particle radius
d_f	average diameter of frazil granules in under-cover transport layer
d_n	nominal diameter of ice particles
d_s	average diameter of bed material
e	border ice equation coefficient
e_{wi}	thermal energy of the water and the suspended frazil (ice-water mixture)
F	frazil particle shape factor
F_{anb}	buoyant force per unit area of anchor ice
F_D	densimetric Froude number
F_d	Froude number immediate downstream of junction
F_{inter}	inter-particle resistance per unit area
F_r	Froude number
F_{r_jux}	maximum Froude number for juxtaposition
F_{r_max}	maximum Froude number for ice cover advancement
f	allowable longitudinal force on the ice cover

f_b	fraction of the main channel covered by border ice
f_{bmax}	maximum allowable fraction of main channel occupied by border ice
f_l	conditional constant in solid ice layer transport equation
g	gravitational acceleration
H	water surface elevation above a specified datum
$H_{measured}$	measured water surface elevation
$H_{simulated}$	simulated water surface elevation
h_{iws}	heat exchange coefficient between anchor ice and substrate flow
h_{sb}	substrate floe depth under anchor ice
h_{wa}	linear heat transfer coefficient between water and air
i	integer index
j_{wa}	linear heat transfer coefficient between water and air
K	form factor (function of ice floe geometry)
K_i	thermal conductivity of ice
K_s	momentum reduction separation factor
$K_{s(Element\ B)}$	momentum reduction separation factor for Element B
$K_{s(Element\ C)}$	momentum reduction separation factor for Element C
K_v	passive pressure coefficient

K_{xy}	lateral stress transfer coefficient
k_b	effective bed roughness height
k_i	effective ice jam roughness height
k_{wa}	linear heat transfer constant
L	length of ice cover between computational nodes
L_{block}	length of block
L_E	length of element
L_i	latent heat of ice
L_{is}	island length
m	coefficient dependent on surface water width in the wind direction
N_u^f	Nusselt number for typical suspended frazil particle
n	number of observations
n_b	Manning's roughness coefficient of the bed
n_c	composite Manning's roughness coefficient
n_i	Manning's roughness coefficient of the ice
n_j	ice jam Manning's roughness coefficient
n_s	sheet ice Manning's roughness coefficient
OB_i	i^{th} observed value

P_b	bed-affected wetted perimeter of the channel
P_i	ice-affected wetted perimeter of the channel
PR_i	i^{th} predicted value
p_a	porosity of anchor ice
p_c	space between ice floes in newly formed ice cover
p_f	frazil slush porosity
p_j	porosity of ice accumulation
Q_{diff}	difference in discharge between iterations at a node
Q_{flux}	volume flux
$Q_{tolerance}$	maximum allowable difference in discharge between iterations at a node
Q_{uit}	total under-cover ice discharge
Q_{uic}	ice transport capacity
$Q_{CM}, Q_{TU}, Q_{TD}, Q_{BU}, Q_{BD}$	water discharges at model sections in parallel channels tests
Q_{LD}, Q_{MD}, Q_{MU}	water discharges at model sections in diverging junction tests
$Q_{measured}$	measured discharge
$Q_{simulated}$	simulated discharge
$Q_{total\ inflow}$	total inflow to the Delta from gauge data

Q_{TOP}, Q_{BOTTOM}	water discharge at inflow boundaries in parallel channels tests
Q_w	water discharge (under and through the ice)
Q_{wA}	water discharge at junction node A
Q_{wB}	water discharge at junction node B
Q_{wC}	water discharge at junction node C
$Q_{wA(Element\ B)}$	portion of Q_{wA} flowing in Element B
$Q_{wA(Element\ C)}$	portion of Q_{wA} flowing in Element C
q_i	ice discharge under ice cover
q_o	net rate of heat exchange between the water surface and atmosphere
R_h	hydraulic radius
R_i	hydraulic radius of the ice affected portion of flow cross sectional area
RD	relative difference
RE	relative error
RMSE	root mean square error
R_{sl}	hydraulic radius of a given slice
r_o	typical frazil particle radius
S_{bed}	channel bed slope

S_f	boundary friction slope
S_{oMain}	bed slope of main channel in diverging junction tests
$S_{oLateral}$	bed slope of lateral channel in diverging junction tests
S_{ui}	source term representing exchange between moving and stationary frazil layers
S_{wBAD}	average water slope for junction Elements B and D
S_{wCAD}	average water slope for junction Elements C and D
$S_{wA(\text{Converging Junction})}$	water surface slop at node A for converging junctions
$S_{wA(\text{Diverging Junction})}$	water surface slop at node A for diverging junctions
T	total width of the channel at the water surface
T_a	air temperature
T_m	melting point of ice
T_w	water temperature
T_{ws}	surface water temperature
T_v	average water temperature in the cross section
t	time variable
Δt	simulation time step
t_{an}	anchor ice thickness
t_b	border ice thickness

t_{block}	thickness of incoming ice block
t_{fs}	frazil slush layer thickness
t'_f	new frazil pan thickness
t_i	ice thickness
t_{if}	mean thickness of transported ice floe
t_j	ice jam thickness
t_{jA}	ice jam thickness at Node A
$t_{jA(\text{Element B})}$	ice jam thickness at Node A in Element B
$t_{jA(\text{Element C})}$	ice jam thickness at Node A in Element C
t_{le}	thickness of ice at the leading edge
t_s	sheet ice thickness
t_{si}	solid ice layer thickness
t'_{si}	initial ice thickness of newly formed solid ice between stationary ice pans
t_{ui}	thickness of under-cover moving frazil layer
U_c	critical water velocity upstream of leading edge for block stability
U_{cr}	maximum velocity for dynamic border ice growth
U_i	ice velocity
U_{i_re}	the ice velocity threshold criteria for re-entrainment

U_u	average flow velocity under the ice cover
U_{ui}	velocity of under-cover moving frazil layer
U_w	average water velocity in the cross section
U_{wind}	wind velocity
U_{wl}	local depth-averaged water velocity at the edge of border ice
V_b	buoyant velocity of frazil ice
V_c	maximum observed water velocity for frazil accretion
V_{max}	erosion velocity
V_s	local water velocity in the open water adjacent to border ice edge
V_{sl}	average velocity of a given slice
V_v	mean vertical velocity
v'_z	vertical fluctuating component of water velocity due to turbulence
W_{bed}	submerged width per unit area of bed material
W_{Bottom}	width of bottom channel in parallel channels tests
$W_{Connector}$	width of connector channel in parallel channels tests
$W_{Lateral}$	width of lateral channel in diverging junction tests
W_{Main}	width of main channel in diverging junction tests
W_{Top}	width of top channel in parallel channels tests

ΔW	incremental growth in the border ice over a given time period
X_i	ice front location
x	streamwise space variable
Y	mean flow depth immediately upstream of the leading edge
Y_{eq}	equilibrium stage (depth to free surface) for equivalent single channel jam
Y_{min}	minimum stage (depth to free surface) along island with ice jam
Y_{normal}	normal stage (depth to free surface)
α_{wi}	coefficient of turbulent heat exchange
β	momentum flux correction coefficient
β_{re}	rate of surface ice re-entrainment
γ	frazil accretion rate
γ_e	specific weight of ice jam
η	rate of frazil rise
Θ	dimensionless flow strength
Θ_c	critical flow strength
θ	model implicitness
θ_B	junction angle for Element B

θ_C	junction angle for Element C
μ	composite jam stress parameter
μ_1	bank friction coefficient
ξ	discharge ratio
ρ_i	density of ice
ρ_w	density of water
ρ_s	density of bed material
τ_a	shear stress due to wind
τ_c	ice (jam) cohesion
τ_g	weight component of the ice cover
τ_i	shear stress on underside of ice jam due to flowing water
Φ	dimensionless ice transport capacity
ϕ_{ia}	net rate of heat exchange between water and air through the floating ice layer
ϕ_{fw}	net rate of heat exchange per unit surface area between frazil particles and water
ϕ_{pz}	short wave radiation absorbed by anchor ice
ϕ_{wa}	net rate of heat exchange between water and air
ϕ_{wi}	net rate of heat exchange between water and ice

ϕ_s net incoming solar radiation

$\varDelta\phi$ incremental heat loss per unit surface area from water

List of Abbreviations

AEA   Alaska Energy Authority

ADCP   Acoustic Doppler Current Profiler

CDG   characteristic-dissipative-Galerkin

CGG05   Canadian Gravimetric Geoid 2005

ESM   Environmental Susitna Monitoring

ESS   Alaska Energy Authority station on the Susitna River for Surface water

HDR   HDR Alaska, Inc.

HRD   Hay River Delta

IPY-SCARF   Canadian International Polar Year project entitled Study of the Canadian Artic River-delta Fluxes

m, a.s.l.   metres above sea level

MD   Mackenzie Delta

RTK-GPS   Real Time Kinetic Global Positioning System

USGS   United States Geological Survey

WSC   Water Survey of Canada

1.   Introduction and Objectives

1.1   Overview

Ice affects most northern rivers for a significant portion of the year.   So understanding how ice affects a river's regime is important because of its potential to impact river ecology / morphology and to cause severe flooding. River ice models are important tools for both engineers and researchers because they can be used in both the analysis of past events and the forecasting of future scenarios. Many one-dimensional (1D) river ice models exist, but they all have their limitations.

The objective of the work in this thesis is to improve on the river ice modelling capabilities in the University of Alberta's *River1D* model. Improvements made here are part of a long-term goal to develop a public-domain comprehensive river ice process model that is capable of handling complex natural river systems from compound single channels to river deltas with multiple junctions and islands.

1.2   Background

Rivers in cold regions experience ice conditions for a significant part of the year. River ice can cause ice jam flooding, impact hydropower generation operations, and affect a river's ecological and morphological conditions. Many ice processes are highly dynamic and are affected by meteorological / hydrodynamic conditions, and river geomorphology. The first two types of ice commonly observed at freeze-up are skim ice and border ice. Skim ice forms on the water surface in slow-moving regions. If flow velocities permit,

sheets of skim ice can be transported downstream to create a skim ice run. Border ice grows out laterally from the river banks towards the river centerline. In regions of the channel where the water is moving quickly, turbulence prevents ice from forming on the water surface and the water temperature will drop slightly below zero, a phenomenon known as supercooling. Once the water is supercooled, ice particles, called 'frazil', will start to form in the water column. The frazil particles can stick to underwater objects such as the river bed or water intake structures, forming anchor ice. Frazil particles will also adhere to each other to form larger flocs. If buoyancy can overcome downward mixing effects, the flocs float to form surface ice floes, which can come together to form pans and rafts. Surface ice is transported down the river until something prevents the ice from passing a particular location, such as an artificial obstruction in the river or a constriction in the channel, either due to channel morphology or due to border ice encroaching the flow. Once ice bridging occurs, incoming surface ice accumulates in the upstream direction, forming an ice cover. With continued heat loss, the water in the void space within and between the ice floes will freeze and the ice cover will thicken.

The upstream progression of an ice cover is highly dependent on the geometry of the incoming ice floes and the flow conditions at the leading edge of the ice cover (Pariset and Hausser, 1961). Incoming floes may come to rest edge to edge forming a juxtaposed ice cover when water velocities are low, or they may become unstable and entrained into the flow passing under the leading edge when water velocities are high. Entrained floes may be deposited downstream resulting in a 'hydraulically thickened' ice cover or be swept downstream and will not contribute to the ice cover progression. The ice cover

that forms due to a combination of juxtaposition and hydraulic thickening is also referred to as narrow channel jam formation (Pariset and Hausser, 1961). The ice cover may collapse and thicken if the strength of the ice cover and bank resistance cannot withstand the applied external forces, due to gravity and water drag. This 'mechanical thickening' will continue until a new equilibrium is achieved and is also referred to as wide channel jam formation (Pariset and Hausser, 1961).

River ice breakup, although usually in spring, can be triggered at any point when warmer weather and/or increasing river flows occur. If the river flows remain fairly steady during a period of mild weather, the ice cover will likely undergo a thermal breakup, characterized by in-place thermal decay of the ice cover, minimal ice jamming, and low water levels (Beltaos, 2003). In comparison, if the river flow increases rapidly prior to any significant thermal deterioration of the ice cover, a mechanical breakup is more probable where ice runs and ice jams are far more likely to occur and could result in flooding. A river's geomorphology can also play a role in the breakup process. For example, braided rivers and shallow streams where the ice cover is likely to freeze to the bed rarely experience ice runs (Ashton, 1986) whereas river confluences can be more prone to ice jamming due to concentration of ice at the junction (Ettema et al., 1999). Additionally, multi-channel networks, like river deltas, are highly prone to ice jamming due to low channel gradients, mid-channel islands, and channel junctions which all contribute to reducing the ice conveyance capacity of the channel (Nafziger et al., 2019).

River ice can be very challenging to study due to the risks and costs associated with data collection in harsh winter conditions. One of the most economical and efficient

approaches to study river ice processes and to evaluate the effects of ice on a river's regime is to use numerical model simulations. Models can also be indispensable tools for quantifying the possible effects on river ice due to future regulation or climate change. Existing models range from component models, which consider only a specific ice process like the simulation of static ice jams, to comprehensive models, developed to simulate the entire river ice regime (Shen, 2010). Both one-dimensional (1D) and two-dimensional (2D) comprehensive river ice process models exist, commercially and within the public domain. 2D models provide a better representation of the variability of river ice processes in complex natural channel or multi-channel systems. However, they are not typically applied to long reaches or channel networks because costly field data and lengthy computational requirements render them operationally less practical. It is therefore more practical to model real-world river ice processes using a 1D model. Unfortunately, most existing 1D river ice models typically solve unsteady flow equations using solution algorithms that become unstable when the flow approaches critical or for mixed subcritical/supercritical flow regimes. Additionally, 1D river ice models with channel network modelling capabilities assume the equality of water surface elevations through junctions. These two solution approaches may hinder model application to flow scenarios such as ice cover consolidation and ice jam release in rivers with complex geometries.

1.3   Literature Review

Development of a comprehensive river ice model is no small task. In order for a model
to be able to simulate a river's ice regime it needs to calculate river hydraulics and
consider a large number of river ice processes. Over the past five decades many have
endeavored to develop a comprehensive river ice model. Some of these have
approximated the flow with steady state hydraulics while others have considered the full
solution to the unsteady flow equations. In some models, multi-channel systems can be
simulated whereas others are restricted to single channel analysis. Some have been
developed for application to a specific river and have therefore only considered the ice
processes dominant to the study river whereas others have been developed commercially
intended for application to any river. The following provides an overview of the river
hydraulics and river ice processes used in 1D river ice modelling.

1.3.1   River Hydraulics

1.3.1.1 Steady flow

Steady flow computations are commonly used in engineering analysis. In some cases,
the situation at hand is well approximated by steady flow and does not warrant the
computational burdens that come with unsteady flow modelling. In 1D models, steady
state water surface profiles are typically calculated by solving the gradually varied flow
equation using the standard step method. The *SIMGLACE* model and the *ICESIM* model
are examples of comprehensive river ice models that were developed with steady state

hydraulics. These models approximate unsteady hydraulics with a series of steady state solutions.

Development for the *SIMGLACE* model (Petryk, 1995; Petryk et al., 1981) started in 1977. At its inception, it was originally entitled "Simulation of Ice Conditions in Channels". This 1D model simulates water cooling, ice generation, ice cover formation, melting and breakup processes as function of time in conjunction with steady state backwater computations using the standard step method. In *SIMGLACE* four criteria are used to calculate ice cover thickness: maximum possible velocity for the ice cover to progress by juxtaposition or hydraulic thickening; ice cover stability assuming wide channel jam theory with no cohesion; user specified limiting average flow velocity for border ice stability; and limiting flow velocity for erosion under hanging dams or ice jams.

ICESIM was originally developed in 1973 by Acres International (now Hatch Energy) in order to address river ice problems associated with the design of hydroelectric generating stations on the Nelson River, Manitoba (Carson and Groeneveld, 1997). At each time step the model considers a number of ice processes: rate of ice generation, leading edge advancement by juxtaposition based on a Froude number criterion, ice erosion/deposition/transport, border ice growth, ice retreat by shoving, ice cover advance by staging, and anchor ice growth (Carson et al., 2011). The model approximates unsteady hydraulics with a series of steady state solutions. This is achieved by iterating between the solutions of the ice parameters and the water surface profile at each time step until a converged final solution is obtained for the given time step increment (Carson et

al., 2011). The use of steady state hydraulics in *ICESIM* prevented it from being used in more dynamic applications, which led to the restructuring of the model in a new version called *ICEDYN* (Carson and Groeneveld, 1997). This version of the model uses the same approach to represent the ice processes but replaces the steady hydraulics with a hydrodynamic solution to the Saint-Venant equations. Most recently a MATLAB® based version of *ICESIM* has been developed called *ICESIMAT* (Ghareh Aghaji Zare et al., 2015). In addition to the existing *ICESIM* functionality, the *ICESIMAT* model contains new subroutines to calculate the thermal growth and decay of the ice cover and estimates of the sediment bed load under ice cover conditions.

Steady flow calculations are also used in static ice jam profile models. These models solve for steady 1D non-equilibrium ice jam conditions based on jam stability theory developed by Pariset et al. (1966) and Uzuner and Kennedy (1976). *ICEJAM* (Flato and Gerard, 1986; Flato, 1988) and *RIVJAM* (Beltaos and Wong, 1986; Beltaos, 1988, 1993) are both examples of static ice jam models. Both were developed to calculate the longitudinal variation in ice thickness and water surface elevation for a cohesionless wide channel ice jam. There are subtle differences between the two models. *RIVJAM* accounts for seepage though the voids in the accumulation which is important for very thick and grounded ice jams (Beltaos, 1993); this is neglected in *ICEJAM*. *ICEJAM* employs a decoupled approach to iteratively solve the gradually varied flow and jam stability equations. The steady state solution procedure alternates between the standard step backwater equation proceeding in the upstream direction and the ice jam stability equation solved from the upstream jam head to the downstream jam toe until the water

surface elevations and ice jam thicknesses converge to a specified tolerance. *RIVJAM* employs a simplified gradually varied flow equation that neglects the velocity head gradient (Healy and Hicks, 1999). This simplified equation is coupled with an ice jam stability equation and solved simultaneously over the length of the channel. Some of the available hydraulic models include a static ice jam profile routine. These include the Corp of Engineers Hydraulic Engineering Center's River Analysis System (Brunner 2020a, 2020b), better known as *HEC-RAS;* and *MIKE-ICEJAM* for *MIKE11* (Carson et al., 2011). Both these models solve for steady state ice jam thickness and water surface profiles based on jam stability theory and standard step backwater calculation. The computation approach in *HEC-RAS* is similar to the decoupled approach in *ICEJAM*. Like *RIVJAM*, *MIKE-ICEJAM* also considers the effects of water seepage through the jam (Carson et al., 2011).

Ice jam formation is considered to be a highly dynamic process. As a result, steady state static ice jam models like these may not be able to correctly represent real ice jams (Healy and Hicks, 2006). Also, these models tend to over predict ice jam thickness and stage in channels with islands. This is because they combine the channel widths on either side of the island and neglect the island bank resistance when calculating the thickness profile. Jasek (1995) overcame this limitation by simulating flow around a single island with separate channel segments linked together by boundary conditions at the channel junctions. Although this approach was successfully implemented to estimate the likely effect of islands on ice jam profiles and associated water levels, it requires additional computation routines be set up to link separate segments together and it also requires that

8

junction hydraulics be known, thus making it difficult for engineers to use in practical

situations.

1.3.1.2 Unsteady flow

Because the approximation of unsteady flow with steady state hydraulics limits a model's

application, most 1D comprehensive river ice models simulate unsteady flow by solving

some form of the Saint-Venant Equations. These include *JJT* (Huokuna, 1990); *RIVICE*

(Environment Canada, 2013; Lindenschmidt, 2017); *RICE* (Lal and Shen, 1991); *RICEN*

(Shen et al., 1995); *CRISSP1D* (Shen, 2005, 2006); *River1D* (Andrishak and Hicks, 2005,

2008 ; She and Hicks, 2006; She et al., 2009); *ICEDYN* (Carson and Groeneveld, 1997);

and the *Mike-Ice* module (Timalsina et al., 2013; Theriault et al., 2010) for use with the

Danish Hydraulic Institute's (DHI) *MIKE11* hydrodynamic module (DHI, 2021).

With the exception of *River1D*, these models are based on a four-point implicit finite

difference solution to the differential form of the Saint-Venant equations. The four-point

implicit numerical scheme tends to become numerically unstable when the Froude

number approaches critical or for mixed subcritical/supercritical flow regimes (Fread et

al., 1996). *CRISSP1D* employ the Local Partial Inertia (LPI) solution technique (Fread et

al., 1996) to improve model stability in mixed flow regimes. The LPI method applies a

reduction factor to the two inertia terms in the momentum equation as the Froude number

of the flow approaches a user defined threshold. If the Froude number reaches or exceeds

the threshold, the inertia terms are set to zero and the solution reduces to that of a

diffusive wave. *MIKE11* similarly suppresses the convective acceleration term in the

momentum equation to maintain numerical stability when the Froude number is greater than one (DHI, 2021). *RIVICE* is limited to channels conveying discharge under subcritical conditions (Environment Canada, 2013) and the *JJT* model prevents the Froude number from exceeding 0.98 to maintain stability (Huokuna, 1990). Although these techniques will improve model stability in instances where supercritical flow occurs, preventing the flow from exceeding critical or suppressing the dynamic terms so the solution is more diffusive in nature may compromise solution accuracy when simulating dynamic events. In the case of an ice jam release wave, downstream flood levels could be under predicted. This could be very important if the wave encounters a downstream ice jam.

River1D, the University of Alberta's public-domain modelling system, solves the Saint-Venant equations using the characteristic-dissipative-Galerkin (CDG) finite element method (Hicks and Steffler, 1990, 1992). When applied to the conservation formulation of the Saint-Venant equations for rectangular channels of varying width, the CDG method is able to conserve mass and momentum (Hicks and Steffler, 1990) and is consistently more stable and accurate than other finite element methods and the four-point implicit finite difference scheme particularly when modelling extremely dynamic events (Hicks et al., 1992).

1.3.1.3 Network modelling

Ice jams have a tendency to occur in rivers with complex geometries. Ice jams are prone to occur at river confluences (Ettema et al., 1999), near islands (Turcotte and Morse,

2013), and within river deltas (Beltaos et al., 2012). Despite this, the majority of 1D comprehensive river ice models only consider a single channel and do not have the ability to model channel networks. Most models that do have network modelling capabilities assume equality of water levels at the junctions. In the *MIKE11* hydrodynamic module (DHI, 2021), branched and looped networks are modelled by equating the specific force across junctions (momentum equation neglecting frictional and gravitational forces). Although based on the same conceptual setup as the Environment Canada's One-Dimensional Hydrodynamic Model (*ONE-D*) which is capable of modelling dendritic and looped networks, the current version of *RIVICE* cannot perform simulations where multiple reaches are connected to a node (Environment Canada, 2013). The *RICEN* model (Shen et al., 1995) is a refined version of the *RICE* model (Lal and Shen, 1991). Shen et al. (1995) extended the single channel *RICE* model for application to channel networks with floodplains using the four-point implicit model for river networks developed by Potok and Quinn (1979) which assumes equality of water surface elevations at model junctions. Andrishak and Hicks (2011) adapted the *River1D* hydrodynamic model to simulate flows in channel networks for application to the Peace-Athabasca Delta (PAD). They assumed the water levels were constant through the junction, which they felt was reasonable when water surface gradients are expected to be low. *HEC-RAS*, although not considered a comprehensive river ice model, does have both river networking modelling and non-equilibrium ice jam profile modelling capabilities. However, no details are provided for how an ice jam profile is calculated if

it extends through a channel junction. None of these models that do include network modelling capabilities provide details about how ice physics are handled within junctions.

Although the equal water level assumption is commonly used in river ice models with junction modelling capabilities, it may be inaccurate since energy losses may be significant through the junction. Garcia-Navarro and Savirón (1992) demonstrated that the equality of water levels is only valid for cases of low Froude number. Another approach to modelling junctions is to apply conservation of momentum together with mass continuity through the junction. Using these principles, Shabayek (2002) developed an approach to modelling junctions (both converging and diverging) that is commensurate with the level of approximation of the Saint-Venant equations. This momentum based approach to junctions compared favourably with existing experimental data.

1.3.2   River Ice Processes

1.3.2.1 Heat Transfer

In order to simulate the thermal processes on a river such as water warming / cooling and ice formation / decay, quantification of the heat fluxes is a necessity. To do this, there are a number of approaches available. The most detailed approach is to use a full energy budget. Detailed energy budget calculations typically consider solar radiation, long wave radiation, evaporative heat flux, and convective heat flux (e.g. Hicks, 2016; Ashton, 2013). The calculations may also consider heat flux from other sources such as precipitation, river bed and banks and groundwater (Hicks, 2016). *JJT, SIMGLACE,*

CRISSP1D and *Mike-Ice* all offer a detailed energy budget approach. The challenge with using this approach is usually the lack of the necessary meteorological data. As a result, the more simplified linear heat transfer approach is a practical alternative used in river ice modelling. Andrishak and Hicks (2008) implemented the following linear heat transfer model in *River1D* for calculating the net rate of heat exchange between the water and air:

$$\phi_{wa} = -\phi_s + h_{wa}\left(T_w - T_a\right) - j_{wa}T_a + k_{wa} \qquad [1.1]$$

where ϕ_s is the net rate of incoming solar radiation, T_w is the water temperature, T_a is the air temperature; h_{wa} and j_{wa} are linear heat transfer coefficients; and k_{wa} is a heat transfer constant. In some cases, the above model is even further simplified to consider only the second temperature difference term. Positive values of ϕ_{wa} represent a net heat loss from the water to the air (water cooling or freezing) while negative values represent a net heat gain (water warming or melting).

The simplest approach for quantifying heat flux is the degree-day method. This approach assumes that all heat fluxes can be quantified using accumulated degree-days. Estimates of ice thickness are commonly predicted with accumulated degree-days of freezing, *ADDF*, using the empirical equation commonly called the Stefan equation for ice thickness (Ashton and Beltaos, 2013):

$$t_i = a_s \sqrt{ADDF} \qquad [1.2]$$

where t_i is the predicted ice thickness (m) and a_s is a site specific coefficient (m/°C$^{\frac{1}{2}}$ day$^{\frac{1}{2}}$). Ashton and Beltaos (2013) and Hicks (2016) both offered caution when applying

this approach to predict river ice thicknesses since this method assumes the ice is thermal in origin which is not always the case in river ice where snow ice and frazil slush can contribute to ice thickness. Although this approach has gained widespread use because of its simplicity, it is not commonly used in comprehensive river ice modelling. *SIMGLACE* and *RIVICE* are however two examples of comprehensive river models that do employ *ADDF*. The *SIMGLACE* model estimates the volume of frazil ice generated in open water as a linear function of *ADDF* (Petryk et al., 1981). *RIVICE* calculates the total width of border ice at a cross section as a linear function of *ADDF* in one of the three available methods for border ice formation (Environment Canada, 2013).

1.3.2.2 Water temperature and suspended frazil

Water temperature conditions can vary significantly over the length of a river due to spatial and temporal variability of atmospheric conditions and also due to thermal inputs along the river (e.g. warmer/colder tributaries and industrial effluents). Additionally, the timing and spatial distribution of supercooled water will dictate where and when ice will initially form. Frazil ice formed in suspension is carried with the river flow and may rise to the surface when frazil buoyancy can overcome downward turbulent effects. As a result, the longitudinal distribution of water temperature and suspended frazil are important to the simulation of a river's ice regime. These can be simulated by considering transport equations for the conservation of thermal energy of the river water and conservation of suspended frazil ice mass.

Models such as *JJT*, *RICE*, *RIVICE,* and previous versions of *River1D* only simulate the water temperature down to the freezing point. Once the modelled water temperature drops to zero, additional heat loss to the atmosphere is used for frazil production. *RICEN*, *CRISSP1D,* and *Mike-Ice* all simulate water supercooling. This is achieved by including the heat transfer between the water and the ice in the thermal energy conservation equation (Shen, 2010). In these models, heat flux between the water and suspended frazil is a function of volumetric suspended frazil concentration, Nusselt number, the water temperature, the thermal conductivity of water, and the average frazil particle geometry (Shen et al., 1995; Theriault et al., 2010).

Once frazil starts to form, the size of particles will vary as a result of crystal growth, flocculation of particles to form larger particles (Ye and Doering, 2004), and breaking apart of particles due to collisions with hard surfaces (Daly, 2013). Laboratory experiments of frazil particle size have found that the size distributions generally follow a lognormal distribution (Ye et al., 2004; Clark and Doering, 2006; McFarlane et al., 2014, 2015). If frazil particles become large enough, their buoyancy will overcome the downward effects of turbulence and the frazil will rise to the surface. A number of theoretical equations have been derived for calculating rise velocity as function of frazil particle geometry (e.g. Gosink and Osterkamp, 1983; Wuebben, 1984; Daly, 1984; Shen and Wang, 1995, McFarlane et al., 2014). At present, these relationships are not considered in 1D comprehensive river ice models since neither particle size nor particle size distribution is simulated. Existing comprehensive river ice models that do simulate suspended frazil and frazil rise (e.g. *JJT*, *RICE*, *RICEN*, *Mike-Ice*, *River1D*, and

CRISSP1D), model frazil rise as a net rate of suspended ice supply to the surface ice. This net rate is calculated as a function of the suspended frazil concentration and a user specified parameter representing the rate of frazil crystals rising to the surface. Without field measurements, the frazil rise parameter is usually indirectly calibrated when it is adjusted so that simulated ice cover progression rates, water levels and ice thicknesses match observed values (Jasek et al., 2011).

1.3.2.3 Skim and border ice

When a river starts to freeze, one of the first types of ice to form is a thin skim of ice at the water surface. Skim ice formation in faster moving water may develop into a skim ice run. In regions of calm water, a stationary skim ice cover may develop. Also observed at the onset of freeze-up is border ice which grows out horizontally from the river banks into the flow. Border ice formation occurs either due to heat loss at the water-air interface in the form of stationary skim ice at the banks of the river (static border ice formation) or due to frazil accretion of moving surface ice floes to the river bank or to the edge of stationary ice (dynamic border ice formation).

Matousek (1984a) formulated conditions for different types of ice runs at freeze-up as a function of the surface water temperature, T_{ws} (°C), average water temperature in the cross section, T_v (°C), the vertical fluctuating component of the water velocity due to turbulence, v'_z (m/s), and the buoyant velocity of frazil ice, V_b (m/s):

- when $T_{ws} \geq 0$ °C, no ice will form;
- when -1.1 °C < T_{ws} < 0 °C and $v'_z \leq V_b$ skim ice will form and run with the water (skim ice run);

16

- when -1.1 °C $< T_{ws} < 0$ °C, $v'_z > V_b$, and $T_v \leq 0$ °C frazil ice will form; and
- when $T_{ws} \leq$ -1.1 °C a skim ice cover (static ice cover) will form.

Matousek (1984a) provided the following empirical relationships for evaluating the above conditions.

$$T_{ws} = T_v + \frac{q_o}{1130 U_w + mU_{wind}} \quad\quad [1.3]$$

$$V_b = -0.025 T_{ws} + 0.005 \quad\quad [1.4]$$

$$v'_z = \frac{\sqrt{g}}{5\sqrt{(0.7 C_s + 6) C_s}} U_w \qu\quad [1.5]$$

where m is a calibration coefficient dependent on surface water width in the wind direction, ranging from 15 to 45 (J/m³/°C); U_w is the average water velocity in the cross section (m/s); U_{wind} is the wind velocity at an elevation of 2 m above the water surface (m/s); q_o is the net rate of heat exchange between the water surface and atmosphere (W/m²), and C_s is Chézy's coefficient (m$^{\frac{1}{2}}$/s).

Matousek (1984b) proposed that the criterion for the formation of a static ice cover is also applicable to border ice formation and suggested that the mean vertical velocity, V_v, meet the following condition for border ice to form:

$$V_v \leq \frac{q_o}{1130(-1.1 - T_v)} - \frac{mU_{wind}}{1130} \quad\quad [1.6]$$

17

Empirical lateral border ice growth models have been developed by Newbury (1968), Michel et al. (1982), and Miles (1993). Using field observations along the St. Anne River in Québec, Michel et al. (1982) developed the following equation for dynamic lateral border ice growth:

$$\Delta W = 14.1 C_i^{1.08} \left(\frac{V_s}{V_c} \right)^{-0.93} \frac{\Delta \phi}{\rho_w L_i} \qquad [1.7]$$

where ΔW is the incremental growth in the border ice over a given time period (m); C_i is the surface ice concentration; $\Delta \phi$ is heat loss per unit surface area from the water over the same time period (kJ/m²); V_s is the local water velocity in the open water adjacent to the edge of the border ice (m/s); V_c is the maximum observed water velocity for frazil adherence = 1.2 m/s; and L_i is the latent heat of ice (kJ/kg). Michel et al. (1982) indicated that when $C_i < 0.1$ border ice will only grow in thermal or static mode and, in that case, this equation can be used with $C_i = 0.1$ to account for the static growth. It is also only valid when $0.167 < V_s / V_c < 1.0$.

Comprehensive ice models vary with respect to border ice modelling capabilities. Previous versions of the *River1D* model did not consider border ice. Andrishak and Hicks (2008) recognized the importance of border ice formation on large rivers, however they felt the use of rectangular sections to approximate river cross sections excluded the portions of the channel near to the river banks where border ice is expected to form. The *SIMGLACE* model considers border ice growth as a thermal ice cover with its stability governed by a user input limiting average flow velocity value (Petryk et al., 1981). In the

JJT model (Huokuna, 1990), static border ice is formed according to the mean vertical velocity criteria in equation [1.6]. To apply the criteria, the cross sectional area is divided into vertical slices of a user input width and local velocities are calculated for the slices using a weighted conveyance approach:

$$V_{sl} = \left\{ \frac{(1/n)R_{sl}^{2/3}}{(1/n)AR^{2/3}} \right\} Q$$ [1.8]

where V_{sl} and R_{sl} are the average velocity and hydraulic radius of a given slice, respectively; A, R, and Q are the cross sectional area, hydraulic radius, and the discharge, respectively; and n is the Manning resistance coefficient. The *Mike-Ice* module simulates border ice progression based on cooling rate and maximum local flow velocity criteria (Timalsina et al., 2013). Local flow velocities are computed using an approach presented in Theriault et al. (2010). In *RIVICE* (Environment Canada, 2013), the user has three options for simulating border ice advancement:

1. User defined – calculates the border ice width at a cross section as a function of channel top width, a time step to total simulation time ratio, and user input coefficients.
2. Newbury Empirical Method – calculates total border ice at a cross section as function of *ADDF*, average flow velocity at the cross section, and user input coefficients.
3. Matousek Method – establishes a static ice cover according to the velocity criterion in equation [1.6].

The *CRISSP1D* model was developed based on *RICEN* which is a refinement of *RICE*. As a result, they all use very similar approaches to simulating skim and border ice. In all

three models skim ice runs and static border ice formation are based on criteria as proposed by Matousek (1984a); but in *CRISSP1D* equation [1.5] is replaced with an equation that considers both bed and wind shear effects. Dynamic border ice formation is based on equation [1.7]. *CRISSP1D* employs a stream-tube method developed by Shen and Ackermann (1980) to calculate local water velocity, V_s.

1.3.2.4 Anchor Ice

When river water is supercooled, frazil ice can become 'anchored' to the bed material of the river. Anchor ice can also develop on structures within the river such as water intakes and trash racks. There are two processes for anchor ice growth: accretion of active frazil particles to submerged objects and underwater nucleation (Malenchak and Clark, 2013). Once anchor ice has formed, it can release if the bonds between the anchor ice and the anchoring surface are melted or if the buoyancy forces of the anchor ice exceed the resistive forces keeping the ice anchored.

A number of mathematical models have been developed for simulating anchor ice. Malenchak and Clark (2013) provide an excellent review of the models presented in the literature. Earlier models only considered a single process for anchor ice buildup. For example, Marcotte and Robert (1986) used detailed heat transfer to calculate anchor ice volume but did not account for frazil accretion. In contrast, Tsang (1988) assumed that growth of frazil crystals on the bed is of secondary importance and therefore only considered the accretion of frazil in the development of a 1D model for the prediction of river cooling and the formation of frazil and anchor ice. A more comprehensive

20

analytical formulation for anchor ice formation and evolution was developed by Wang

and Shen (1993) as presented in Shen et al. (1995). This model considers anchor ice

growth due to frazil accretion and thermal growth and decay of anchor ice due to

turbulent heat exchange between anchor ice and the river water. The model also

considers anchor ice release due to thermal and mechanical triggers. The rate of change

of anchor ice thickness is described using:

$$\frac{dt_{an}}{dt} = \frac{1}{(1-p_a)}\left(\gamma C_f - \frac{\phi_{wi}}{\rho_i L_i}\right)$$ [1.9]

where t_{an} is the anchor ice thickness on the top surface of the substrate; p_a is the porosity

of the anchor ice; γ is the frazil accretion rate; C_f is the volumetric concentration of

suspended frazil; ϕ_{wi} is the heat flux from the water to the anchor ice; ρ_i is the density of

ice; and L_i is the latent heat of fusion of ice. The frazil accretion rate in the model is set

to zero when frazil is not in its active state (when the water temperature rises above zero).

Shen et al. (1995) recognized as anchor ice forms, it may not completely fill the void

space in the bed material and assumed that anchor ice would thermally release when the

substrate flow depth under the anchor ice, h_{sb}, reached a critical substrate flow depth.

The rate of change of substrate flow depth can be calculated by (from Shen 2005):

$$\frac{dh_{sb}}{dt} = \frac{1}{(1-p_a)\rho_i L_i}\left(h_{iws}(T_w - T_m) + \phi_{pz}\right)$$ [1.10]

where h_{iws} is the heat exchange coefficient between the anchor ice and the substrate flow;

ϕ_{pz} is the short wave radiation absorbed by the anchor ice; and T_m is the melting point of

ice. The model assumes that the ice will mechanically release from the substrate when the buoyant force of anchor ice exceeds the resistive forces (submerged weight of bed material plus inter-particle resistance):

$$F_{anb} > W_{bed} + F_{inter} \qquad\qquad [1.11]$$

where F_{anb} is the buoyant force per unit area of the anchor ice; W_{bed} is the submerged weight per unit area of bed material; and F_{inter} is the inter-particle resistance per unit area.

Kerr et al. (2002) performed a laboratory study on anchor ice evolution in channels with gravel beds. They found that when the anchor ice initially started to form, the channel roughness started to increase above that of the ice-free gravel bed, but that as more of the bed became covered in ice, the roughness decreased. Once the entire bed was covered in anchor ice, the roughness decreased towards a minimum value that was lower than that of the ice-free gravel bed. Pan et al. (2020) performed an analysis to study the effects of anchor ice on river hydraulics. They looked at the effect on river flow due to changes in bed elevation due to anchor ice, changes in mass flux of anchor ice growth and release, and changes ice-bed roughness. Of these three, they found that change in ice-bed roughness to be the dominating factor causing the most significant fluctuations in water level and discharge. They also found that ice-bed roughness varied with the evolution of anchor ice, as suggested by Kerr et al. (2002), but were unable to obtain an analytical relationship and suggested further research in order to develop a formulation on the relationship between anchor ice thickness and ice-bed roughness.

Because anchor ice growth occurs only in supercooled water, simulation of supercooling and anchor ice formation tend to go hand-in-hand. *RICEN*, *CRISSP1D* and *Mike-Ice*, which all simulate water supercooling, also simulate anchor ice formation, decay and release. The anchor ice models in *RICEN* and *CRISSP1D* are based on the formulation developed by Wang and Shen (1993), as presented above. In *CRISSP1D*, it is assumed that inter-particle resistance is zero when evaluating the mechanical release condition as presented in equation [1.11]. In both *RICEN* and *CRISSP1D*, when anchor ice releases, it is assumed that all anchor ice rises to the surface and becomes part of the surface ice run rather than being entrained in the flow. Recently, Pan et al. (2020) modified the hydrodynamic equations in both *RICEN* and *CRISSP1D* to account for the effects of anchor ice on water levels and discharge. Details of anchor ice treatment in *Mike-Ice* are provided in Timalsina et al. (2013). The model considers anchor ice formation due to frazil accretion and heat exchange between anchor ice and supercooled water in a similar way to equation [1.9]. Anchor ice release in *Mike-Ice* is controlled by a release rate which is calculated as function of thermal effects and buoyancy.

1.3.2.5 Ice Cover Progression

When an ice floe approaches the leading edge of an ice cover, it will either come to rest at the upstream edge of the ice cover (juxtaposition) or it will become unstable and pass under the leading edge and may be deposited downstream adding to the thickness of the stationary ice cover (hydraulic thickening). Many investigators have looked at the stability of incoming ice floes. One of the earliest investigations into ice floe stability was conducted by Pariset and Hausser (1961). Through mathematical analysis and

laboratory tests they found that the stability of incoming ice blocks to be a function of the

flow velocity immediately upstream of the leading edge (expressed here in term of

Froude number, F_r):

$$F_r \leq F_{r\_jux} = K\sqrt{2\frac{t_{block}}{Y}\left(1-\frac{\rho_i}{\rho_w}\right)\left(1-\frac{t_{block}}{Y}\right)} \qquad [1.12]$$

where K is a form factor that is a function of the ice floe geometry; t_{block} is the thickness

of the incoming ice block; Y is the mean depth of flow immediately upstream of the

leading edge; and F_{r_jux} is the critical Froude number for juxtaposition. Since this early

study by Pariset and Hausser (1961), numerous studies have investigated the stability

incoming ice blocks (see literature reviews in Beltaos, 2013; and Dow Ambtman et al.,

2011a, 2011b). These studies have revealed that there are two different processes by

which ice blocks become unstable. They are either vertically submerged also called

"sinking" or they rotate about their downstream edge also called "underturning".

Uzuner and Kennedy (1972) performed laboratory experiments to determine the critical

Froude number for underturning as a function of t_{block}/Y, t_{block}/L_{block}, and ρ_i/ρ_w, where

L_{block} is the length of the block. They observed that short thick blocks ($t_{block}/L_{block} > 0.8$)

and long thin blocks ($t_{block}/L_{block} < 0.1$) submerge by sinking. Using the experimental

results of Uzuner and Kennedy (1972) and a simplified moments analysis, Ashton (1974)

found that ice block stability was more dependent on t_{block}/Y and that t_{block}/L_{block} was less

important. He also found that it is more applicable to express ice block stability criterion

in terms of densimetric Froude number, rather than the Froude number of the incoming

flow. Based on his findings, he developed the following relationship for ice-block

stability:

$$F_D = \frac{U_c}{\sqrt{g t_{block}\left(1-\dfrac{\rho_i}{\rho_w}\right)}} = \frac{2\left(1-\dfrac{t_{block}}{Y}\right)}{\sqrt{5-3\left(1-\dfrac{t_{block}}{Y}\right)^2}} \qquad [1.13]$$

where F_D is the densimetric Froude number; and U_c is the critical velocity of the water

upstream of the leading edge for block stability. Because this criterion involves the

evaluation of just one equation, it is easy to apply and is widely used (Dow Ambtman et

al. 2011b). Recasting equation [1.13] in terms of Froude number:

$$F_r \leq F_{r\_jux} = \frac{2\left(1-\dfrac{t_{block}}{Y}\right)\sqrt{\dfrac{t_{block}}{Y}\left(1-\dfrac{\rho_i}{\rho_w}\right)}}{\sqrt{5-3\left(1-\dfrac{t_{block}}{Y}\right)^2}} \qquad [1.14]$$

Equating equations [1.12] and [1.14], K can be evaluated using (Ashton, 1986):

$$K = \frac{\sqrt{2}}{\sqrt{5-3\left(1-\dfrac{t_{block}}{Y}\right)^2}} \qquad [1.15]$$

where K ranges from 0.63 (for $t_{block}/Y = 1.0$) to 1.0 (for $t_{block}/Y = 0$). Dow Ambtman et al.

(2011b) evaluated the stability of floating ice blocks through a force-moment analysis.

They compared results of their analysis with data from a number of studies (Uzuner and

Kennedy, 1972; Larsen, 1975; and Daly and Axelson, 1990) and found good agreement

between calculated and observed critical densimetric Froude numbers. Their analysis

also demonstrated the importance of block length on block stability. Specifically, they

compared Ashton's equation [1.13] to the results of their moment analysis and found that

Ashton's equation matches well to the moment analysis for the case of $t_{block}/L_{block} = 0.5$

but that Ashton's equation would under predict the critical densimetric Froude number

for values of t_{block}/L_{block} less than 0.5. As a result, they recommended that block length

not be neglected in assessing block stability.

Once an incoming ice floe becomes unstable, it can be deposited downstream of the front,

hydraulically thickening the ice cover. Based on the seminal work by Pariset and

Hausser (1961), and adapted by Michel (1971) to include the effects of porosity of the

accumulation, p_j, the thickness of the ice at the leading edge, t_{le} of an ice cover that

results due to submergence and deposition of incoming ice floes can be estimated from

the following relationship:

$$\frac{U_w}{\sqrt{gY}} = \sqrt{2\frac{t_{le}}{Y}\left(1-p_j\right)\left(1-\frac{\rho_i}{\rho_w}\right)\left(1-\frac{t_{le}}{Y}\right)}$$
[1.16]

This equation is based on the assumption that the leading edge of the ice cover does not

submerge under the water, also called the "no spill" condition. The formation of an ice

cover due to hydraulic thickening is also referred to as narrow channel jam formation.

Examination of equation [1.16] reveals that there is a maximum Froude number above

which all incoming ice is swept under the ice front and the ice cover will cease to

progress in the upstream direction. This occurs when $t_{le}/Y = 1/3$. Assuming $\rho_i/\rho_w = 0.92$, the maximum Froude number for ice cover progression is:

$$F_{r\_max} = 0.154\sqrt{\left(1 - p_j\right)} \qquad\qquad [1.17]$$

Most laboratory data lie between $F_{r\_max} = 0.08$ and 0.13 (Ashton, 1986). But field observations and calibrated values in modelling studies suggest that the upper limit for F_{r_max} may be closer to 0.09 (Calkins, 1984; Sun and Shen, 1988; Lal and Shen, 1991).

Ice cover leading edge advancement in the *ICESIM* model is described by Judge et al. (1997). In slow moving water, leading edge progression will occur by juxtaposition. Once a critical user input Froude number is exceeded, incoming ice floes are swept under the leading edge. Hydraulic thickening will occur until $t_{le}/Y = 1/3$ at which point additional ice will be swept downstream under the stationary ice cover until lower velocities allow it to be deposited. Ice cover progression by juxtaposition will resume once the accumulated ice causes the water level to stage up and the Froude number at the leading edge to drop below the critical value.

Progression of the leading edge by juxtaposition in *Mike-Ice* is described by Timalsina et al. (2013) as a function of local flow velocity, Froude number and ice thickness. If the local velocity and Froude number do not exceed user defined values for stable leading edge progression, the thickness of the advancing cover is calculated using equation [1.16]. If the Froude number exceeds the user defined critical Froude number at the

leading edge, the ice cover will advance with a thickness of $t_{le} = Y/3$, suggesting that the ice cover continues to advance regardless of flow conditions.

In the *JJT* model (Houkuna, 1990), the leading edge will progress upstream in juxtaposition if the velocity is less than the critical velocity (from the critical Froude number for juxtaposition) calculated from equation [1.14] with an ice cover thickness equal to the thickness of the incoming ice floes. If the velocity is greater than the critical velocity, the ice cover progresses with a thickness calculated by equation [1.16]. The ice cover progress will cease if the Froude number at the leading edge exceeds the critical Froude number for submergence as given by equation [1.17].

In the *SIMGLACE* model, the front progression of the ice cover employs the narrow jam criterion (Petryk, 1995). Andrishak and Hicks (2008) implemented a simplified conservation of surface ice discharge into *River1D* to track the ice front location. The front location is calculated as function of the surface concentration of the ice, the ice velocity (assumed to travel at the same velocity as the water), and a user defined calibration parameter that empirically accounts for hydraulic and mechanical thickening of the ice cover at the leading edge. *RIVICE* provides the user with three options for evaluating the stability of incoming ice floes at the leading edge: stability according to equation [1.16]; stability according to equation [1.13]; or a user defined leading edge thickness value (Environment Canada, 2013).

In *RICE*, *RICEN* and *CRISSP1D* ice cover progression can occur in three different modes: juxtaposition mode, hydraulic thickening mode; and mechanical thickening mode (Shen et al., 1995; Shen, 2005). The ice cover will advance by juxtaposition when the

Froude number is less than the user defined critical Froude number for juxtaposition. When this value is exceeded, the ice cover will progress either in hydraulic thickening mode with leading edge thickness calculated based on equation [1.16] or it will proceed in mechanical thickening mode with leading edge thickness assuming equilibrium wide channel jam conditions according Pariset and Hausser (1961). The model calculates the thickness using both narrow and wide channel jam equations; the controlling process is the one that produces the larger ice thickness (Shen, 2005). Ice cover will not progress upstream if the Froude number exceeds a user defined maximum Froude number for ice cover progression.

1.3.2.6 Undercover Transport

Ice floes and frazil slush approaching the lead edge of an ice cover will either contribute to the ice cover advancement or they will be swept downstream and transported with the flow on the underside of the stationary ice cover. Transported frazil tends to deposit in areas of lower velocity which can lead to the development of hanging dams. An under ice accumulation will thicken until the local flow velocity has reached some critical value (Ashton, 1986). The accumulated frazil may be eroded and transported downstream if the flow velocity increases.

Pariset and Hausser (1961) suggested that under ice transport of frazil could be simulated with bed load theory and adopted the use of the empirical Meyer-Peter formulation for bed load transport in rivers:

$$1000\frac{U_u^{\,2}}{C_s^{\,2}} = 3.75t_{if} + 5q_i^{\,2/3} \qquad\qquad [1.18]$$

where U_u is the average flow velocity under the ice cover (ft/s); t_{if} is the mean thickness of the transported ice floe (ft); C_s is Chezy's coefficient; and q_i is the ice discharge under the ice cover (lb/ft). If the incoming ice discharge exceeds the ice carrying capacity of the flow under the ice cover, deposition will occur.

Shen and Wang (1995) also suggested under cover transport of frazil behaves as a cover load, analogous to bed load transport. They proposed the following relationship between transport capacity, Φ, and flow strength, Θ:

$$\Phi = 5.487\left(\Theta - \Theta_c\right)^{1.5} \quad \text{when } \Theta \geq \Theta_c = 0.041 \qquad\qquad [1.19]$$

in which Φ is the dimensionless ice transport capacity; Θ is the dimensionless flow strength, Θ_c is the critical flow strength (below which there is no ice transport). These dimensionless parameters are defined as:

$$\Phi = \frac{q_i}{Fd_n\sqrt{gd_n\left(\dfrac{\rho_w - \rho_i}{\rho_w}\right)}} \qquad\qquad [1.20]$$

$$\Theta = \frac{\tau_i}{F^2\rho_w gd_n\left(\dfrac{\rho_w - \rho_i}{\rho_w}\right)} \qquad\qquad [1.21]$$

where d_n is the nominal diameter of ice particles; and τ_i is the shear stress on the underside of the frazil accumulation. The critical velocity approach to undercover accumulations of frazil based on user defined inputs is the most common method use in river ice modelling (e.g. *ICESIM*, *JJT*, *RICE*, *Mike-Ice*). *SIMGLACE* estimates the undercover ice erosion using the Meyer-Peter relation (Petryk et al., 1981). In *RIVICE* deposition can be controlled by a user-defined critical velocity, the Meyer-Peter equation, or a critical densimetric Froude number whereas erosion options include a user-defined maximum velocity or maximum tractive forces (Environment Canada, 2013). The *RICEN* and *CRISSP1D* models both simulate under cover transport of frazil based on the ice transport capacity developed by Shen and Wang (1995).

1.3.2.7 Ice Cover Stability

At lower surface ice concentrations, interaction between surface ice floes is minimal and ice will generally be transported at the surface water velocity. When surface concentrations are high, resistive forces on the ice floes will come into play and will cause the ice to slow down. Unless ice dynamics are simulated, the unsteady effects of the ice must be approximated by some other means. While theories of leading edge stability are used to determine the rate of ice cover progression, the stability of the downstream ice cover should also be addressed since it may collapse and thicken if the strength of the ice cover and bank resistance cannot withstand the applied external forces, due to gravity and water drag. Pariset et al. (1966) developed a bell-curve approach for evaluating the stability of an ice cover. This approach is used on SIMGLACE (Petry et al., 1981). However, this approach is not applicable near the leading edge and was

designed for simplified channels of constant width and geometry (Environment Canada, 2013). Another approach to simulating ice cover stability is to incrementally evaluate the forces on the ice cover starting at the lead edge and working downstream. If the stability conditions are not satisfied, the leading edge is moved down to the unstable location and the ice cover continues to progress from this new location. Assuming steady uniform flow, Lal and Shen (1991) presented the following stability condition that must be satisfied for the ice cover to shove:

$$2\left(\tau_c t_i + \mu_1 f\right) < \left(\tau_i + \tau_g + \tau_a\right) B_o \qquad [1.22]$$

where τ_c is the cohesion of the ice; t_i is the ice thickness; μ_1 is a bank friction coefficient; f is the allowable longitudinal force on the ice cover (expressed in terms of the strength of the ice cover); τ_i is the shear stress on the underside of the ice; τ_g is the weight component of the ice cover; τ_a is the shear stress due to wind; and B_o is the width of the open water between border ice. This incremental approach has been implemented in a number of models including *RICE, RICEN, CRISSP1D* and *RIVICE*.

Since theories on static surface ice accumulations / jams cannot be used to predict the initiation of ice covers or ice jams, Shen et al. (1990) developed a 1D equation formulation for dynamic ice transport. The governing equations solve ice velocity, surface ice concentration, and ice thickness. They used two different constitutive laws to define the internal ice resistance depending on whether the ice movement was considered rapid or slow. Shen et al. (2000) formulated the internal ice resistance using Hibler's viscous-plastic law. She et al. (2009) developed a new constitutive model for

determining the internal ice resistance based on a one-mth power function and found that it provides a better representation of the stress strain rate relationship than Hibler's viscous-plastic constitutive law, as well as improved accuracy. This new constitutive law has been included in the ice dynamics modelling component of *River1D*.

1.3.3 Discussion

There are many 1D ice models in existence ranging from those that have limited applicability to those that are very sophisticated and comprehensive. Since the most sophisticated ones tend to be proprietary (eg. *CRISSP1D*, *Mike-Ice*), there is still a need for state-of-the-art comprehensive river ice process modelling tools available in the public domain. Also, there is a need for these comprehensive modelling capabilities within a model with accurate and stable solutions to river hydraulics so that the most complex scenarios can be effectively simulated (e.g. dynamic ice jam formation within a river delta system).

1.4 Study Objectives

The long-term goal of this research is to develop a comprehensive public-domain river ice process model that is capable of handling complex natural channel geometry and channel networks for the full spectrum of scenarios, from simple (known) steady ice conditions to highly dynamics cases, such as ice jam formation or release. The study had three specific objectives towards this long-term goal, which are outlined below.

The first objective was to enhance the University of Alberta's *River1D* model to simulate

river ice processes based on natural channel geometry. Significant progress has been

made in the development of the University of Alberta's *River1D* model with respect to

river ice processes. However, previous versions of the model were limited to rectangular

channel geometry and did not include a number of important river ice processes, such as

border ice formation, anchor ice evolution, and under ice cover transport of frazil.

Although the rectangular channel approximation has been shown to reliably route flood

flows, it may not simulate water levels accurately. In order to accurately assess the flood

risk associated with ice-related events, the ability to model channels using natural

channel cross section data is required. To meet this first objective, the hydrodynamic

component was first modified to accommodate natural channel geometry and the river ice

processes component was then enhanced to be more comprehensive. Validation of these

new enhancements was achieved with the simulation of freeze-up on the Susitna River in

Alaska. This work is presented in Chapter 2.

The second objective was to implement channel junction modelling capabilities in the

hydrodynamic module of the University of Alberta's *River1D*. A new approach was

implemented based on the 1D momentum conservation approach to model channel

junctions developed by Shabayek (2002). The adapted approach eliminates the equal

water level assumption used in previous versions of *River1D*, and instead takes into

account the significant physical effects at channel junctions (such as gravity and flow

separation forces, and channel resistance). The adapted approach is also equipped with

the ability to dynamically change junction configurations (i.e. diverging to converging or

vice versa) as the result of flow reversals. The new momentum based approach to model junctions was assessed using a series of steady and unsteady tests using a 2D model for comparison. The model was then applied to the Mackenzie Delta to simulate flow conditions during the 2008 breakup. This work is presented in Chapter 3.

The third objective was to extend the junction modelling approach applied to *River1D's* hydrodynamic module to model ice jam profiles in complex natural channel systems with channel junctions. The proposed approach is unique in that it considers the effect of the junction discharge ratio on channel junction elements when solving the ice jam stability equation and can simulate ice jam profiles that extend through complex channel networks with multiple junctions and islands. The model was first compared to a series of ice jam simulations in channels with islands. The model was then validated with simulations of ice jam profiles in the Hay River Delta during the 2009 breakup. This work is presented in Chapter 4.

References

Andrishak, R., Hicks, F.E. 2005. Impact of Climate Change on the Peace River Thermal Ice Regime. In: CGU HS Committee on River Ice Processes and the Environment Proc., 13th Workshop on Hydraulics of Ice Covered Rivers, September 15-16, 2005, Hanover, NH, 21-40.

Andrishak, R., Hicks, F. 2008. Simulating the effects of climate change on the ice regime of the Peace River. Canadian Journal of Civil Engineering 35: 461-472.

Andrishak, R., Hicks, F. 2011. Ice effects on flow distributions within the Athabasca Delta, Canada. River Research and Applications 27: 1149-1158.

Ashton, G.D. 1974. Froude criterion for ice-block stability. Journal of Glaciology 13: 307-313.

Ashton, G.D. (Ed.) 1986. River and Lake Ice Engineering. Water Resources Publications, Littleton, Colorado, 485 pp.

Ashton, G., Beltaos, S. 2013. Chapter 8: Thermal Growth of Ice Cover. In: Beltaos, S. (ed) River Ice Formation. CGU HS Committee on River Ice Processes and the Environment, 257-296.

Beltaos, S. 1988. Configuration and properties of a breakup jam. Canadian Journal of Civil Engineering, Ottawa, 15(4): 685-697.

Beltaos, S. 1993. Numerical computation of river ice jams. Canadian Journal of Civil Engineering, Ottawa, 20(1): 88-99.

Beltaos, S. 2003. Numerical modelling of ice-jam flooding on the Peace-Athabasca delta. Hydrological Processes, 17, 3685-3702 (2003).

Beltaos, S. 2013. Chapter 7: Freezeup Jamming and Formation of Ice Cover. In: Beltaos, S. (ed) River Ice Formation. CGU HS Committee on River Ice Processes and the Environment, 181-255.

Beltaos, S., Carter, T., & Rowsell, R. 2012. Measurements and analysis of ice breakup and jamming characteristics in the Mackenzie Delta, Canada. Cold Regions Science and Technology, 82: 110-123.

Beltaos, S., Wong, J. 1986. Downstream transition of river ice jams. Journal of Hydraulic Engineering, ASCE, 112(2): 91-110.

Brunner, G.W. 2020a. HEC-RAS, River Analysis System Hydraulic Reference Manual Version 6.0 Beta. U.S. Army Corps of Engineers Hydrologic Engineering Center. 466 pp.

Brunner, G.W. 2020b. HEC-RAS River Analysis System User's Manual Version 6.0 Beta. U.S. Army Corps of Engineers Hydrologic Engineering Center. 721 pp.

Calkins, D.J. 1984. Instream Ice Calibration of Computer Model. Alaska Power Authority Document no. 1122. 111 pp.

Carson, R., Beltaos, S., Groeneveld, J., Healy, D., She, Y., Malenchak, J., Morris, M. Saucet, J. Kolerski, T., Shen, H. T. 2011. Comparative testing of numerical models of river ice jams. Canadian Journal of Civil Engineering, 38(6): 669-678.

Carson, R., Groeneveld, J. L. 1997. Evolution of the ICESIM Model. In: CGU HS Committee on River Ice Processes and the Environment Proc., 9th Workshop on River Ice, September 24-26, 1997, Fredericton, NB, 289-302.

Clark, S., Doering, J. 2006. Laboratory experiments on frazil-size characteristics in a counterrotating flume. Journal of Hydraulic Engineering, 132: 94-101.

Daly, S.F. 1984. Frazil ice dynamics. U.S. Army Cold Regions Research and Engineering Laboratory, Hanover, N. H., 46 pp.

Daly, S.F. 2013. Chapter 4: Frazil Ice. In: Beltaos, S. (ed) River Ice Formation. CGU HS Committee on River Ice Processes and the Environment, 107-134.

Daly, S.F. and Axelson, K.D. 1990. Stability of floating and submerged blocks. Journal of Hydraulic Research 28: 737-752.

DHI, 2021. MIKE 11, A Modelling System for Rivers and Channels, Reference Manual, 500 pp.

Dow Ambtman, K. E., Hicks, F. E., & Steffler, P. M. 2011a. Experimental Investigation of the Pressure Distribution beneath a Floating Ice Block. Journal of Hydraulic Engineering, 137: 399-411.

Dow Ambtman, K. E., Steffler, P. M., & Hicks, F. E. 2011b. Analysis of the Stability of Floating Ice Blocks. Journal of Hydraulic Engineering, 137: 412-422.

Environment Canada, 2013. RIVICE Model - User's Manual. RIVICE Steering Committee, Environment Canada, January 2013, 185 pp.

Ettema, R. Muste, M., Kruger, A. 1999. Ice jams in river confluences. US Army Corps of Engineering, Cold Regions Research and Engineering Laboratory, Report 99-06, 61 pp.

Flato, G. 1988. Calculation of ice jam profiles. Master's Thesis, University of Alberta, Edmonton, Alberta, 177 pp.

Flato, G., Gerard, R. 1986. Calculation of ice jam thickness profiles. Proc., 4th Workshop on Hydraulics of River Ice, Subcommittee of Hydraulics of Ice Covered Rivers, National Research Council of Canada, Montreal, C-3.1-18.

Fread, D.L., Jin, M., Lewis, J. M., 1996. An LPI Numerical Solution for Unsteady Mixed Flow Simulation, North American Water Congress, Anaheim, CA June 22-28, 1996, American Society of Civil Engineers, 1-7.

Garcia-Navarro, M. P., Savirón, J. M. 1992. Numerical simulation of unsteady flow at open channel junctions. Journal of Hydraulic Research, 30(5): 595-609.

Ghareh Aghaji Zare, S., Ansari, S., Rennie, C.D., Seidou, O., Groenveld, R., Ahsan, R., Malenchak, J., Ahmari, H. 2015. Simulation of river ice processes in a regulated ice covered river. In: CGU HS Committee on River Ice Processes and the Environment Proc., 18th Workshop on Hydraulics of Ice Covered Rivers, Quebec City, Quebec.

Gosink, J.P., Osterkamp, T.E. 1983. Measurements and analyses of velocity profiles and frazil ice-crystal rise velocities during periods of frazil-ice formation in rivers. Annals of Glaciology, 4: 79-84.

Healy, D., Hicks, F. 1999. Comparison of ICEJAM and RIVJAM Ice Jam Profile Models. Journal of Cold Regions Engineering, 13(4): 180-198.

Healy, D., Hicks, F.E. 2006. Experimental Study of Ice Jam Formation Dynamics, Journal of Cold Regions Engineering, 30(4): 117-139.

Hicks, F. 2016. An introduction to River Ice Engineering for Civil Engineers and Geoscientists, 159 pp.

Hicks, F.E., Steffler, P.M. 1990. Finite element modeling of open channel now. Water Resources Engineering Report No. 90-6. Department of Civil Engineering, University of Alberta, Edmonton, AB, 356 pp.

Hicks, F.E., Steffler, P.M. 1992. A Characteristic Dissipative Galerkin Scheme for Open Channel Flow. ASCE Journal of Hydraulic Engineering 118: 337-352.

Hicks, F.E., Steffler, P.M., Gerard, R. 1992. Finite element modeling of surges propagation and an application to the Hay River, N.W.T. Canadian Journal of Civil Engineering 19 (3): 454-462.

Huokuna, M. 1990. The Finnish River Ice Research Project – the Numerical River Ice Model in Use. In: Proceedings of 10th IAHR International Symposium on Ice, Espoo, Finland. Volume 3: 215-230.

Jasek, M. 1995. Ice jam simulations in rivers with islands. Proceedings of the 8th Workshop on the Hydraulics of Ice Covered Rivers, Kamloops, BC, 421-441.

Jasek, M., Ghobrial, T., Loewen, M., Hicks, F. 2011. Comparison of CRISSP modeled and SWIPS measured ice concentrations on the Peace River. In: CGU HS Committee on River Ice Processes and the Environment Proc., 16th Workshop on River Ice, September 18-22, 2001, Winnipeg, MB, 249-273.

Judge, D.G., Lavender, S.T., Carson, R.W., Ismail, S. 1997. Headpond Ice Jams – Where Will They Occur? In: CGU HS Committee on River Ice Processes and the Environment Proc., 9th Workshop on River Ice, September 24-26, 1997, Fredericton, N.B, 73-87.

Kerr, D.J., Shen, H.T., Daly, S.F. 2002. Evolution and hydraulic resistance of anchor ice on gravel bed. Cold Regions Science and Technology, 35 (2):101-114.

Lal, A.M. W. and Shen, H. T. 1991. A Mathematical for River Ice Processes, Journal of Hydraulic Engineering, ASCE, 117(7): 851-867.

Larsen, P. 1975. Notes on the stability of floating ice blocks. Proceedings IAHR Third International Symposium on Ice Problems, Hanover, NH, 305-313.

Lindenschmidt, K.E. 2017. RIVICE - A Non-Proprietary, Open-Source, One-Dimensional River-Ice Model. Water, 9(5), 314: 1-15.

Malenchak, J., Clark, S. 2013. Chapter 5: Anchor Ice. In: Beltaos, S. (ed) River Ice Formation. CGU HS Committee on River Ice Processes and the Environment, 135-157.

Marcotte, N., Robert, S. 1986. Elementary mathematical modelling of anchor ice. In: Proceedings of 8th IAHR International Symposium on Ice, Iowa City, Iowa, Iowa Institute of Hydraulic Research, Volume 1: 493-506.

Matousek, V. 1984a. Types of Ice Run and Conditions for their Formation, In: Proceedings of 7th IAHR International Symposium on Ice, Hamburg, Germany. Volume 1: 315-327.

Matousek, V. 1984b. Regularity of the Freezing-up of the Water Surface and Heat Exchange between water body and water surface, In: Proceedings of 7th IAHR International Symposium on Ice, Hamburg, Germany. Volume 1: 187-200.

McFarlane, V., Loewen, M., Hicks, F. 2014. Laboratory measurements of the rise velocity of frazil ice particles. Journal of Cold Regions Science and Technology. 106-107 (2014): 120-130.

McFarlane, V., Loewen, M., Hicks, F. 2015. Measurements of the evolution of frazil ice particle size distributions. Journal of Cold Regions Science and Technology. 120: 45-55.

Michel. B. 1971. Winter regime of rivers and lakes. Cold Regions Science and Engineering Monograph III-B1a. U.S. Army Cold Regions Research and Engineering Lab, Hanover, NH. 131 pp.

Michel, B., Marcotte, N., Fonseca, F., Rivard, G. 1982. Formation of Border Ice in the Ste. Anne River, In: CGU HS Committee on River Ice Processes and the Environment Proc., 2nd Workshop on the Hydraulics of Ice Covered Rivers, 38-61.

Miles, T. 1993. A study of border ice growth on the Burntwood River. M. Sc. Thesis, University of Manitoba, Winnipeg, Canada.

Nafziger, J., She, Y., Hicks, F. 2019. Dynamic river ice processes in a river delta network. Cold Regions Science and Technology, 158: 275-287.

Newbury, R. W. 1968. Nelson River: A study of subarctic river processes. Ph.D. Thesis, Johns Hopkins University, Baltimore, Maryland.

Pan, J., Shen, H.T., Jasek, M. 2020. Anchor ice effects on river hydraulics. Cold Regions Science and Technology, 174 (2020) 103062.

Pariset, E., Hausser, R. 1961. Formation and evolution of ice covers on rivers. Transactions of the Engineering Institute of Canada 5: 41-49.

Pariset, E., Hausser, R., Gagnon, A. 1966. Formation of ice covers and ice jams in rivers. ASCE Journal of the Hydraulics Division 92(HY6): 1-24.

Petryk, S., 1995. Chapter 5: Numerical Modeling. In: Beltaos, S. (ed) River Ice Jams. Water Resources Publication, L.L.C. Colorado, USA.

Petryk, S., Panu, U.S., Kartha, V.C., Clement, F., 1981. Numerical Modeling and Predictability of Ice Regime in Rivers. 6th IAHR International Symposium on Ice, Quebec City, Canada, Volume 1: 426-435.

Potok, A.J., Quinn, F.H. 1979. A Hydraulic Transient Model of the Upper St. Lawrence River for Water Resources Research, Water Resources Bulletin, American Water Resources Association, 15(6): 1538-1555.

Shabayek, S. 2002. Conservation Equations for Subcritical Flow in Open Channel Junctions. PhD. thesis, University of Alberta, Edmonton, AB, 210 pp.

She, Y., Hicks, F. 2006. Modeling ice jam release waves with consideration for ice effects. Journal of Cold Regions Science and Technology 73: 41-49.

She, Y., Hicks, F., Steffler, P., Healy, D. 2009. Constitutive Model for Internal Resistance of Moving Ice Accumulations and Eulerian Implementation for River Ice Jam Formation. Journal of Cold Regions Science and Technology 45: 137-147.

Shen, H.T. 2005. CRISSP1D Version Programmer's Manual. In CEATI Report No. T012700-0401. Department of Civil Engineering, Clarkson University, Potsdam, N.Y.

Shen, H.T. 2006. A one-dimensional comprehensive river ice model. In: Proceedings of the 18th IAHR International Symposium on Ice, Sapporo, Japan, 61-68.

Shen, H.T. 2010. Mathematical modeling of river ice processes. Cold Regions Science and Technology 62: 3-13.

Shen, H.T., Ackermann, N.L. 1980. Wintertime Flow Distribution in River Channels, Journal of the Hydraulics Division, ASCE, 106(HY5): 805-817.

Shen, H.T., Shen, H., Tsai, S.-M. 1990. Dynamic transport of river ice. Journal of Hydraulic Research 28 (6): 659-671.

Shen, H.T., Wang, D.S. 1995. Under Cover Transport and Accumulation of Frazil Granules, Journal of Hydraulic Engineering, ASCE, 121(2): 184-194.

Shen, H.T., Wang, D.S., Lal, A.M. W. 1995. Numerical Simulation of River Ice Processes. Journal of Cold Regions Engineering, ASCE, 9: 107-118.

Sun. Z. C. and Shen, H.T. 1988. A field investigation of frazil ice jam in Yellow River. In: CGU HS Committee on River Ice Processes and the Environment Proc., 5th Workshop River Ice / Ice Jams, Winnipeg, Canada, 157-175.

Theriault, I., Sucet, J.-P., Taha, W. 2010. Validation of the Mike-Ice model simulating river flows in presence of ice and forecast of changes to the ice regime of the

Romaine River due to hydroelectric project. In: Proceedings of the 20th IAHR International Symposium on Ice, Lahti, Finland.

Timalsina, N., Charmasson, J., Alfredsen, K.T. 2013. Simulation of the ice regime in a Norwegian regulated river. Cold Regions Science and Technology, 94: 61-73.

Tsang, G. 1988. Development of mathematical modelling for prediction of river cooling and frazil and anchor ice formation. In: CGU HS Committee on River Ice Processes and the Environment Proc., 5th Workshop River Ice / Ice Jams, Winnipeg, Canada, 393-416.

Turcotte, B., Morse, B. 2013. Ice jam mitigation at the St. Félicien Zoo. In: 17th CGU HS Committee on River Ice Processes and the Environment Proc., 17th Workshop on Hydraulics of Ice Covered Rivers, Edmonton, Alberta, July 21-24, 2013.

Uzuner, M.S. and Kennedy, J.F. 1972. Stability of Floating Ice Blocks. ASCE Journal of the Hydraulics Division 98 (HY12): 2117-2133.

Uzuner, M.S., Kennedy, J.F. 1976. Theoretical Model of River Ice Jams. ASCE Journal of the Hydraulics Division 102 (HY9): 1365-1383.

Wang, D.S., Shen, H.T. 1993. Frazil and anchor ice evolution in rivers. Report 93-09, Department of Civil and Environmental Engineering, Clarkson University, Potsdam, New York.

Wuebben, J.L. 1984. The rise pattern and velocity of frazil ice. In: CGU HS Committee on River Ice Processes and the Environment Proc., 3rd Workshop on the Hydraulics of Ice Covered Rivers, Fredericton, New Brunswick, Canada, 297-316.

Ye, S.Q., Doering, J. 2004. Simulation of the supercooling process and frazil evolution in turbulent flows. Canadian Journal of Civil Engineering, 31: 915-926.

Ye, S.Q., Doering, J., Shen, H.T. 2004. A laboratory study of frazil evolution in a

counter-rotating flume. Canadian Journal of Civil Engineering, 31: 899-914.

# 2.	A comprehensive public-domain river ice process model and its application to a complex natural river

## 2.1	*Introduction*

Most northern rivers experience ice conditions for part or all of winter. River ice can significantly affect a river's regime, and in some cases, plays a larger role in flooding compared to open water conditions. The different types of river ice, and their interaction with moving river water, can affect the regime in a variety of ways. For example, as border ice grows out into the channel, the partial stationary ice cover can increase the channel resistance causing a reduction in flow under the border ice and an increase in flow in the open portion of the river (Tsang, 1970). In supercooled turbulent water, the formation of anchor ice on the river bed can affect the hydraulic resistance of the bed (Kerr et al., 2002), and its release can send waves downstream that produce measurable changes in discharge and water levels (Jasek et al., 2015). As surface ice floes travel downstream, an ice cover may be initiated if the floes come to rest due to a constriction or obstacle in the river. The ice cover progression is highly dependent on the geometry of incoming ice floes and the flow conditions at the leading edge of the ice cover (Pariset and Hausser, 1961). Incoming floes may come to rest edge to edge forming a juxtaposed ice cover when water velocities are low, or they may become unstable and entrained into the flow passing under the leading edge when water velocities are high. Entrained floes may be deposited on the underside of the downstream ice resulting in a 'hydraulically thickened' accumulation, or may be swept downstream and will not contribute to the

upstream progression of the leading edge. The accumulation may collapse and thicken if its internal strength and the resistance at the banks cannot withstand the applied external forces, due to gravity and water drag. This 'mechanical thickening' will continue until a new equilibrium is achieved. As the ice front passes a location, the stage can increase dramatically and rapidly due to the sudden increase in flow resistance from the stationary ice. Once the accumulation is stable, it will freeze into an ice cover. Thickening of the ice cover can occur thermally but it can also thicken when frazil that is generated in upstream open areas is transported and deposited on the underside of the ice cover. This can also lead to the formation of hanging dams. In some cases, hanging dams can become extremely thick, reducing the flow area and increasing the under-ice velocities, which may result in bed scour (Beltaos, 2013).

These regime changes can have implications for engineering structures and aquatic ecology. Frazil ice can accumulate and block the flow to water intakes. In some severe cases, frazil ice blockage can result in collapse of the intake structure (Daly, 1991). Anchor ice can be problematic for hydropower generation. For example, anchor ice formation downstream of Manitoba Hydro's Limestone Generation Station at Sundance Rapids has caused stage increases that have resulted in millions of dollar in lost power generation revenue (Girling and Groenevald, 1999; Malenchak, 2011). Frazil and anchor ice can also affect fish. Brown and Mackay (1995) found that cutthroat trout were excluded from overwintering pools with extensive frazil and anchor ice growth. Brown et al. (2000) reported that common carp and brown trout evacuated a pool where frazil ice had formed a hanging dam. Although freeze-up jams do not normally pose a risk to

flooding since flows are typically much lower in fall and winter compared to those in

spring when breakup jam occurs, they are known to pose problems to hydropower

generation (Beltaos and Prowse, 2001).

River ice processes can be very challenging to study due to the risks and costs associated

with data collection in remote locations, especially under harsh winter conditions.

Numerical models can provide valuable insight into a river's current ice regime where

data are sparse. They can also be indispensable tools for quantifying changes to the

regime due to potential future conditions such as regulation and climate change. Existing

models range from component models, which consider only specific ice processes, to

comprehensive models, developed to simulate the entire river ice regime (Shen, 2010).

Both one-dimensional (1D) and two-dimensional (2D) comprehensive river ice process

models exist, commercially and within the public domain. 2D models provide a better

representation of the variability of river ice processes in complex natural channel

systems. However, they are not typically applied to long reaches or channel networks

because costly field data and lengthy computational time render them operationally

impractical. It can therefore be more practical to model real-world river ice processes

over lengthy reaches using a 1D model. Most existing 1D river ice process models

typically solve unsteady flow equations using implicit finite difference schemes (e.g.

CRISSP1D (Shen, 2006); *MIKE-Ice* (Theriault et al., 2010; Timalsina et al., 2013); and

RIVICE (Lindenschmidt, 2017)) that may become unstable when the flow approaches

critical or for mixed subcritical/supercritical flow situations. In order to prevent model

instabilities in these cases, techniques such as the local partial inertia (LPI) technique

(Fread et al., 1996) are applied to the finite difference solution to suppress the inertial terms in the Saint-Venant equations so that the solution is reduced to the more stable but less accurate diffusive wave description. These types of flow regime transitions are commonly encountered when modelling long reaches of natural rivers due to the presence of rapids, waterfalls and steep canyons. For example, the Athabasca River upstream of Fort McMurray, AB, is characterized by numerous rapids that instigate dynamic breakup and a cascade of ice jam events almost yearly (Hutchison and Hicks, 2007). The upper reach of the Hay River, NWT, contains two major waterfalls and a very steep gorge section. Ice jams often occur in this section and their release ultimately result in the ice run causing peak water level and possible flooding in the Town of Hay River (Kovachis, 2011). The rapids in the Devils Canyon on the Susitna River, Alaska, periodically jam in winter but the jams typically fail and the channel remains open at these locations and they continue to produce frazil throughout winter (HDR, 2014). Furthermore, calibration and validation of the existing models were conducted towards various elements such as water levels, flows, water temperatures, ice front locations, surface ice conditions, and border ice extent, but not all of them (e.g. Timalsina et al., 2013; Thériault et al., 2010; Malenchak, 2011; Andrishak and Hicks, 2008). Without a comprehensive range of data metrics, it is difficult to correctly evaluate a given model's performance. For example, more than one combination of model parameters may create the same ice cover advancement rates, but simulated ice cover thicknesses could be drastically different for each combination of parameters.

The ultimate goal of this research is to develop a highly robust 1D comprehensive river ice process model that is capable of simulating dynamic ice processes in natural river systems with complex ice and flow regimes, and that is also available in the public domain. This paper presents new developments to the University of Alberta's public-domain river ice process model, *River1D*. The enhancements over the previous versions of the model are first described. An overview of the model's governing equations and solution procedure is then provided, followed by its application to the Susitna River in Alaska to demonstrate its new capabilities in a complex natural river system. The model results agreed favourably with observations of water levels, flows, water temperatures, surface ice concentrations, border ice widths, ice cover progression rates, as well as ice thicknesses.

2.2   Model Description

The new river ice process model is built on the University of Alberta's public-domain software *River1D*. The model was originally developed as an open water hydrodynamic model, solving the Saint-Venant equation using the characteristic-dissipative-Galerkin (CDG) finite element scheme (Hicks and Steffler, 1990, 1992). This method conserves both mass and momentum perfectly (Hicks and Steffler, 1992) and it has been proven to be consistently more stable and accurate than other schemes (finite element and implicit finite difference) particularly when modelling extreme dynamic events (Hicks et al., 1992). Previous versions of the model were adapted to include several thermal (water cooling, frazil formation and rise, and ice cover formation) and dynamic (ice jam

formation and release) ice processes (Andrishak and Hicks, 2005 and 2008; She et al., 2009). However for these previous versions, the model application was limited to rectangular cross section geometry and site-specific ice components. In order to better simulate river ice processes in complex natural river systems, the *River1D* model was reformulated to accommodate natural channel geometry. The ice processes considered in this new natural channel geometry version of the model follow those of Andrishak and Hicks (2008) with enhancements to include water supercooling, frazil accretion, frazil re-entrainment, anchor ice formation and release, border ice formation, and under-cover transport of frazil. Additionally, ice cover formation leading edge stability criteria were implemented to simulate the ice cover progression. This accounts for the dynamic processes (i.e. hydraulic and mechanical thickening) that reduce the rate of ice cover advancement, which were modelled empirically in previous versions (Andrishak and Hicks, 2005 and 2008).

2.2.1 Hydrodynamic Equations

Accounting for the presence of a floating ice cover and anchor ice on the river bed, the conservation equation for water flow under and through the ice is:

$$\frac{\partial A}{\partial t} + \frac{\partial Q_w}{\partial x} = \frac{\rho_i}{\rho_w}\frac{\partial A_i}{\partial t} + (1 - p_a)\frac{\partial A_{an}}{\partial t} \qquad [2.1]$$

where A is the cross sectional area to the water surface; Q_w is discharge of water under and through the ice; A_i is the cross sectional area of the surface ice including border ice

and under-cover moving frazil; A_{an} is the cross sectional area of the anchor ice; ρ_i and ρ_w are the densities of the ice and water, respectively; p_a is the porosity of the anchor ice; t represents time; and x represents the streamwise path of the river.

The momentum equation of the water flow under and through the ice is:

$$\frac{\partial Q_w}{\partial t} + \frac{\partial(\beta Q_w U_w)}{\partial x} + gA_w \frac{\partial H}{\partial x} + gA_w S_f = 0 \qquad [2.2]$$

where A_w is the flow cross sectional area; U_w is the average flow velocity (Q_w / A_w); H is the water surface elevation above a specified datum; β is the momentum flux correction coefficient calculated based on Fread (1988); and S_f is the boundary friction slope. The flow cross sectional area is related the cross sectional area to the water surface through:

$$A = A_w + \frac{\rho_i}{\rho_w} A_i + (1 - p_a)A_{an} \qquad [2.3]$$

The friction slope is evaluated using Manning's equation. When a stationary ice cover is present, the composite Manning's roughness coefficient, n_c, is calculated from the general form of the Sabaneev equation (Uzuner, 1975):

$$n_c = n_b \left(\frac{1 + \frac{P_i}{P_b}\left(\frac{n_i}{n_b}\right)^{3/2}}{1 + \frac{P_i}{P_b}} \right)^{2/3} \qquad [2.4]$$

where n_b and n_i are the Manning's roughness coefficients for the bed and surface ice layer, respectively; and P_b and P_i are the bed-affected and ice-affected wetted perimeters

of the channel, respectively. The Manning's roughness coefficient for the surface ice

layer can either be user specified or it can be calculated as a function of thickness based

on coefficients of Manning's roughness of the under surface of frozen slush ice obtained

by Nezhikovskiy (1964). If ice roughness is calculated, the user must specify the type of

ice and roughness is interpolated based on the simulated ice thickness according to

Nezhikovskiy's roughness coefficients for slush-ice cover formed principally 'from loose

slush', 'from dense (frozen) slush', or 'from ice'.

2.2.2 Ice Equations

The newly enhanced *River1D* model considers water cooling and supercooling, frazil ice

formation, frazil rise and re-entrainment, border ice growth and decay, surface ice

transport, thermal ice growth and decay, anchor ice evolution, under-cover transport of

frazil, and ice cover progression based on leading edge stability criteria. All transport

equations are solved using the Streamline Upwind Petrov-Galerkin finite element method

(Brooks and Hughes, 1982). Figure 2.1 illustrates the vertical ice processes considered in

the model.

2.2.2.1 Water Cooling and Supercooling

Water temperature is simulated by considering the conservation of thermal energy of the

water and the suspended frazil ice (ice-water mixture) following Shen (2010):

$$\frac{\partial\left(A_w e_{wi}\right)}{\partial t}+\frac{\partial\left(Q_w e_{wi}\right)}{\partial x}=-\underbrace{\frac{B_o\left(1-C_i\right)}{\rho_w}\phi_{wa}}_{\substack{\text{net heat exchange}\\ \text{between water}\\ \text{and air}}}-\underbrace{\frac{\left(B_o C_i+f_b B_{ws}\right)}{\rho_w}\phi_{ia}}_{\substack{\text{net heat exchange}\\ \text{between water and air}\\ \text{through the ice cover}\\ \text{air when } T_w>0\ ^\circ\text{C}\\ \text{and } T_a<0\ ^\circ\text{C}}}$$

$$-\underbrace{\frac{\left(B_o C_i+P_b C_{an}+f_b B_{ws}\right)}{\rho_w}\phi_{wi}}_{\substack{\text{net heat exchange}\\ \text{between water}\\ \text{and ice}}}+\underbrace{B_o\frac{\rho_i}{\rho_w}L_i\eta C_f}_{\substack{\text{frazil rise}\\ \text{when } T_w<0\ ^\circ\text{C}}}+\underbrace{P_b C_{an}\frac{\rho_i}{\rho_w}L_i\gamma C_f}_{\substack{\text{frazil accretion to}\\ \text{bed when } T_w<0\ ^\circ\text{C}}} \qquad [2.5]$$

$$-\underbrace{B_o C_i\frac{\rho_i}{\rho_w}L_i\beta_{re}\left(t_{si}+t_{fs}\left(1-p_f\right)\right)}_{\substack{\text{re-entrainment of surface ice}\\ \text{to suspended frazil layer}\\ \text{when } U_i>U_{i\_re}\text{ and } U_i>0}}-\underbrace{B_o C_i\frac{\rho_i}{\rho_w}L_i\beta_{re}\left(t_{ui}\left(1-p_f\right)\right)}_{\substack{\text{re-entrainment of under-cover}\\ \text{moving frazil to suspended frazil layer}\\ \text{when } U_w>U_{i\_re}\text{ and } U_i=0}}$$

where e_{wi} is the thermal energy per unit mass of the ice-water mixture ($e_{wi} = C_p(1-C_f)T_w - \rho_i\,C_f\,L_i/\rho_w$); C_p is the specific heat of water; T_w is the water temperature; C_f is the volumetric concentration of suspended frazil ice; L_i is the latent heat of ice (set to 334 kJ/kg); B_{ws} is the total width of the channel at the water surface for the main channel excluding any overbank flow; f_b is the fraction of the main channel covered by border ice; B_o is the width of the water surface not covered by border ice, $B_o = (1-f_b)B_{ws}$; C_i is the surface ice concentration; C_{an} is the fraction of the bed covered by anchor ice (user specified); ϕ_{wa}, ϕ_{ia}, ϕ_{wi} are the net rates of heat exchange per unit surface area between water and air, between water and air through the floating ice layer, and between water and ice, respectively, all quantified based on Andrishak and Hicks (2008); η is the rate of frazil rise (user specified); γ is the rate of frazil ice accretion to the bed (user specified); β_{re} is the rate of surface ice re-entrainment (user specified) that will occur when the ice velocity, U_i, is greater than the ice velocity threshold for re-entrainment, U_{i_re}; t_{si} is the

thickness of the solid ice layer; t_{fs} is the thickness of the frazil slush layer; p_f is the frazil

slush porosity; and t_{ui} is the thickness of the under-cover moving frazil layer. Heat

exchange between the water and air uses the linear heat transfer approach to approximate

the energy budget equation (Andrishak and Hicks, 2008):

$$\phi_{wa} = -\phi_s + h_{wa}\left(T_w - T_a\right) - j_{wa}T_a + k_{wa} \qquad [2.6]$$

where ϕ_s is the net incoming solar radiation; h_{wa} and j_{wa} are linear heat transfer

coefficients; k_{wa} is a linear heat transfer constant; and T_a is the air temperature.

2.2.2.2 Suspended Frazil Production and Transport

Once the water becomes supercooled, frazil ice will form in the water column. The

concentration of suspended frazil ice changes with the thermal growth and decay of frazil

ice in the water column and mass transfer between the surface ice, under-cover moving

frazil, and anchor ice layers:

$$
\begin{aligned}
\frac{\partial\left(A_w C_f\right)}{\partial t} + \frac{\partial\left(Q_w C_f\right)}{\partial x} &= \underbrace{\frac{\phi_{fw}}{\rho_i L_i}}_{\substack{\text{growth and}\\\text{decay}}} - \underbrace{B_o \eta C_f}_{\text{frazil rise}} - \underbrace{P_b C_{an} \gamma C_f}_{\substack{\text{frazil accretion}\\\text{to bed}}} \\
&+ \underbrace{B_o C_i \beta_{re}\left(t_{si} + t_{fs}\left(1 - p_f\right)\right)}_{\substack{\text{re-entrainment of surface ice}\\\text{to suspended frazil layer}\\\text{when } U_i > U_{i\_re} \text{ and } U_i > 0}} + \underbrace{B_o C_i \beta_{re}\left(t_{ui}\left(1 - p_f\right)\right)}_{\substack{\text{re-entrainment of under-cover}\\\text{moving frazil to suspended frazil}\\\text{layer when } U_w > U_{i\_re} \text{ and } U_i = 0}}
\end{aligned}
\qquad [2.7]
$$

where ϕ_{fw} is the net rate of heat exchange per unit surface area between suspended frazil

particles and water and is evaluated in a similar manner to Shen et al. (1995):

55

$$\phi_{fw} = -\frac{2N_u^f K_w}{d_e r_o}\left(C_f + C_{fo}\right)A_w T_w \qquad [2.8]$$

where N_u^f is the Nusselt number of a suspended frazil particle; K_w is the thermal conductivity of water; d_e is the typical frazil particle thickness; r_o is the typical frazil particle radius; and C_{fo} is the frazil seeding concentration. Except for K_w, set to 0.566 W/m/°C (Shen, 2016), all parameters are user specified.

2.2.2.3 Border Ice Formation

The model simulates border ice growth from both static and dynamic processes. Static border ice is assumed to develop in the form of skim ice when the following criteria, based on Matousek (1984a), are satisfied: $T_w < 0°C$; $T_a < 0°C$; and $U_{wl}/U_{cr} < 0.167$ where U_{wl} is the local depth-averaged water velocity in the open water adjacent to the edge of the border ice; and U_{cr} is the maximum water velocity for border ice accretion. The model considers lateral accretion of border ice using the following equation:

$$\frac{dB_b}{dt} = aC_i^b\left(\frac{U_{wl}}{U_{cr}}\right)^d \frac{\phi_{wa}}{\rho_i L_i} + e\frac{\phi_{DDF}}{\rho_i L_i} \qquad [2.9]$$

where B_b is the border ice width from a given bank; ϕ_{DDF} is the rate of heat loss based on the degree-days of freezing; and a, b, d, and e are user defined coefficients. The first term is based on the empirical dynamic border ice model developed by Michel et al. (1982). This term is only active when $0.167 < U_{wl}/U_{cr} < 1.0$ and $C_i > 0.1$. The second term was introduced to account for border ice growth that is not accounted by dynamic

border ice formation (first term) and skim ice formation and is fashioned after the simple

degree-day equation for border ice growth developed by Haresign et al. (2011). Since the

first term requires the calibration of three parameters (*a, b, and d*), which may not be

practical, the second term also offers the user a simpler model for border ice growth that

only requires the calibration of one parameter (*e*). Equation [2.9] is evaluated at both the

left (B_{bl}) and right (B_{br}) banks to obtain the total border ice width for a given cross section

(B_{btotal}). The local depth-averaged water velocity, U_{wl}, is estimated using the following

relationship:

$$U_{wl} = U_w \left(\frac{D_{wl}}{D_w} \right)^{2/3} \qquad\qquad [2.10]$$

where D_{wl} is the local water depth at the edge of the border ice; D_w ($=A_w/T$) is the mean

hydraulic depth of the water; and T is the total width of the channel.

In Clark (2013), border ice is described as "a wedge-shaped ice sheet extending from the

shoreline, with the thickest portion closest to the shore and the thinnest portion actively

growing laterally" as shown in Figure 2.1. This description has directed the approach

used to simulate the border ice thickness, t_b, and cross sectional area, A_b, in the model.

The rate of growth and decay of border ice thickness, t_b, is modelled using the following

equation:

$$\frac{dt_b}{dt} = \frac{-h_{wa}T_a - \phi_s}{\underbrace{\rho_i L_i \left(1 + \dfrac{h_{wa}t_b}{K_i}\right)}_{\text{growth and decay}}} - \underbrace{\frac{\phi_{wi}}{\rho_i L_i}}_{\text{decay}}$$ [2.11]

where K_i is the thermal conductivity of ice. The border ice thickness calculation begins

once the border ice starts to grow laterally and represents the border ice thickness at each

bank. It is assumed that the thickness reduces to zero at the border ice edge protruding

into the channel. The average of these two thicknesses ($t_b/2$) is used to estimate the cross

sectional area of the border ice:

$$A_b = \frac{B_{btotal}t_b}{2}$$ [2.12]

2.2.2.4 Anchor Ice Formation and Release

The rate of change of anchor ice thickness due to frazil accretion and thermal growth and

decay at a given cross section is defined by (Shen, 2010):

$$\frac{dt_{an}}{dt} = \underbrace{\frac{\gamma C_f}{(1-p_a)}}_{\substack{\text{growth due to accretion} \\ \text{when Tw} < 0°C}} - \underbrace{\frac{\phi_{wi}}{\rho_i(1-p_a)L_i}}_{\text{thermal growth and decay}}$$ [2.13]

The cross sectional area occupied by the anchor ice is defined by:

$$A_{an} = C_{an}P_b t_{an}$$ [2.14]

58

Anchor ice release is a very important but complicated process that can occur due to mechanical and thermal processes (Malenchak, 2011). In the enhanced version of the *River1D* model, anchor ice release occurs if either the water temperature rises above zero (denoted as condition 1), or if the buoyancy forces of the anchor ice exceed the gravitational forces on the anchor ice (denoted as condition 2). Assuming tightly packed bed material based on a hexagonal close packing arrangement and negligible anchor ice growth down into the bed material pore space, condition 2 can be expressed as:

$$t_{an} > \frac{\pi}{3\sqrt{3}} \frac{d_s(\rho_s - \rho_w)}{(1-p_a)(\rho_w - \rho_i)} \tag{2.15}$$

where d_s and ρ_s are the average diameter and density of the bed material, respectively (both user specified).

2.2.2.5 Surface Ice Evolution and Transport

The surface ice in the model is defined by solid and frazil slush layers, assumed to travel at velocity U_i until the layers come to rest to form a stationary ice cover or accumulation. The variation in the surface ice concentration along the channel is described by:

$$\frac{\partial \left(B_o C_i \right)}{\partial t} + \frac{\partial \left(U_i B_o C_i \right)}{\partial x} = \underbrace{\frac{B_o \left(1 - C_i \right) \eta C_f}{t'_f \left(1 - p_f \right)}}_{\text{frazil rise}} + \underbrace{\frac{B_o \left(1 - C_i \right) \phi_{wa}}{t'_{si} \, \rho_i L_i}}_{\substack{\text{freezing between ice} \\ \text{pans once ice has stopped} \\ \text{when } U_i = 0 \text{ and } T_a < 0}}$$

$$+ \underbrace{\frac{\left(1 - C_i \right) S_{ui}}{\left(1 - p_f \right) t_{ui}}}_{\substack{\text{transfer from} \\ \text{under-cover moving} \\ \text{frazil layer}} } - \underbrace{B_o \beta_{re} C_i}_{\substack{\text{re-entrainment} \\ \text{of surface ice} \\ \text{when } U_i > U_{i\_re}}}$$

$$[2.16]$$

Where t'_f is the thickness of new frazil pans; t'_{si} is the initial thickness of newly formed solid ice between the ice pans once the ice has stopped moving; and S_{ui} is a source term representing the exchange between the under-cover moving (A_{ui}) and stationary (A_{fs}) frazil layers.

The conservation of mass equation for the frazil slush layer is described by:

$$\frac{\partial A_{fs}}{\partial t} + \frac{\partial U_i A_{fs}}{\partial x} = \underbrace{\frac{B_o \eta C_f}{\left(1 - p_f \right)}}_{\substack{\text{frazil rise} \\ \text{when } U_i > 0}} - \underbrace{\frac{B_o C_i \phi_{ia}}{\rho_w p_f L_i}}_{\substack{\text{pore water} \\ \text{freezing when} \\ A_{fs} > 0 \text{ and} \\ T_a < T_w \leq 0 \text{ °C}}} - \underbrace{\frac{B_o C_i \phi_{wi}}{\rho_i \left(1 - p_f \right) L_i}}_{\substack{\text{decay at} \\ \text{water-ice interface} \\ \text{when } A_{fs} > 0 \\ \text{and} T_w > 0 \text{ °C}}}$$

$$- \underbrace{B_o C_i \beta_{re} t_{fs}}_{\substack{\text{re-entrainment} \\ \text{of surface ice} \\ \text{when } U_i > U_{i\_re} \\ \text{and when } U_i > 0}} + \underbrace{\frac{S_{ui}}{\left(1 - p_f \right)}}_{\substack{\text{transfer from} \\ \text{under-cover} \\ \text{moving} \\ \text{frazil layer}}}$$

$$[2.17]$$

where A_{fs} is the cross sectional area of the frazil slush layer ($A_{fs} = B_o C_i t_{fs}$).

For the solid ice layer, the mass conservation equation is expressed as:

60

$$\frac{\partial A_{si}}{\partial t} + \frac{\partial U_i A_{si}}{\partial x} = f_1 \underbrace{\frac{B_o C_i \phi_{ia}}{\rho_i L_i}}_{\text{growth and decay}} - \underbrace{\frac{B_o C_i \phi_{wi}}{\rho_i L_i}}_{\substack{\text{growth and} \\ \text{decay at} \\ \text{water-ice interface} \\ \text{when } A_{fs} = 0}}$$

$$+ \underbrace{\frac{B_o(1-C_i)\phi_{wa}}{\rho_i L_i}}_{\substack{\text{freezing between ice pans} \\ \text{once ice has stopped} \\ \text{when } U_i = 0 \text{ and } T_a < 0}} - \underbrace{B_o C_i \beta_{re} t_{si}}_{\substack{\text{re-entrainment} \\ \text{of surface ice} \\ \text{when } U_i > U_{i\_re} \\ \text{and when } U_i > 0}}$$

[2.18]

where A_{si} is the cross sectional area of the solid ice layer ($A_{si} = B_o C_i t_{si}$) and f_1 is a

conditional constant that is defined as follows.

$$f_1 = \begin{cases} 1 & \text{when } \phi_{ia} < 0,\, A_{si} > 0,\, \text{and } T_a > 0\,°\text{C} \\ & \text{(melting of solid ice)} \\ 1 & \text{when } \phi_{ia} > 0,\, A_{fs} = 0,\, \text{and } T_w \leq 0\,°\text{C} \\ & \text{(freezing of water column)} \\ \rho_i(1-p_f)/\rho_w p_f + 1 & \text{when } \phi_{ia} > 0,\, A_{fs} > 0 \text{ and } T_w \leq 0\,°\text{C} \\ & \text{(freezing of pore water)} \\ 0 & \text{otherwise} \end{cases}$$

[2.19]

The border ice, under-cover moving frazil ice, and surface ice are related through:

$$A_i = A_{si} + (1 - p_f)(A_{fs} + A_{ui}) + A_b$$

[2.20]

2.2.2.6 Ice Cover Progression

Ice cover formation is assumed to occur based on a single bridging location that is user

specified. Once bridging occurs, incoming ice will accumulate to form a stationary ice

cover in the upstream direction either by floe juxtaposition, hydraulic thickening, or

mechanical thickening based on the Froude number immediately upstream of the leading

edge, F_r, defined as $U_w / \sqrt{gY}$. The ice front location, X_i, is tracked using the following

equation (Uzuner and Kennedy, 1976):

$$X_i^{t+\Delta t} = X_i^t - \frac{C_i\left(t_{si} + (1-p_f)t_{fs}\right)U_i\Delta t}{t_{le}(1-p_j) - C_i\left(t_{si} + (1-p_f)t_{fs}\right)} \qquad [2.21]$$

where t and $t+\Delta t$ are the model times corresponding to the ice front location; Δt is the

simulation time step; t_{le} and p_j are the thickness and porosity of the ice accumulation,

respectively, that are expected once the ice cover forms. The location of the ice front,

also called the leading edge, is used to specify the velocity of the ice in the model, as

shown in Figure 2.2.

Upstream of the leading edge, the surface ice (frazil slush and solid ice layers) is assumed

to travel at the speed of the water ($U_i = U_w$). Downstream of the leading edge, the surface

ice is assumed to be stationary ($U_i = 0$) and the under-cover frazil transport layer is

assumed to travel at the speed of the water ($U_{ui} = U_w$). Estimates for t_{le} are dependent on

the ice cover progression mode as described in Shen (2016). Specifically, when F_r is less

than the user specified maximum Froude number for juxtaposition, F_{r_jux}, the ice cover

progresses upstream in juxtaposed mode, and the value of t_{le} is set to the thickness of the

incoming ice floes ($t_{si} + t_{fs}$). Whereas, when the Froude number is between F_{r_jux} and the

maximum Froude number for ice cover advancement, F_{r_max}, the ice cover will progress

upstream in either hydraulic thickening or mechanical thickening mode. Values of t_{le} are

calculated using narrow ice jam and equilibrium ice jam theory (Pariset and Hausser,

1961; Pariset et al., 1966); the governing theory is determined by the one that produces the larger value of t_{le}. The equilibrium ice jam equation requires values be input for μ, a composite jam stress parameter (involving internal friction properties and porosity of the ice accumulation), and τ_c, the ice cohesion. The porosity of the ice accumulation is estimated using (Shen, 2016):

$$p_j = p_c + (1 - p_c)\left(\frac{p_f t_{fs}}{t_{si} + t_{fs}}\right) \tag{2.22}$$

where p_c represents the space between the ice floes in the newly formed ice cover.

In the model, the surface ice and under-cover transport layers are confined to the width of the channel between the border ice. Since frazil does not accumulate below the border ice, the flow may never stage up to the level that it would in nature to allow the Froude number to drop below $Fr_{\_max}$ and simulated ice cover advance rates may be slowed or stalled compared to observed rates.

2.2.2.7 Under-cover Transport of Frazil

Transport of frazil along the underside of the stationary ice cover is defined by:

$$\frac{\partial A_{ui}}{\partial t} + \frac{\partial U_{ui} A_{ui}}{\partial x} = \underbrace{\frac{B_o \eta C_f}{(1 - p_f)}}_{\substack{\text{frazil rise} \\ \text{when } U_i = 0}} - \underbrace{B_o C_i \beta_{re} t_{ui}}_{\substack{\text{re-entrainment} \\ \text{of under-cover moving} \\ \text{frazil when } U_{ui} > U_{i\_re} \\ \text{and when } U_i = 0}} - \underbrace{\frac{S_{ui}}{(1 - p_f)}}_{\substack{\text{transfer to} \\ \text{frazil slush} \\ \text{layer}}} \tag{2.23}$$

where $A_{ui} = B_o C_i t_{ui}$ is the cross sectional area of the under-cover moving frazil layer; and U_{ui} is the velocity of this layer. In discrete form, the source term, S_{ui}, which represents the

rate of transfer between the undercover and stationary frazil slush layers, is evaluated as follows:

$$S_{ui} = \frac{Q_{uit} - Q_{uic}}{L} \qquad [2.24]$$

where L is the length of the ice cover between computational nodes (approximated in the model by the streamwise discretization); Q_{uit} is the total under-cover ice discharge ($A_{ui}U_{ui}(1\text{-}p_f) + A_wC_fU_w$); and Q_{uic} is the ice transport capacity which follows Shen and Wang (1995):

$$Q_{uic} = 5.487 F d_f B_o \sqrt{g d_f \left(\frac{\rho_w - \rho_i}{\rho_w} \right)} (\Theta - \Theta_c)^{1.5} \quad \text{when } \Theta \geq \Theta_c \qquad [2.25]$$

and the dimensionless flow strength, Θ, is:

$$\Theta = \frac{\tau_i}{F^2 g d_f (\rho_w - \rho_i)} \qquad [2.26]$$

where τ_i is the shear stress on the underside of the stationary frazil slush and solid ice layers; F is the frazil particle shape factor; and d_f is the average diameter of frazil granules in the under-cover transport layer. When Θ is less than the critical flow strength, Θ_c, there is no under-cover frazil transport ($Q_{uic} = 0$).

2.3   *Model Application*

2.3.1   Study Site and Available Data

The newly enhanced *River1D* ice process model was applied to the Susitna River, located in south-central Alaska. The Susitna River, shown in Figure 2.3, stretches 504 km from its headwaters at the Susitna Glacier, in the Alaska Range to the Cook Inlet in the Gulf of Alaska with a drainage area of 51,800 km^2 and an average discharge at the mouth of 1444 m^3/s (Kammerer, 1990). The model study reach extends from the location of the proposed Susitna-Watana Dam site down to the confluence with the Yetna River, a length of approximately 241 km. The study reach was categorized into seven subreaches based on channel geomorphology (e.g. planform pattern, channel slope, and roughness features) as shown in Figure 2.4. Stationing is measured starting from the model upstream boundary at the location of the proposed dam.

All data for this modelling study were made available by HDR Alaska, Inc. (HDR) as part of the Alaska Energy Authority's (AEA) license application for the Susitna-Watana Hydroelectric Project (Project). For the Project, a total of 246 cross sections were surveyed along the study reach. Cross sections were interpolated with a maximum spacing between sections of 322 m for a total of 875 modelled cross sections.

Inflows to the study reach were provided at five locations along the study reach: one inflow boundary and four lateral inflow boundaries (Figure 2.4). Two of the lateral inflows were provided to account for ungauged tributaries entering the study reach (Ungauged 1 and Ungauged 2) while the other two were to account for the inflows from

the Chulitna and Talkeetna Rivers. Gauge data (water levels and flows) at Susitna River at Gold Creek (USGS 15292000) and Susitna River near Sunshine (USGS 15292780) were provided for comparison with model results. Continuous water level, water temperature, and air temperature data were available at nine Project stations along the study reach, labelled with the prefix ESS (Alaska Energy Authority station on the Susitna River for Surface water). Water temperatures at the five inflow boundaries were provided by HDR and were also available at USGS 15292780 for comparison with model results. Net incoming solar radiation data were available at two ESM (Environmental Susitna Monitoring) stations: ESM1 and ESM3. However, due to potential data quality and orographic effects at ESM3, only the data from ESM1 was used in the modelling. USGS, ESS, and ESM station locations are shown in Figure 2.4. Air temperature data at the ESS stations were applied to each cross section in the model based on the nearest station to the cross section. The net solar radiation from ESM1 was applied to all cross sections. Ice data for model freeze-up calibration and validation included incoming surface frazil at the upstream boundary (estimated from hourly photos taken at ESS70); ice cover progression from the time of bridging onward; and winter ice thickness, water level and discharge data at a few selected cross sections. The data also included observations of surface ice concentration, border ice widths, and anchor ice areal coverage, all obtained from aerial photos, aerial video, or from remote cameras installed at a number of the ESS stations. No water level data were available at the downstream boundary. For this reason a constant water level was assumed at this boundary for both open water and ice covered conditions. A value of 13.7 m was selected to ensure

66

minimal backwater effects based on a sensitivity analysis (13.7 ± 1.5 m only affects the water levels within the last 19 km of the model domain which is more than 64 km downstream of the most downstream gauge, USGS 15292780, used in the model calibration and validation).

2.3.2   Open Water Calibration and Validation

The model was calibrated and validated for six open water events in 2012 and 2013. Model calibration was completed by adjusting the main channel roughness values within each of the seven subreaches. Calibrated Manning's roughness values range from 0.025 in the braided reach to 0.050 in the canyon (known as the Devils Canyon). Floodplain roughness values were set based on engineering judgement by HDR with a value of 0.15 at most cross sections. For open water, a calibration tolerance of 0.3048 m (1 foot) was selected by taking into account the magnitude of potential errors in measuring water levels on a river of this size and type (e.g. wave effects, instrument error, and survey error) as well as two dimensional effects (such as flow super-elevation).

At the two USGS stations, the model results showed good agreement with the observed flows with a Nash-Sutcliffe model efficiency (Nash and Sutcliffe, 1970) of no less than 0.96 for all events. For the events, the mean absolute errors in the water levels are less or equal to the 0.3048 m tolerance at all stations except at ESS35 where it is above this tolerance for one event (0.46 m). Since this station is immediately downstream of the confluence with the Chulitna River, where the flow is likely very two-dimensional in nature, the model is not expected to perform particularly well at this location. Figure 2.5

shows simulated and observed results at the USGS stations for one of the events. Water

levels are reported in metres above sea level (m, a.s.l.).

2.3.3 Freeze-up Calibration and Validation

Data collected during the 2012-2013 freeze-up period were used for model calibration;

the 2013-2014 data set was used for model validation. Calibration of the model ice

parameters was performed in steps. The first step was to calibrate the parameters that

control the water temperature. These parameters include the heat transfer coefficients in

the heat exchange between the water and air, ϕ_{wa} (Equation [2.6]). For the heat transfer

coefficient, h_{wa}, a value of 20 W/m²/°C was found to be the most appropriate. Figure 2.6

provides a comparison between the modelled and observed water temperature at ESS50

and USGS 15292780 for the calibration period. The same stations are compared for the

validation period in Figure 2.7. Although the linear heat transfer model has additional

parameters (i.e. j_{wa}, k_{wa}), they were set to zero as it was found that the modelled

temperature corresponded well to the observed using only h_{wa} and the net incoming solar

radiation, ϕ_s. For both the calibration and validation period, the model was able to

simulate both the variation in the water temperature through the cool down period and

also the point in time when the water reached (and generally stayed at) zero degrees,

demarking the start of the freeze-up. The differences between the simulated and

observed values at USGS 15292780 that occur after October but before the water drops to

zero may be the result of assumptions that were made in order to fill gaps in the data

needed for model inputs. Because water temperature data were not available for the

Chulitna and Talkeetna Rivers, input values at these two inflow boundaries were assumed

68

to be equal to the water temperatures at ESS35. Additionally, input air temperature data collected at ESS30 were used to represent the air temperatures for the last 100 km of the domain. Lastly, net incoming solar radiation was only available at the upstream end of the domain at ESM1 which is approximately 100 km away from USGS 15292780. Because of the orographic effect of the mountainous terrain, the differences between the assumed and actual values for any of these model inputs could be significant and negatively impact the simulated water temperatures.

The next step was to calibrate the ice modelling parameters that relate to the river ice but prior to the formation of a stationary ice cover (e.g. frazil, anchor and border ice). Where available, collected data were used to directly set parameters; otherwise, the values were adjusted so that simulated values best matched observed ones using the range of values found in the literature as guidance. Table 2.1 summarizes the adopted values for the ice modelling parameters for the freeze-up simulations.

In order to properly calibrate the frazil formation component of the model, data quantifying the amount of frazil in the river is needed. Since only areal ice coverages were collected during freeze-up (no thicknesses), it was difficult to calibrate the ice production in the model. For this reason, the frazil production parameters (C_{fo}, d_e, r_o, N_{uf}) were taken from values in the literature (see Table 2.1). The thickness of newly formed ice pans, t'_f, was set based on the average thickness of incoming frazil pans at the upstream boundary during the 2012 freeze-up period, 0.2 m. The rate of frazil rise, η, was adjusted so that modelled surface ice concentrations matched reasonably well with the observed. Figure 2.8 shows a comparison of observed surface ice concentrations with

simulated values for late November for both the calibration (2012) and validation (2013) events. Although there is significant variability between the observed and simulated ice concentrations, the simulated values are generally similar to the observed ones in terms of magnitude. The average simulated surface ice concentration on November 28th, 2012 for the first 95 km of the domain (upstream of the simulated ice front) is 37%, while the observed average for the same reach on that day is 40%. Similarly, the average simulated surface ice concentration on November 29th, 2013 is 40% upstream of the simulated ice front (first 109 km) and the observed average is 66%. The validation data do not agree as well; however, there were fewer data points to calculate the average for 2013 compared to 2012. Additionally, variability between the observed and simulated concentrations may be due in part to model results being output at a specific point in time whereas the observed ice concentrations were recorded at various times through the day.

It was noticed that the model underestimated the border ice widths when only the skim and dynamic border ice components were simulated and parameters in the dynamic component (i.e. a, b, d, and U_{cr}) were set based on the values in Michel et al. (1982). Rather than adjusting the parameters in the dynamic border ice component of the border ice model, in order to simulate the widths that were in better agreement with the observed ones, the parameter e was adjusted until the simulated and observed values matched reasonably well. The maximum fraction of the channel that can be occupied by border ice, f_{bmax}, was set to 0.7. This was set to prevent the channel from completely closing at any section upstream of the ice front, since the model can presently only accommodate bridging at a single location. Figure 2.9 shows simulated and observed total border ice

widths in early December for both the calibration and validation events. For the calibration event, where border ice widths were reported at most cross sections upstream of Talkeetna (km 139), the model did quite a good job of capturing the variability in the data. For example, the observed and simulated values are both generally around or below 50 m in the reach between km 35 and km 52. Unfortunately, the same level of detail was not available for the validation border ice data but the reported values do show the same trend of around 50 m or less compared to the simulated values for the same reach.

Data for the anchor ice component included areal coverages and bed material sizes. The fraction of the channel that gets covered by anchor ice in the model, C_{an}, was calculated based on anchor ice widths observed during the 2012 freeze-up period. These widths were converted to a percent coverage and the average was taken. The percent coverage values collected in the first 140 km of the domain between October and December 2012 are presented in Figure 2.10. The figure illustrates the significant presence of anchor ice in the river during the freeze-up process and the need to include this process in the model. The bed material average diameter, d_s, in the anchor ice release model, was set to 0.05 m based on the weighted average of bed material sizes reported in Tetra Tech, Inc. (2013). Since anchor ice thicknesses were not available to calibrate the anchor ice accretion rate, γ, and the anchor ice porosity, p_a, these parameters were set based on the values in the literature.

The last step was to calibrate the model's ability to simulate the ice cover progression during freeze-up. Time of bridging at the downstream boundary and ice front location data were provided for the calibration and validation events. The ice cover was observed

to bridge at other locations along the domain but a general ice front progression was interpreted from the data (by neglecting open leads and intermediary bridging locations) for comparison with the simulated ice front progression. The maximum Froude number for juxtaposition, $Fr_{\_jux}$, was set to 0.06 based on Lal and Shen (1991). However, the ice cover progression was not found to be sensitive to this parameter indicating that the ice cover generally progressed in either hydraulic thickening or mechanical thickening mode. Two values of $Fr_{\_max}$ were used to simulate the ice cover progression. For most of the domain $Fr_{\_max} = 0.097$ best fit the general progression; however, a value of $Fr_{\_max} = 0.15$ was required in the braided reach downstream of USGS 15292780, which is outside of the range of expected values for this parameter (Table 2.1). A possible reason for this is that the one-dimensional modelling approach is not able to accurately simulate the flow properties in the braided reach where the flow is expected to be more two-dimensional in nature. The composite jam stress parameter, μ, was set to 1.28, based on values in the literature (see Table 2.1) and the ice cohesion, τ_c, was set to 700 Pa as this value was used in a previous ice model of the Susitna River (Calkins, 1984). The simulated ice cover progressions are compared to the interpreted general ice front locations in Figure 2.11 for both the calibration and validation events.

Overall the model is capable of capturing the general progression of the ice front up to the downstream end of the canyon (km 53). However, the data show that the ice cover does initiate at multiple bridging locations which cannot be simulated by the current version of the model. This limitation is something that should be addressed in the future to allow for more accurate simulation of an ice cover with multiple ice fronts. The

simulated ice cover progression stalls in the canyon (km 30 to km 53) which is consistent with freeze-up observations that the channel remains mostly open through the canyon throughout winter (HDR, 2014). But because the model does not currently consider stability of the ice cover once the ice cover has formed, the model is not able to simulate the retreat of the ice front due to jam failure in the canyon as reported by HDR (2014). Therefore, future model developments should also include a means of evaluating ice cover stability to determine whether the ice cover may collapse and cause retreat of the ice front.

Water level data, available at a number of USGS and ESS stations, were used to calibrate and validate the ice roughness parameter in the model. Ice roughness values were interpolated based on ice thickness using the 'from ice' option. Simulated water levels are compared to observed levels in Figure 2.12 at four of the stations that were operational for both the calibration and validation events. Unfortunately the gauges failed at the USGS stations during the validation event. If the gauge was 'taken out' when the ice front passed, then the results suggest that the model is doing a good job of simulating the timing of the ice front at the USGS gauges for both the calibration and validation events. The timing of the water level rise is not well captured at ESS45 in either the calibration or the validation event. The model is late in predicting the rise for the calibration event but predicts it early for the validation event. The cause of poor performance at this station is unclear; however, it is located immediately upstream of a two mile reach of the river containing mid-channel islands. These islands may be creating two-dimensional forces on the water and ice that impacting the ice cover

progression through this reach and therefore the arrival time of the ice front at ESS45. Although the timing is off, the model has predicted the magnitude of the water level rise quite well.

Parameters for the under-cover transport follow those suggested by Shen and Wang (1995). Although no data were available to directly calibrate this process, winter ice thickness measurements indicated the presence of significant frazil slush under the solid ice cover, confirming the importance of under-cover transport in the Susitna River's ice regime. Data from winter ice surveys were provided for a few selected cross sections during the freeze-up period. This survey data included bed elevation, top and bottom of frazil slush layer, top and bottom of solid ice layer, water level and flow at the time of survey. This information was used to calculate the cross sectional area of the frazil slush and solid ice layers for the surveys. Average ice thicknesses were calculated from the areas by dividing by the width of the channel at the time of survey. Simulated and observed values at the time of the surveys are presented in Table 2.2.

Generally the model did a good job of simulating solid ice thickness and cross sectional area. For the most part, the simulated values are between the average and maximum observed thicknesses. The model did not perform as well in simulating the frazil slush. Only at ESS50 were the frazil slush thickness and cross section area in agreement with the observed values. At the other stations, the model either over or underestimated the amount of ice. But considering the temporal nature of undercover ice transport and the 1D approach used to simulate this complex process, the results are reasonable. The simulated flows agree very well with observed ones except on January 29, 2013. On this

date, the flow at USGS 15292000 (upstream of ESS40) is reported ranging from 64.1 to 64.3 m³/s. The simulated flows at USGS 15292000 on this date range from 63.3 to 64.4 m³/s. Since the model and observed flows are in agreement at the USGS station, the discrepancy at ESS40 is possibly due to survey error. However, it is possible that at the USGS stations, which were used to create the model inflows, flows are not being reported correctly since gauge rating curves do not normally account for the effects of an ice cover. But since all other simulated and observed flows in Table 2.2 agree so well, it is more likely that the lack of agreement for the 2013 survey is attributable to survey error.

2.4   Conclusions and Recommendations

This paper presents new development of the University of Alberta's comprehensive river ice process model, *River1D*. This public-domain model has been enhanced to include the ability to simulate natural channel geometry, water supercooling, anchor ice formation and release, border ice formation, under-cover transport of frazil, and ice cover progression based on leading edge stability criteria. *River1D* is the first public-domain model to include supercooling and anchor ice evolution. An unprecedentedly comprehensive calibration and validation of the model were conducted with data of the Susitna River, including water levels, flows, water temperatures, surface ice concentrations, border ice widths, ice cover progression rates, and ice thicknesses. Favourable agreements between the modelled and observed data demonstrate the ability of the newly enhanced model for simulating the freeze-up process on this complex natural river. The new natural channel capabilities facilitated good simulation of water

75

levels in both open water and ice covered conditions compared to the observed levels. The new border ice component was able to capture the variability in the observed border ice widths. An additional term, based on a degree-day approach, has been included in the border ice model which provides the user with additional means to calibrate the border ice growth and/or a simpler border ice model that only requires calibration of a single parameter. The new supercooling capabilities allowed for the simulation of anchor ice which, as observations indicate, is an important process on the Susitna River. The presence of significant frazil slush under the solid ice cover confirmed the importance of under-cover transport of frazil in the Susitna River's ice regime and the need to include this process in the simulations. Future developments to *River1D* ice process model are recommended to include the capability to simulate multiple bridging locations and a means of evaluating the stability of the ice cover once it has formed. Lastly, detailed data describing anchor ice evolution and under-cover transport and accumulation are really needed in order to properly evaluate these model components.

Figures

Figure 2.1: Cross section definition sketch of the vertical processes considered in the model for (a) moving surface ice layers, (b) anchor ice, and (c) stationary surface ice layers with moving under-cover frazil layer adapted from Andrishak and Hicks (2008).

77
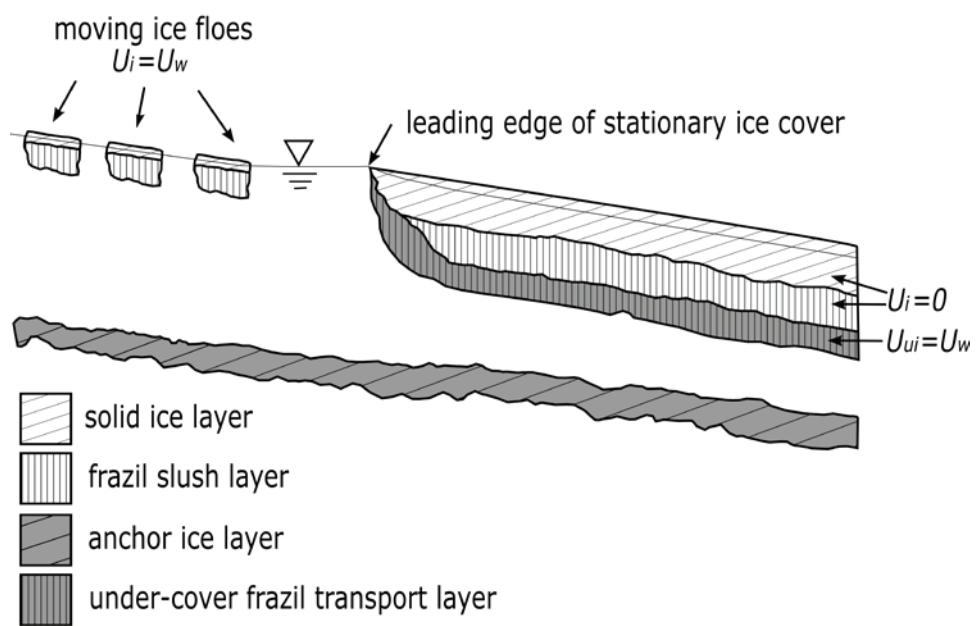
Figure 2.2: Longitudinal profile definition sketch showing the modelled ice layers.
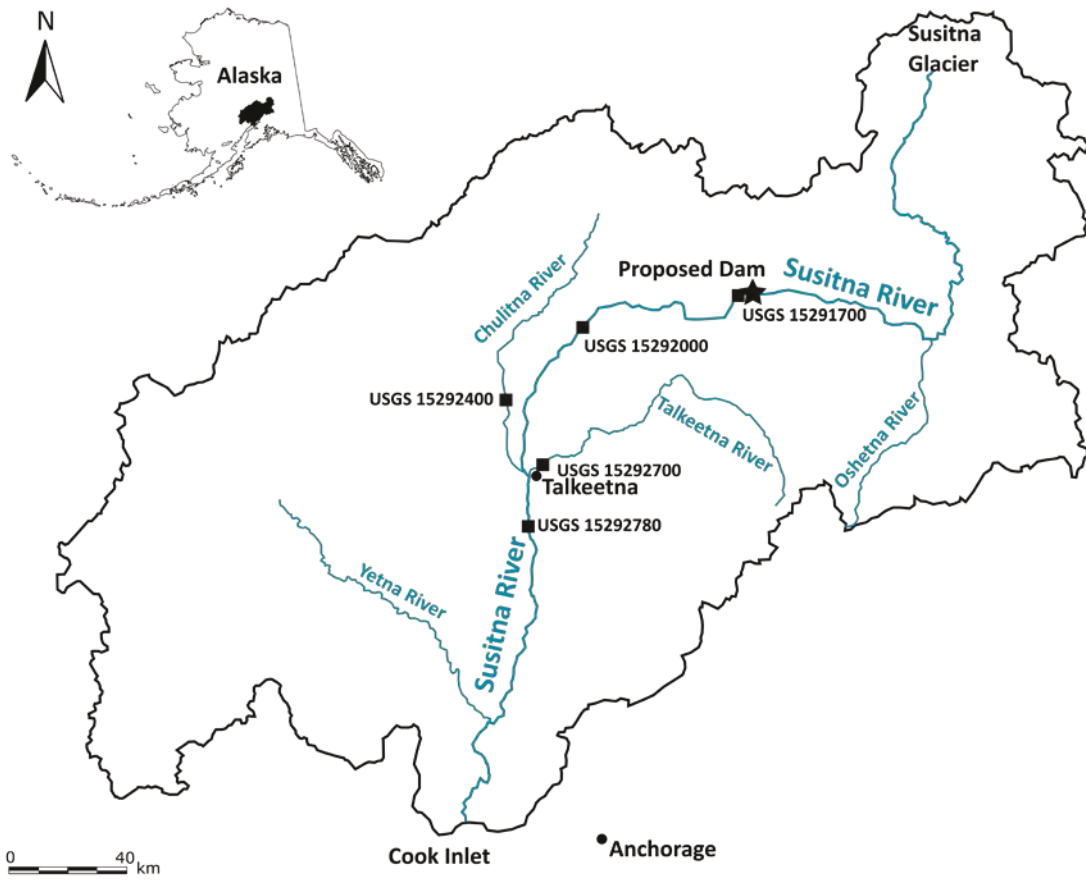
Figure 2.3: The Susitna River basin.
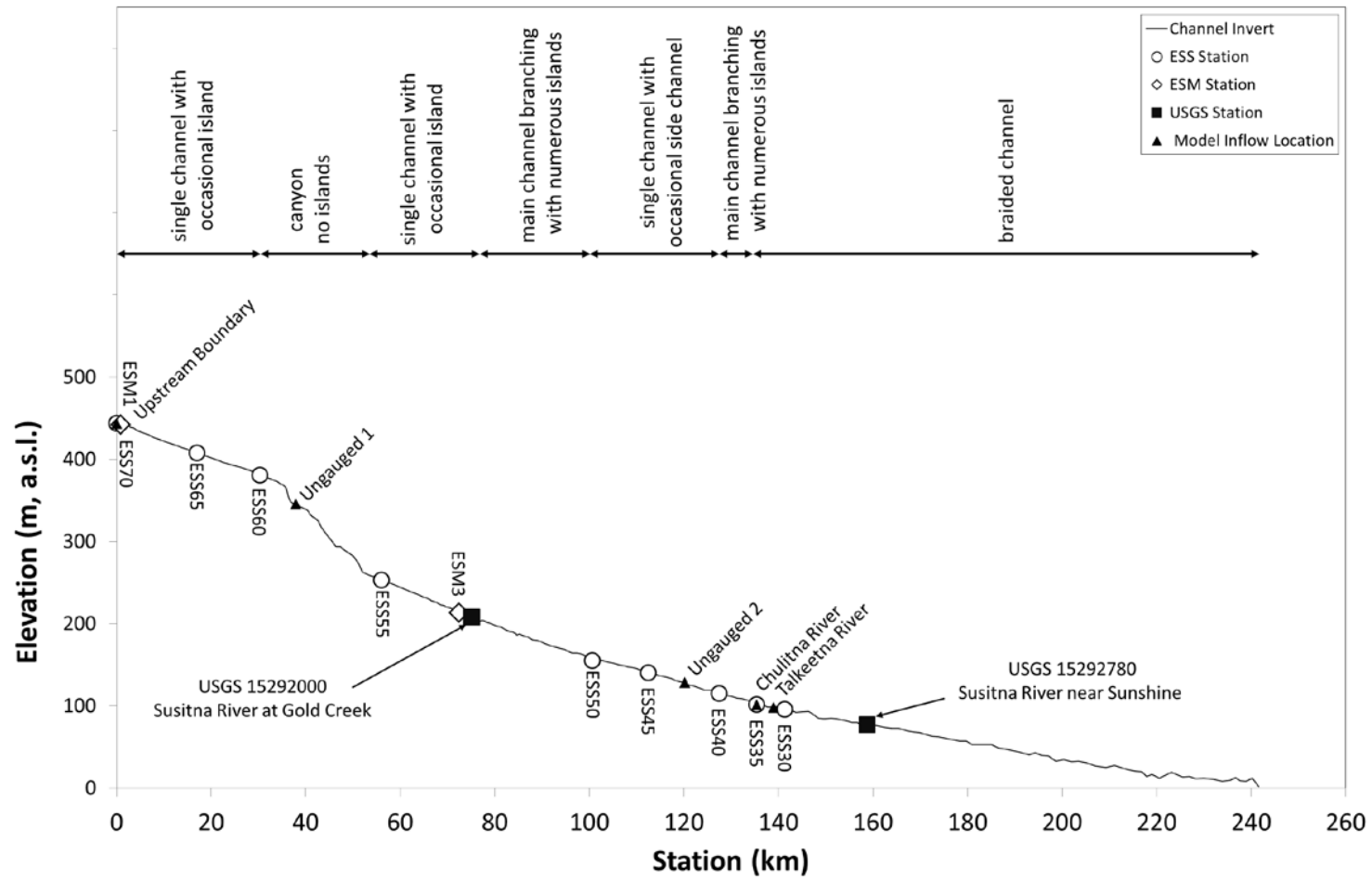
Figure 2.4: Susitna River profile showing channel invert, sub reach descriptions, USGS and ESS station locations, and model inflow locations.
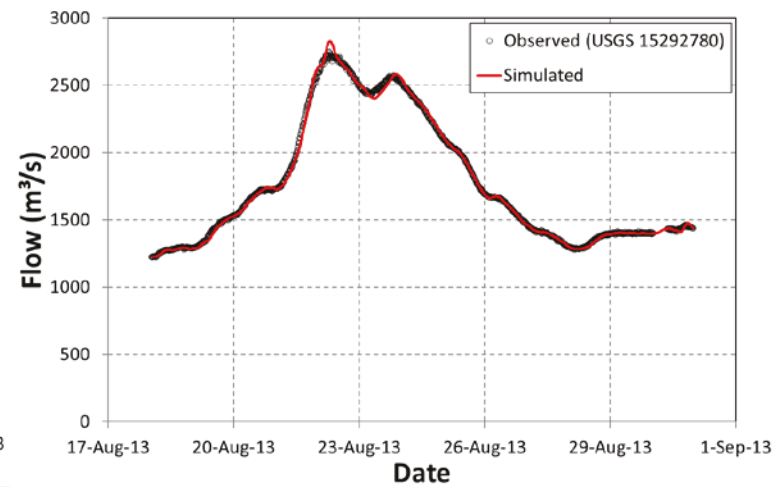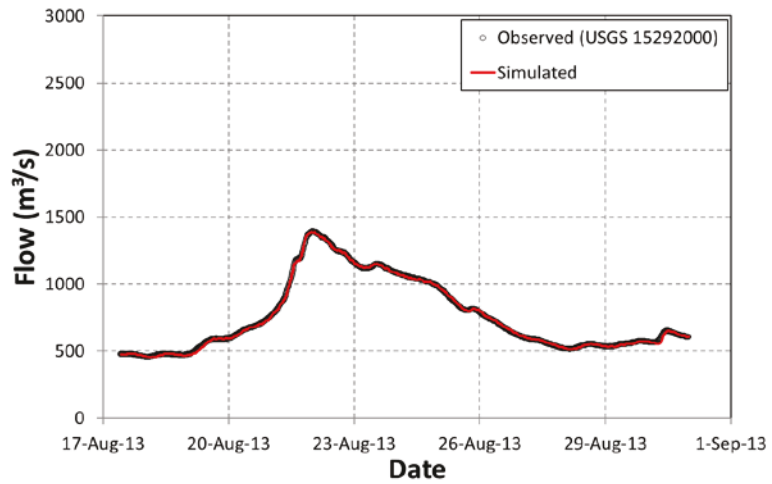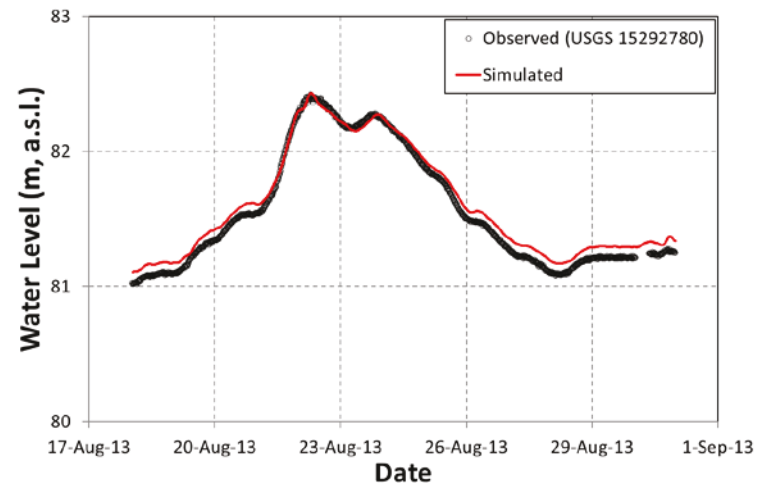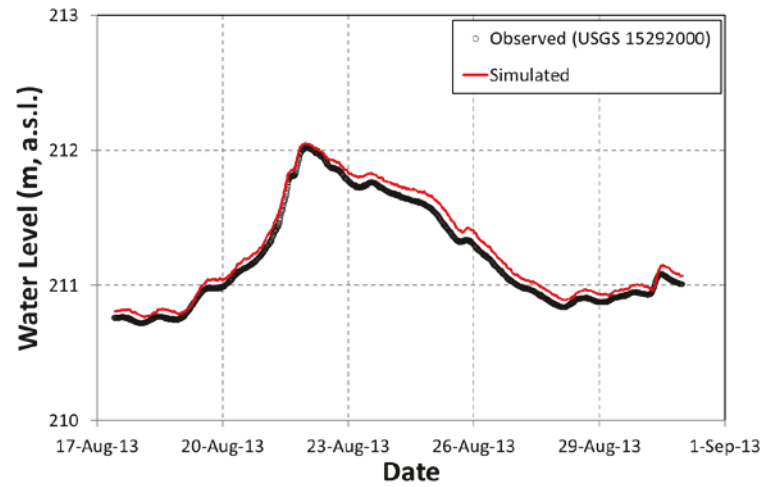
Figure 2.5: Simulated and observed water levels and flows at USGS 15292000 and USGS 15292780.
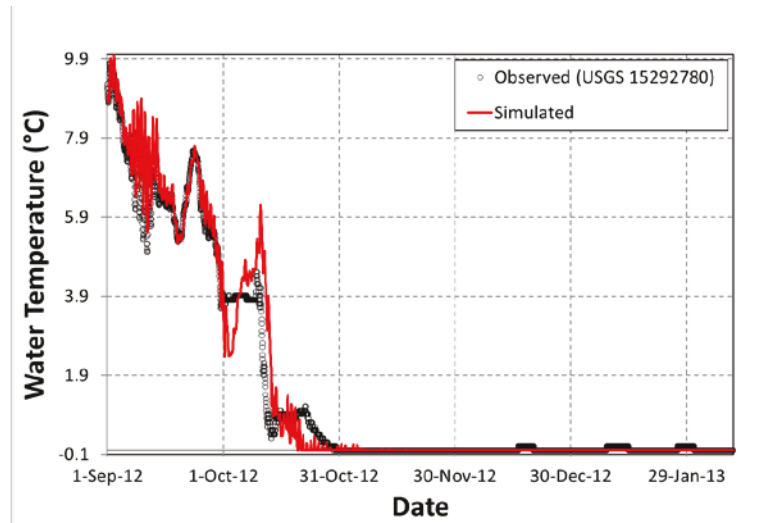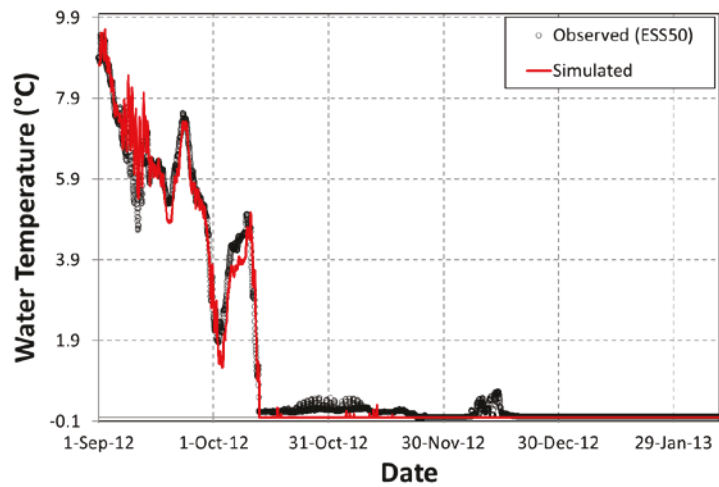
Figure 2.6: Simulated and observed water temperatures at ESS50 and USGS 15292780 for the 2012-2013 calibration period.
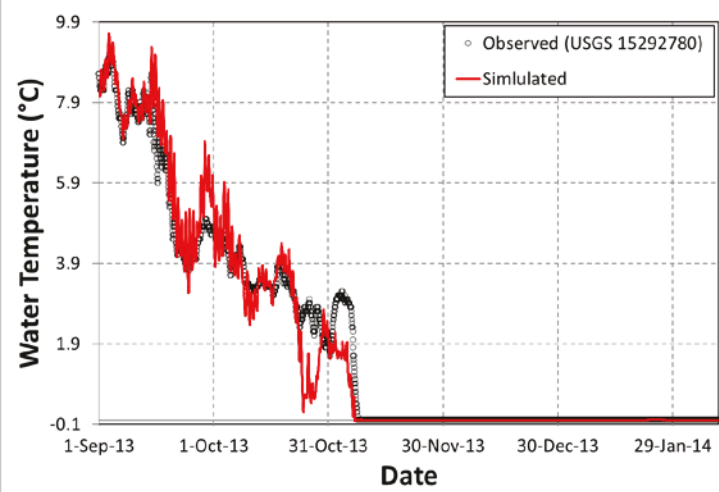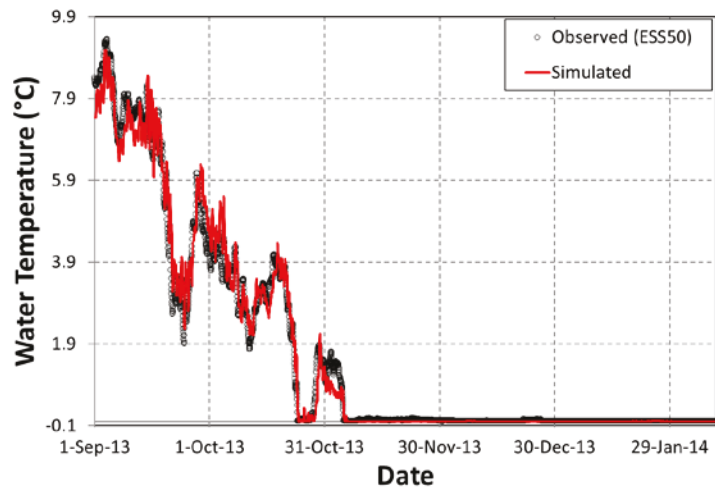
Figure 2.7: Simulated and observed water temperatures at ESS50 and USGS 15292780 for the 2013-2014 validation period.
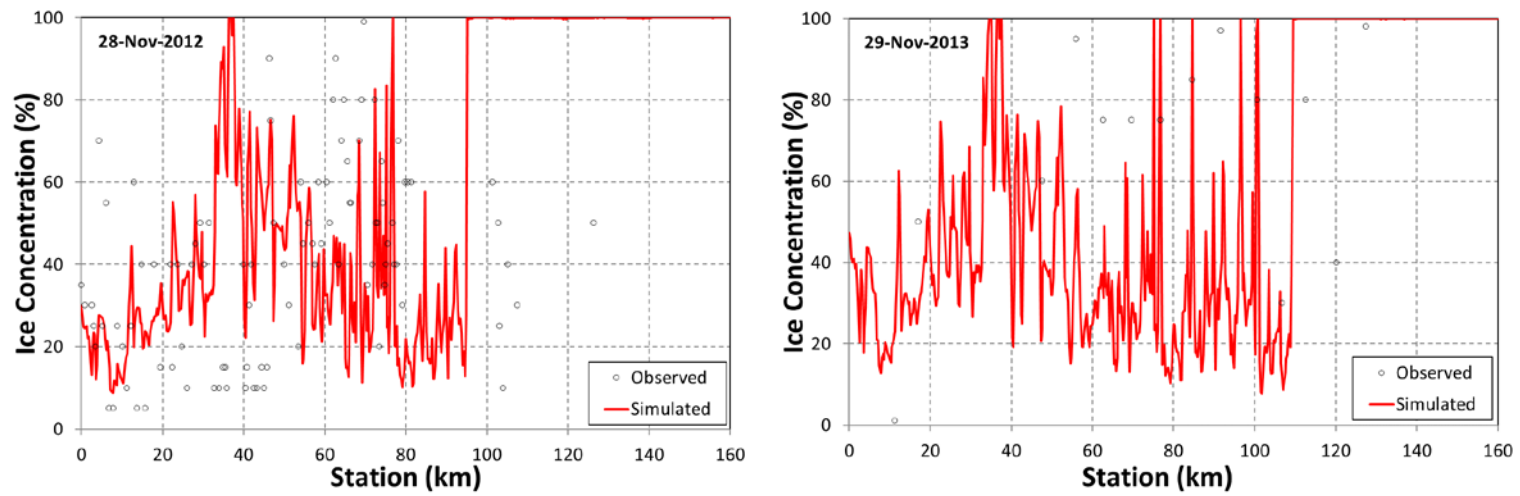
Figure 2.8: Simulated and observed surface ice concentrations in late November for the calibration and validation events.
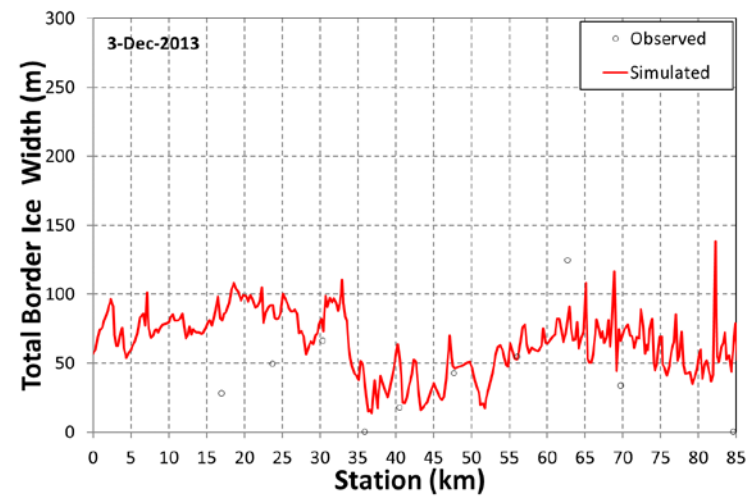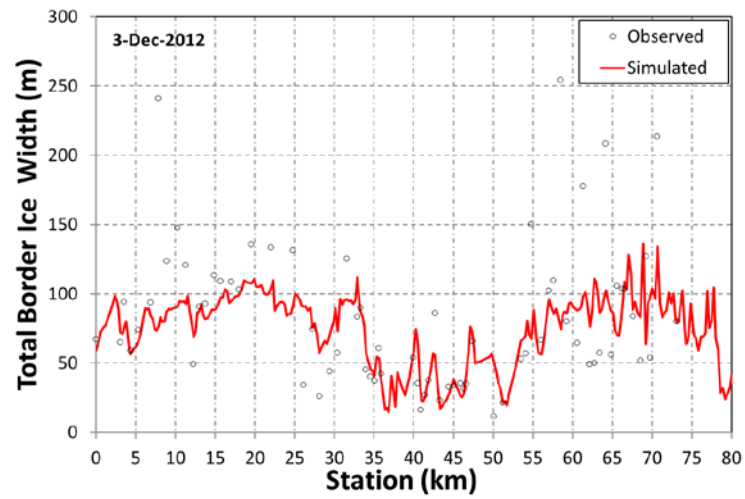
Figure 2.9: Simulated and observed border ice widths in early December for the calibration and validation events.
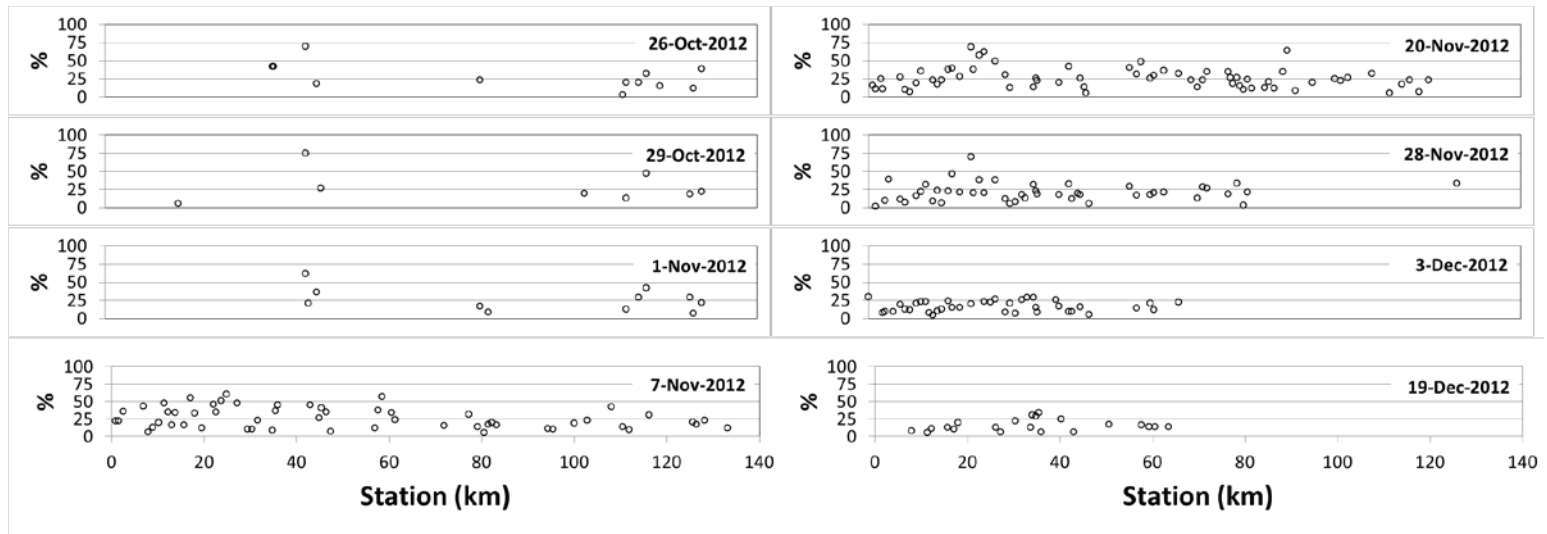
Figure 2.10: Observed percent coverage of anchor ice along the domain on various days through the 2012 freeze-up period.
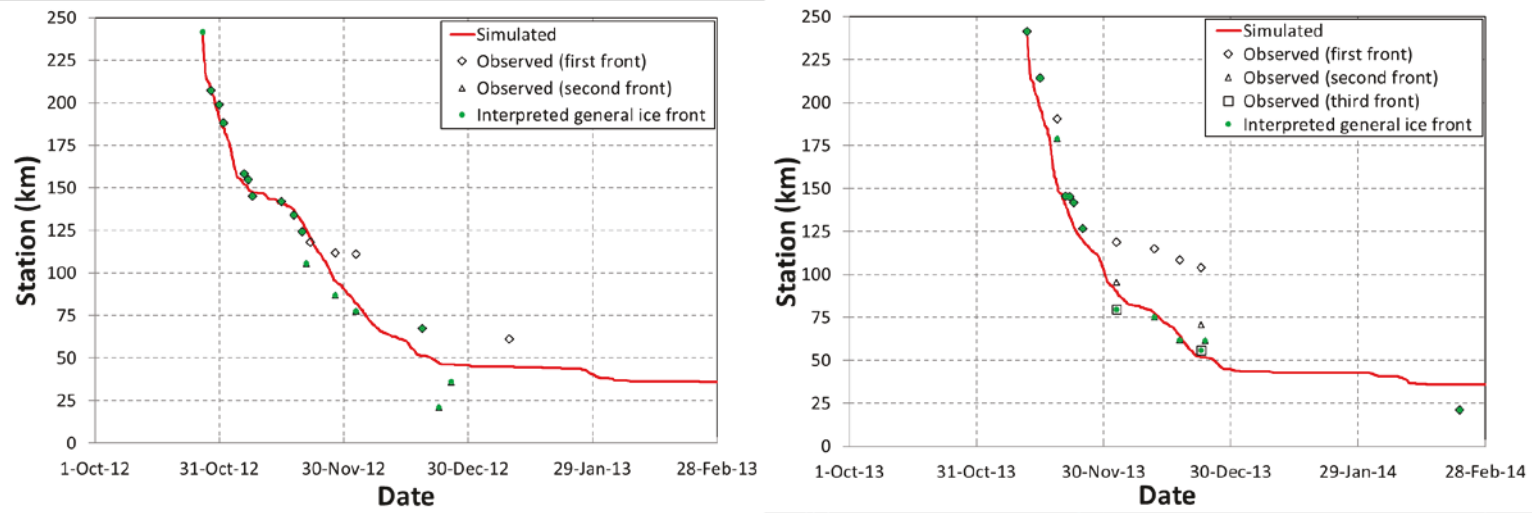
Figure 2.11: Simulated and observed ice front progression for the calibration and validation events.
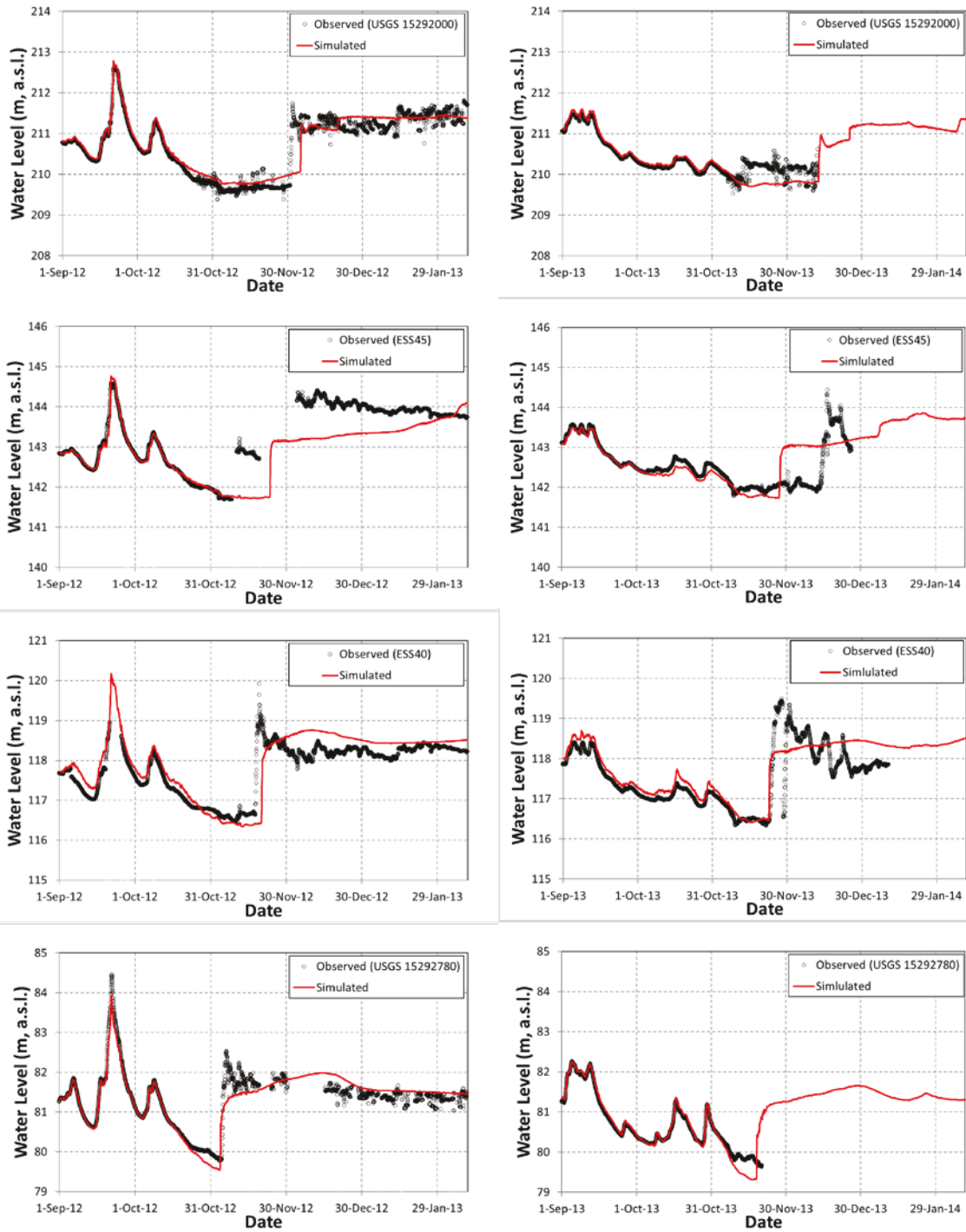
Figure 2.12: Simulated and observed water levels at USGS 15292000, ESS45, ESS40, and USGS 15292780 for the calibration and validation events.

Tables

Table 2.1: Adopted values for ice modelling parameters.

(*Continued on next three pages*).

Ice modelling parameter	Adopted Value	Values in Literature
Density of ice, ρ_i (kg/m³)	917	Lal and Shen (1991)
Heat transfer coefficient, h_{wa} (W/m²/°C)	20	19.7 (Lal and Shen,1991) 15 (Andrishak and Hicks, 2008) 20 (Timalsina et al., 2013; Calkins, 1984)
Frazil seeding concentration, C_{fo}	0.00001	
Typical frazil particle thickness, d_e (m)	0.0003	0.0003 (Wang, et al., 1995) 0.00013 (Malenchak, 2011)
Typical frazil particle radius, r_o (m)	0.001	0.001 (Wang et al., 1995; Malenchak, 2011)
Nusselt number for typical suspended frazil particle, Nu^f	4.0	4.0 (Wang et al., 1995; Malenchak, 2011)
Coefficient of turbulent heat exchange, α_{wi} (Ws$^{0.8}$/m$^{2.6}$/°C)	1187	1187 (Ashton, 1973; Andrishak and Hicks, 2008)
Rate of frazil rise, η (m/s)	0.0005	0.001(Wang et al., 1995) 0.0001 (Andrishak and Hicks, 2008) 0.0004 (Jasek et al., 2011) 0.00009 (Timalsina et al., 2013)

Table 2.1: Adopted values for ice modelling parameters (*continued*)**.**

Ice modelling parameter	Adopted Value	Values in Literature
Rate of surface ice re-entrainment, β_{re} (1/s)	0.00001	0.00001 (Wang et al., 1995; Malenchak, 2011)
Re-entrainment velocity threshold, U_{i_re} (m/s)	1.06	
Porosity of frazil slush layer, p_f	0.4	0.5 (Andrishak and Hicks, 2008) 0.4 (Lal and Shen, 1991)
New frazil pan thickness, t'_f (m)	0.2	0.3 (Andrishak and Hicks, 2008) 0.2 (Timalsina et al., 2013)
Solid ice initial thickness, t'_{si} (m)	0.001	0.001 (Lal and Shen, 1991)
Frazil particle shape factor, F	1.0	1.00 ± 0.03 (Beltaos, 2013) 1.0 (Shen and Wang, 1995)
Average diameter of frazil granules in cover load, d_f (m)	0.01	0.01 (Shen and Wang, 1995)
Critical flow strength for under-cover frazil transport, Θ_c	0.041	0.041 (Shen and Wang, 1995)
Porosity of anchor ice, p_a	0.4	0.4 (Malenchak, 2011)
Frazil accretion rate, γ (m/s)	0.00001	0.000001 (Wang et al., 1995) 0.000005-0.00025 (Malenchak, 2011) 0.0001 (Timalsina et al., 2013)

Table 2.1: Adopted values for ice modelling parameters (*continued*).

Ice modelling parameter	Adopted Value	Values in Literature
Fraction of bed covered by anchor ice, C_{an}	0.25	
Bed material average diameter, d_s (m)	0.05	
Bed material density, ρ_s (kg/m³)	2650	2650 (Malenchak, 2011)
Border ice equation coefficient, a	14.1	14.1 (Michel et al., 1982)
Border ice equation coefficient, b	1.08	1.08 (Michel et al., 1982)
Border ice equation coefficient, d	-0.93	-0.93 (Michel et al., 1982)
Border ice equation coefficient, e	9.75	
Maximum fraction of channel covered by border ice, f_{bmax}	0.7	
Maximum velocity for dynamic border ice growth, U_{cr} (m/s)	1.2	1.2 (Michel et al., 1982)
Maximum Froude number for juxtaposition, F_{r_jux}	0.06	0.06 (Lal and Shen, 1991)
Maximum Froude number for ice cover progression, F_{r_max}	0.097, 0.15	0.08 to 0.13 (Ashton, 1986) 0.09 (Lal and Shen, 1991) 0.094 (Calkins, 1984) 0.08 (Timalsina et al., 2013)
Space between ice floes in newly formed cover, p_c	0.4	Shen (2016)

Table 2.1: Adopted values for ice modelling parameters (*continued*)**.**

Ice modelling parameter	Adopted Value	Values in Literature
Composite jam stress parameter, μ	1.28	1.28 (Pariset and Hausser, 1961; Pariset et al., 1966; Lal and Shen, 1991)
Ice cohesion, τ_c (Pa)	700	700 (Calkins, 1984) 980 (Lal and Shen, 1991)

Table 2.2: Simulated and observed values for ice surveys.

	Station and Date				
	ESS40	**ESS40**	**ESS45**	**ESS50**	**ESS55**
	29-Jan-13	**26-Jan-14**	**24-Jan-14**	**23-Jan-14**	**25-Jan-14**
Average observed solid ice thickness, t_i (m)	1.15	0.75	0.67	0.55	0.62
Maximum observed solid ice thickness, t_i (m)	1.63	1.09	1.13	1.14	0.92
Simulated solid ice thickness, t_i (m)	1.20	1.02	0.86	0.92	1.04
Observed solid ice cross sectional area, A_{si} (m²)	170	103	96	63	59
Simulated solid ice cross sectional area, A_{si} (m²)	169	142	118	56	69
Average observed frazil slush thickness, t_{fs} (m)	1.04	1.78	1.06	2.31	1.71
Maximum observed frazil slush thickness, t_{fs} (m)	2.31	3.53	2.25	5.71	3.26
Simulated frazil slush thickness, t_{fs} (m)	0.90	0.93	2.33	4.28	1.23
Observed frazil slush cross sectional area, A_{fs} (m²)	153	245	152	262	164
Simulated frazil slush cross sectional area, A_{fs} (m²)	127	129	319	261	82
Observed width, B_o (m)	148	137	143	114	96
Simulated width, B_o (m)	141	138	137	61	66
Observed flow, Q_w (m³/s)	52.4	74.0	71.9	69.6	63.6
Simulated flow, Q_w (m³/s)	73.0	76.5	69.4	66.6	66.6
Observed water level, H (m, a.s.l.)	118.34	118.24	143.34	161.53	256.87
Simulated water level, H (m,a.s.l.)	118.46	118.33	143.86	162.22	256.54

References

Andrishak, R., Hicks, F.E. 2005. Impact of Climate Change on the Peace River Thermal Ice Regime. In: CGU HS Committee on River Ice Processes and the Environment Proc., 13th Workshop on Hydraulics of Ice Covered Rivers, September 15-16, 2005, Hanover, NH, 21–40.

Andrishak, R., Hicks, F. 2008. Simulating the effects of climate change on the ice regime of the Peace River. Canadian Journal of Civil Engineering 35: 461-472.

Ashton, G.D. 1973. Heat transfer to river ice covers. In Proceedings of the 30th Eastern Snow Conference, Amherst, Mass., 8-9 February 1973. Eastern Snow Conference, Monmouth, Maine, 125-135.

Ashton, G.D. (Ed.) 1986. River and Lake Ice Engineering. Water Resources Publications, Littleton, Colorado, 485 pp.

Beltaos, S. 2013. Chapter 7: Freezeup Jamming and Formation of Ice Cover. In: Beltaos, S. (ed) River Ice Formation. CGU HS Committee on River Ice Processes and the Environment, 181-255.

Beltaos, S., Prowse, T. 2001. Climate impacts on extreme ice-jam events in Canadian rivers, Hydrological Sciences Journal, 46(1): 157-181.

Brooks, A.N., Hughes, T.J.R. 1982. Streamline Upwind Petrov-Galerkin Formulations for Convection Dominated Flows with Particular Emphasis on the Incompressible Navier-Stokes Equations. Computer Methods in Applied Mechanics and Engineering. 32(1-3): 199-259.

Brown, R.S., Mackay, W.C. 1995. Fall and winter movements and habitat use by cutthroat trout in the Ram River, Alberta. Transactions of the American Fisheries Society 124: 873-885.

Brown, R.S., Power, G., Beltaos, S., Beddow, T.A. 2000. Effects of hanging ice dams on winter movements and swimming activity of fish. Journal of Fish Biology 57: 1150-1159.

Clark, S. 2013. Chapter 3: Border and Skim Ice. In: Beltaos, S. (ed) River Ice Formation. CGU HS Committee on River Ice Processes and the Environment, 77-106.

Calkins, D.J. 1984. Instream Ice Calibration of Computer Model. Alaska Power Authority Document no. 1122. 111 pp.

Daly, S.F. 1991. Frazil ice blockage of intake trash racks. CRREL Technical Digest 91-1. Army Corps of Engineers Cold Regions Research and Engineering Laboratory. Hanover, New Hampshire, 12 pp.

Fread, D.L. 1988. The NWS DAMBRK Model: Theoretical Background/User Documentation. Office of Hydrology, National Weather Service (NWS), Maryland, U.S.A.

Fread, D.L., Jin, M., Lewis, J. M., 1996. An LPI Numerical Solution for Unsteady Mixed Flow Simulation, North American Water Congress, Anaheim, CA June 22-28, 1996, American Society of Civil Engineers, 1-7.

Girling, W.C., Groeneveld, J. 1999. Anchor Ice Formation Below Limestone Generating Station. In: CGU HS Committee on River Ice Processes and the Environment Proc., 10th Workshop on Hydraulics of Ice Covered Rivers, Winnipeg, Manitoba, Canada, pp. 160-173.

Haresign, M., Toews, J.S., Clark, S. 2011. Comparative testing of border ice growth prediction models. In: CGU HS Committee on River Ice Processes and the Environment Proc., 16th Workshop on River Ice, September 18-22, 2011, Winnipeg, MB, 400-412.

HDR, Alaska Inc. 2014. Ice processes in the Susitna River study, Study plan Section 7.6, Initial Study Report. Prepared for Alaska Energy Authority. 51 pp.

Hicks, F.E. 1996. Hydraulic Flood Routing with Minimal Channel Data: Peace River, Canada. Canadian Journal of Civil Engineering 23(2): 524-535.

Hicks, F. E., McKay, K., Shabayek, S. 1997. Modelling an ice jam release surge on the St. John River, New Brunswick. In: CGU HS Committee on River Ice Processes and the Environment Proc., 9th Workshop on River Ice, September 24-26, 1997, Fredericton, NB, 303-314.

Hicks, F.E., Steffler, P.M. 1990. Finite element modeling of open channel now. Water Resources Engineering Report No. 90-6. Department of Civil Engineering, University of Alberta, Edmonton, AB, 356 pp.

Hicks, F.E., Steffler, P.M. 1992. A Characteristic Dissipative Galerkin Scheme for Open Channel Flow. ASCE Journal of Hydraulic Engineering 118: 337-352.

Hutchison, T.K., Hicks, F. 2007. Observations of ice jam release events on the Athabasca River, AB. Canadian Journal of Civil Engineering 34(4): 473-484.

Jasek, M., Ghobrial, T., Loewen, M., Hicks, F. 2011. Comparison of CRISSP modeled and SWIPS measured ice concentrations on the Peace River. In: CGU HS Committee on River Ice Processes and the Environment Proc., 16th Workshop on River Ice, September 18-22, 2001, Winnipeg, MB, 249-273.

Jasek, M., Shen, H.T., Pan, J, Paslawski, K. 2015. Anchor Ice Waves and their Impact on Winter Ice cover Stability. In: 18th CGU-HS Committee on River Ice Processes and the Environment Proc. 18th Workshop on the Hydraulics of Ice Covered Rivers, Quebec City, Quebec, August 18-20, 2015.

Kammerer, J.C. 1990. Largest rivers in the United States: U.S. Geological Survey Open-File Report 87-242, 2 pp.

Kerr, D.J., Shen, H.T., Daly, S.F. 2002. Evolution and hydraulic resistance of anchor ice on gravel bed. Journal of Cold Regions Science and Technology. 35 (2): 101-114.

Kovachis, N. 2011. Patterns of River Breakup Timing and Sequencing, Hay River, NWT. M.Sc. Thesis, University of Alberta, Edmonton, Canada, 459 pp.

Lal, A.M. W., Shen, H. T. 1991. A Mathematical for River Ice Processes, Journal of Hydraulic Engineering, ASCE, 117(7): 851-867.

Lindenschmidt, K.E. 2017. RIVICE - A Non-Proprietary, Open-Source, One-Dimensional River-Ice Model. Water, 9(5), 314: 1-15.

Malenchak, J. 2011. Numerical modelling of river ice processes on the Lower Nelson River. Ph.D. Thesis, University of Manitoba, Winnipeg, Canada.

Matousek, V. 1984a. Types of Ice Run and Conditions for their Formation, In: Proceedings of 7th IAHR International Symposium on Ice, Hamburg, Germany. Volume 1: 315-327.

Michel, B., Marcotte, N., Fonseca, F., Rivard, G. 1982. Formation of border ice in the Ste. Anne River. Proceedings of the Workshop on Hydraulics of Ice-Covered Rivers, University of Alberta, Edmonton, Alberta, Canada, 38-61.

Nafziger, J., She, Y., Hicks, F., Cunjak, R.A. 2017. Anchor ice formation and release in small regulated and unregulated streams. Journal of Cold Regions Science and Technology. 141: 66-77.

Nash, J. E., Sutcliffe, J. V. 1970. River flow forecasting through conceptual models, Part 1 - a discussion of principles. Journal of Hydrology 10(3): 282-290.

Nezhikhovskiy, R. A. 1964. Coefficients of roughness of bottom surface on slush-ice cover. Soviet Hydrology (American Geophysical Union), 127-150.

Pariset, E., Hausser, R. 1961. Formation and evolution of ice covers on rivers. Transactions of the Engineering Institute of Canada 5: 41-49.

Pariset, E., Hausser, R., Gagnon, A. 1966. Formation of ice covers and ice jams in rivers. ASCE Journal of the Hydraulics Division 92(HY6): 1-24.

She, Y., Hicks, F., Steffler, P., Healy, D. 2009. Constitutive Model for Internal Resistance of Moving Ice Accumulations and Eulerian Implementation for River Ice Jam Formation. Journal of Cold Regions Science and Technology 45: 137-147.

Shen, H.T. 2006. A one-dimensional comprehensive river ice model. In: Proceedings of the 18th IAHR International Symposium on Ice, Sapporo, Japan, 61-68.

Shen, H.T. 2010. Mathematical modeling of river ice processes. Cold Regions Science and Technology 62: 3-13.

Shen, H.T. 2016. Chapter 9: River Ice Processes. In: Wang, L.K., Yang, C.T., Wang, M.-H.S. (eds) Advances in Water Resources Management, Springer International Publishing Switzerland, 483-530.

Shen, H.T., Wang, D.S., Lal, A.M. W. 1995. Numerical Simulation of River Ice Processes. Journal of Cold Regions Engineering, ASCE, 9: 107-118.

Shen, H.T., Wang, D.S. 1995. Under Cover Transport and Accumulation of Frazil Granules, Journal of Hydraulic Engineering, ASCE, 121(2): 184-194.

Tetra Tech, Ice. 2013. Initial Geomorphic Reach Delineation and Characterization, Middle and Lower Susitna River Segments (FERC No. 14241). Prepared for Alaska Energy Authority, February 2013, 24 pp.

Theriault, I., Sucet, J.-P., Taha, W. 2010. Validation of the Mike-Ice model simulating river flows in presence of ice and forecast of changes to the ice regime of the

Romaine River due to hydroelectric project. In: Proceedings of the 20th IAHR International Symposium on Ice, Lahti, Finland.

Timalsina, N., Charmasson, J., Alfredsen, K.T. 2013. Simulation of the ice regime in a Norwegian regulated river. Cold Regions Science and Technology, 94: 61–73.

Tsang, G. 1970. Change of Velocity Distribution in a Cross-Section of a Freezing River and the Effect of Frazil Ice Loading on Velocity Distribution. In: Proceedings of the 1st International Symposium on Ice, Reykjavik, Iceland. International Association of Hydro-Environment Engineering and Research, 1-11.

Uzuner, M.S. 1975. The composite roughness of ice covered streams. Journal of Hydraulic Research 13: 79-102.

Uzuner, M.S., Kennedy, J.F. 1976. Theoretical Model of River Ice Jams. ASCE Journal of the Hydraulics Division 102 (HY9): 1365-1383.

Wang, D.S., Shen, H.T., Crissman, R.D. 1995. Simulation and Analysis of Upper Niagara River Ice-Jam Conditions. Journal of Cold Regions Engineering, 9(3): 119-134.

3. One-Dimensional Channel Network Modelling and Simulation of Flow Conditions During the 2008 Ice Breakup in the Mackenzie Delta, Canada

3.1 Introduction

Networks of open channels are common occurrences in complex natural river systems such as braided rivers and river deltas. River channel junctions are key components to river networks and have an impact on how flows are distributed within a network. Junctions are located where two or more channels intersect resulting in channels coming together (converging junctions) or a channel splitting (diverging junctions). The hydrodynamics at channel junctions are complex and are a function of the junction geometry and flow conditions (Ghostine et al., 2009). Over the past six decades, considerable efforts have gone into the development of mathematical junction models. For subcritical flows, which are the most common in natural river systems, the models range from theoretical and partly empirical one-dimensional (1D) approaches (e.g. García-Navarro and Savirón, 1992; Gurram et al., 1997; Hsu et al., 1998; Shabayek, 2002; Ghostine et al., 2013) to three-dimensional (3D) approaches based on the Reynolds-averaged Navier-Stokes equations (e.g. Huang et al., 2002; Ramammurthy et al., 2007; Pandey et al., 2020).

For northern river systems, unsteady flow models with both multi-channel hydraulics and river ice modelling capabilities can be important predictive tools since ice jams (freeze-

up and breakup) have a tendency to occur at river confluences (Ettema et al., 1999), near islands (Turcotte and Morse, 2013), and within river deltas (Beltaos et al., 2012). Both one-dimensional and two-dimensional (2D) models with river ice modelling capabilities exist, commercially and within the public domain. 2D models, like *CRISSP2D* and *River2D*, provide a better representation of the variability of river ice in complex natural channel or multi-channel systems. Though, they are not typically applied to long reaches or channel networks because costly field data and lengthy computational requirements render them operationally impractical. As a result, it is often more practical to model real-world rivers affected by ice using a 1D model, particularly when modelling large river networks. However, not many 1D models with both multi-channel hydraulics and river ice modelling capabilities exist. Those with junction modelling capabilities and a comprehensive set of river ice modelling capabilities (i.e. water cooling and supercooling, border ice formation, anchor ice formation and release, surface ice evolution and transport, ice cover progression and retreat, and under-cover transport of frazil) are even fewer. The most common approach for modelling junctions in network models is to use conservation of mass and energy at the junction. Because energy losses and differences in velocities heads are difficult to evaluate, the energy equation is typically approximated by equal water levels across the junctions (Shabayek et al., 2002).

HEC-RAS (Hydrologic Engineering Center's River Analysis System) is capable of modelling river networks with stream junctions. For unsteady flow modelling in *HEC-RAS*, the default option is to force equal water levels across the junction, also called the equality model. A newer option allows for balancing energy across the junction to

compute water surfaces at junctions but no documentation is available on how the energy loss at the junction is calculated (Brunner, 2020b). Presently *HEC-RAS* does not have comprehensive ice modelling capabilities and is limited to modelling stationary ice covers and ice jams. *CRISSP1D*, a fully comprehensive 1D river ice model (Shen, 2005), uses a four-point implicit method to model river networks (Potok and Quinn, 1979). The method assumes equal water levels at junctions. A previous version of *River1D*, the University of Alberta's comprehensive river ice process model, (Andrishak and Hicks, 2011) also employed the equality model at junctions in order to study the ice effects on flow distributions within the Athabasca Delta. The Danish Hydraulic Institute's *MIKE11* hydraulic software uses the principles of mass and momentum conservation to predict the depth ratio across a junction (DHI, 2021) but it is not known whether *Mike-Ice* (Ice Generation and Accumulation add-in module) has been adapted for use with channel networks. Timalsina et al. (2013) applied *Mike-Ice* to a single reach of the Orkla River in Norway. Yuan et al. (2020) found that for a simple bifurcation *MIKE11* could not correctly simulate rapidly changing inflows.

The limitations of the equality model have been demonstrated by numerous investigators. García-Navarro and Savirón (1992) found this model is only valid for low Froude numbers. Kesserwani et al. (2008) found that for converging junctions the equality model only agreed well with the compared experimental data when the Froude number immediately downstream of the junction (F_d) remained less than 0.35. They recommended that at higher values of F_d to use a model based on the momentum conservation principle or to handle the junction using a 2D approach.

This paper presents new developments to *River1D's* channel network modelling capabilities, based on the 1D momentum conservation approach to model channel junctions developed by Shabayek (2002). The adapted approach eliminates the equal water level assumption, and instead takes into account the significant physical effects at channel junctions (such as gravity and flow separation forces, and channel resistance). These effects can be critical to dynamic unsteady flow applications such as ice jam formation/release and severe storm surge events. The adapted approach is also equipped with the ability to dynamically change junction configurations (i.e. diverging to converging or vice versa) as the result of flow reversals.

The new momentum based approach to model junctions was assessed using a series of steady and unsteady tests using a 2D model, the University of Alberta's *River2D*, for comparison. The model was then applied to the Mackenzie Delta to simulate flow conditions during the 2008 breakup. The work presented in this paper is a step towards the realization of *River1D* as a comprehensive public-domain river ice process model capable of simulating dynamic ice processes in complex natural river network systems.

3.2   Model Description

The proposed approach to simulating channel networks is built on the University of Alberta's public-domain 1D model, *River1D*, which solves the Saint-Venant equations using the characteristic-dissipative-Galerkin (CDG) finite element scheme (Hicks and Steffler, 1990, 1992). The model was originally developed as a hydrodynamic model for open channel flow in rectangular channels of varying width. Blackburn and She (2019)

reformulated the model to accommodate natural channel cross sections and to account for the presence of a floating ice cover and anchor ice on the river bed.

$$\frac{\partial A}{\partial t} + \frac{\partial Q_w}{\partial x} = \frac{\rho_i}{\rho_w}\frac{\partial A_i}{\partial t} + (1 - p_a)\frac{\partial A_{an}}{\partial t} \qquad [3.1]$$

$$\frac{\partial Q_w}{\partial t} + \frac{\partial(\beta Q_w U_w)}{\partial x} + gA_w\frac{\partial H}{\partial x} + gA_w S_f = 0 \qquad [3.2]$$

where A is the cross sectional area to the water surface; Q_w is discharge of water under and through the ice; A_w is the flow cross sectional area; U_w is the average flow velocity (Q_w / A_w); H is the water surface elevation above a specified datum; β is the momentum flux correction coefficient (1 for rectangular channels, 1.06 for natural channels, and calculated based on Fread (1988) for compound channels); S_f is the boundary friction slope; A_i is the cross sectional area of the surface ice; A_{an} is the cross sectional areas of the anchor ice; ρ_i and ρ_w are the densities of the ice and water, respectively; p_a is the porosity of the anchor ice; t represents time; and x represents the streamwise path of the river. The cross sectional areas of the water and to the water surface are related through:

$$A = A_w + \frac{\rho_i}{\rho_w}A_i + (1 - p_a)A_{an} \qquad [3.3]$$

In the proposed approach to channel junctions, the Saint-Venant equations are solved across the junction, based on Shabayek (2002). Depending on the flow conditions, a channel junction may either experience converging or diverging flow. Figure 3.1 illustrates these two flow configurations, and their computational elements.

104

Applying mass conservation at node A:

$$Q_{wA} = Q_{wA(\text{Element B})} + Q_{wA(\text{Element C})} \qquad [3.4]$$

where Q_{wA} is the discharge at node A; and $Q_{wA(\text{Element B})}$ and $Q_{wA(\text{Element C})}$ are the portions of Q_{wA} flowing in Element B and Element C, respectively. Defining the discharge ratio, ξ, as:

$$\xi = \frac{Q_{wA(\text{Element B})}}{Q_{wA}} \qquad [3.5]$$

then with equation [3.4]:

$$Q_{wA(\text{Element C})} = (1 - \xi) Q_{wA} \qquad [3.6]$$

Assuming the velocity is constant across the channel at node A, then:

$$A_{A(\text{Element B})} = \xi A_A \qquad [3.7]$$

$$A_{A(\text{Element C})} = (1 - \xi) A_A \qquad [3.8]$$

where $A_{A(\text{Element B})}$ and $A_{A(\text{Element C})}$ are the portions of the cross sectional area to the water surface at node A, A_A, contributing to the flow in Element B and Element C, respectively.

The discharge ratio, technically a solution unknown, is determined as follows in the model. Discretization of the Saint-Venant equations using the finite element method, or any other discretization method, results in a set of nonlinear algebraic equations. This

nonlinear system is solved using the Newton-Raphson iterative solution. At every

iteration, the volume fluxed through every element in the computational domain is

calculated as part of the finite element solution:

$$Q_{flux} = \int_0^{L_E} \frac{\partial Q_w}{\partial x} dx \qquad\qquad [3.9]$$

where L_E is the length of the element. The discharge ratio is estimated as the ratio of the

volume flux in the lateral element to the total volume flux in both the lateral and main

elements:

$$\xi \approx \tilde{\xi} = \frac{Q_{flux(\text{Element B})}}{(Q_{flux(\text{Element B})} + Q_{flux(\text{Element C})})} \qquad\qquad [3.10]$$

The estimated discharge ratio is based on the volume flux values from the previous

iteration. As the iterative solution converges, so do the flux values.

In the case of diverging junctions, where the flow split is largely affected by the junction

geometry, a factor is applied to the momentum equation to account for the reduction in

momentum that occurs due to flow separation. For junction elements, the momentum

equation is as follows:

$$\frac{\partial Q_w}{\partial t} + K_s \left[\frac{\partial (\beta Q_w U_w)}{\partial x} \right] + g A_w \frac{\partial H}{\partial x} + g A_w S_f = 0 \qquad\qquad [3.11]$$

Where K_s is the momentum reduction separation factor for diverging juntions. In the current version, values of K_s are calcuated as follows based on the angles of receiving channels as shown in Figure 3.1 (b).

$$K_{s(\text{Element C})} = \cos\theta_C \qquad\qquad [3.12]$$

$$K_{s(\text{Element B})} = \cos\theta_B \qquad\qquad [3.13]$$

The proposed approach has omitted other momentum effects that were included by Shabayek (2002) such as centrifugal effect and interfacial shear. These have not been included in the proposed approach because they require parameters to be calibrated. The intent here was to develop an approach that would permit the simulation of flow in a channel network that includes the more important physical effects at junctions but without the need to adjust model parameters or redefine junctions should a flow reversal occur. As a result, tradeoffs have been made in accuracy in the interest of operational practicality.

The model is also equipped to handle changes to junction configurations due to flow reversals. This is an important feature for modelling flows in channel deltas where water surface gradients are low and flow directions are easily reversed. Should a flow reversal occur at any node defining a junction, the model will reconfigure the junction definition to accomodate the flow reversal. Figure 3.2 illustrates how a diverging junction is reconfigured in the model to a converging junction due to a flow reversal at node B.

Flow directions at model junctions are checked at every time step and junctions are reconfigured accordingly.

3.3   Model Validation

A series of tests were performed to assess the model's junction capabilities. In Shabayek (2002), the proposed models for converging and diverging junctions were validated but the validation was performed for lab scale problems only. Additionally, Shabayek's models were developed and tested solely for steady flow conditions and were never designed to handle flow reversals. For these reasons, the model was setup to test a variety of junction configurations, which were also simulated using the University of Alberta's *River2D* model for comparison. The decision to validate the model with *River2D* was twofold. Firstly, *River2D* has been validated with field data in numerous studies (e.g. Dow et al., 2009; Waddle, 2010; Brayall and Hicks, 2012; Holmquist and Waddle, 2013). Secondly, this allowed for the validation of *River1D* for domains at a scale that are commensurate with the intended application to the Makenzie Delta whereas most junction studies have been conducted at lab scale (e.g. Taylor, 1944; Law, 1965; Hsu et al., 1998; Weber et al., 2001; Rivière et al.; 2014). The tests were performed for both steady and unsteady flow. Two different scenarios were performed: a simple diverging junction and two parallel channels with a perpendicular lateral connecting channel.

3.3.1　Diverging Junction

The general plan view configuration for the diverging junction scenario is shown in Figure 3.3. The domain is defined in terms of a main and a lateral reach. The main and lateral reaches are 40 km and 23 km long, respectively.

Figure 3.3 also shows both the boundary of the 2D domain (dashed grey line) and the alignment of the 1D domain (solid grey line with solid grey dots for node locations) within the 2D domain. For the 1D domain, the model was discretized using 64 nodes with an element length of 1 km. For the 2D domain, the model was discretized with linear triangles. The 2D domains were filled with nodes with a nominal spacing of 100 m. The nodes were triangulated and the mesh was smoothed to regulate triangle shape for optimal computational performance. The number of triangles in each test ranged between 4975 and 6675. The range in the number of triangles is because tests with larger channel widths (500 m versus 250 m) required more triangles to produce similar nodal discretization. Twenty test configurations were performed for different channel width, channel slope, and lateral channel angle, as presented in Table 3.1.

Although *River1D* can use either effective roughness height, k_b, or bed Manning's roughness coefficient, n_b, to calculate channel resistance, *River2D* only employs, k_b. For this reason, all tests (1D and 2D) were performed using effective roughness height, k_b, to calculate channel resistance, which is related the non-dimensional Chezy coefficient, C_s, through:

$$C_s = 2.5 \ln \left(\frac{12 R_h}{k_b} \right) \qquad\qquad\qquad [3.14]$$

where R_h is the hydraulic radius of the flow. For all tests, the effective channel roughness was set to 0.1 m, which translates to a bed Manning's roughness coefficient of approximately 0.026. In *River2D*, it is assumed that vertical wall boundaries are smooth and do not provide any resistance to the flow. For this reason, *River1D* was reconfigured for the tests using this assumption as well. For these subcritical flow tests, the boundary conditions must be specified as discharge at inflow sections and water surface elevation at outflow sections. For the steady tests, the inflow discharge was set to 600 m³/s. For the unsteady tests, an inflow hydrograph was developed using a bell curve shape, as shown in Figure 3.4.

For both steady and unsteady tests the downstream boundary water surface elevations were specified such that a flow depth of 1.5 m was always maintained. This depth was selected in order to maintain drawdown conditions at the downstream boundary and prevent any backwater from affecting flow conditions at the junction. Unsteady tests were run with an implicitness of $\theta = 0.5$ at a time step of $\Delta t = 0.025$ hrs for a total of 30 hrs. For the steady and unsteady tests, model outputs included discharges, water surface elevations, and water depths at the sections *MU* (Main Channel Upstream), *MD* (Main Channel Downstream), and *LD* (Lateral Channel Downstream) as specified in Figure 3.3 (dashed black lines). These sections were placed at the locations of the 1D computational nodes immediately upstream and downstream of the 1D junction node. Depths and water

surface elevations were output from *River2D* at the middle of the output sections to correspond with the 1D node output locations. The discharge and water depth results for the steady tests are presented Table 3.2. In comparing the results for the different tests, of note is how changes to the junction geometry affect the flow split. Changes to the slope and channel width significantly change the flow split while changes to the junction angle have minimal effect.

Overall *River1D* simulated the steady state discharge exceptionally well compared to *River2D* for all test configurations. All 1D discharge values are within 1.4 m^3/s of the 2D values. Also of note is the performance of momentum separation reduction factor, K_s, in *River1D*. Although junction angle has minimal effect on the flow split, the 1D model produced a similar reduction in flow in the lateral channel with increasing junction angle as compared to the 2D model. *River1D* did not perform quite as well with respect to simulated depth. The 1D model depths agree well with the 2D model depths at the sections downstream of the junction (*MD* and *LD*) but *River1D* tends to overestimate the depth at section *MU* for all tests. At the downstream sections, the difference between the 1D and 2D models is always less than 0.01 m. However, at the upstream section, the difference ranged from 0.027 m to 0.097 m. Although the disagreement at the upstream section is considerable, a comparison of depth profile plots for the test configuration with the worse results (test DS15 with depth difference of 0.097 m) show that the depth difference between the two models is most prominent at the junction and reduces in the upstream direction away from the junction, as presented in Figure 3.5 (Main Channel).

For the unsteady tests, *River1D's* performance was evaluated using the root mean square

error (RMSE):

$$RMSE = \sqrt{\frac{\sum_{i=1}^{n}(PR_i - OB_i)^2}{n}}$$ [3.15]

where n is the number of observations in the event, OB_i is the ith observed value, and PR_i

is the ith predicted value. In this case, it is assumed that the *River1D* results are the

predicted values and the *River2D* results are the observed values. A perfect match

between observed and predicted value occurs when the RMSE equals 0. Table 3.3

presents the RMSE values for both the water surface elevation and the volumetric

discharge at each of the three output cross sections for all 20 unsteady tests. For the

transient discharge results, RMSE values for discharge are all very low (2.0 m³/s or less)

indicating an excellent agreement between the 1D and 2D discharge values for all tests.

River1D did not perform as well with respect to the transient water surface elevation.

However, this is not surprising since the steady tests also revealed this less satisfactory

performance. For the sections downstream of the junction (*MD* and *LD*), the agreement

is still excellent with RMSE values for water surface elevation ranging between 0.001 m

and 0.01 m but the RMSE values for section *MU* were as high as 0.101 m (test DT3).

Water surface elevation hydrographs for test DT3 are presented for each of the output

sections in Figure 3.6. *River1D* overestimates the water surface elevation compared to

River2D by approximately 0.1 m over the entire simulation which is consistent with the

RMSE of 0.101 m, since this metric is a measure of the average difference between the predicted and observed values.

All of the steady and unsteady 1D tests were also performed using an element length of 0.5 km in order to investigate whether the discrepancy between the 1D and 2D models could be in part attributable to model discretization. Outputs were generated at the same section locations, but in this case the output sections were placed 2 nodes upstream and downstream of the 1D junction node. For the steady tests, the difference between the 1D and 2D models at the downstream sections (*MD* and *LD*) remain essentially the same at less than 0.01 m. But at the upstream section (*MU*), the maximum difference dropped by almost half and ranged from 0.003 m to 0.059 m. The discharge results were very similar compared to those for the larger discretization with the 1D values all within 1.6 m^3/s of the 2D values. For the unsteady tests, RMSE values for discharge remain low (2.2 m^3/s or less) but slightly higher than for the larger discretization. For the unsteady water surface elevation results, the RMSE values at the sections downstream of the junction (*MD* and *LD*) are essentially unchanged and range between 0.002 m and 0.011 m. The RMSE values for section *MU* improved with a maximum value of 0.061 m, again the maximum error almost halved compared to that for the larger discretization. Although the results suggest that the discrepancies between the two models may in part be attributable to model discretization, the problem with simulating the 1D domain with this smaller discretization is that the length of the junction is essentially reduced by half compared to the 2D domain resulting in the downstream end of the 1D junction elements falling within the junction they are trying to represent. This puts into question the

validity of comparing the two models for this particular set of tests when using this smaller 1D discretization.

The tendency of the 1D model to overestimate the depth /water surface elevation upstream of the junction could also be a result of neglecting the centrifugal force acting on the flow in the main channel as the lateral channel branches off. This force would increase the velocity in the main element (see Figure 3.2a) at and downstream of the junction which would result in a lower depth / water surface elevation at and above the junction. Although the 1D model's performance upstream of the diverging junction could be improved in both steady and unsteady simulations with respect to depth / water surface elevation, the model performance is excellent with respect to depth / water surface elevation and volumetric discharge split at the more crucial locations downstream of the junction. Incorrect predictions at this location would transfer to all cross sections downstream of the junction whereas the poorer performance of the model upstream of the junction appears to affect only a few cross sections in the upstream direction only.

3.3.2   Two parallel channels with perpendicular connecting channel

For this test scenario, the plan view configuration is presented in Figure 3.7. The domain is defined with two parallel channels, both 250 m wide and 40 km long, connected by a 250 m wide and 20 km long channel. The connecting channel is perpendicular to the parallel channels with the 90° junctions halfway along the length of the parallel channels. The two parallel channels have a slope of 0.0005 while the perpendicular connecting channel is flat. For the 1D domain (solid grey line with solid grey dots for node locations

in Figure 3.7), the model was discretized using 101 nodes with an element length of 1 km. The 2D domain (boundary shown as dashed grey line in Figure 3.7) was filled with nodes with a nominal spacing of 100 m, triangulated and smoothed such that the final discretization included 7859 linear triangles. All tests were performed using an effective roughness height of 0.1 m (approximately equivalent to $n_b = 0.026$) to calculate channel resistance and assuming smooth vertical wall boundaries. With this configuration, five steady and two unsteady tests were performed. For the steady tests, the steady flow boundary conditions were set according to Table 3.4.

Depths and discharges were output at the five sections depicted in Figure 3.7 (dashed black lines), specifically sections *TU* (Top Channel Upstream of Junction), *TD* (Top Channel Downstream of Junction), *CM* (Connector Channel at Midpoint), *BU* (Bottom Channel Upstream of Junction), and *BD* (Bottom Channel Downstream of Junction). The sections in the parallel channels are exactly 1 km upstream and downstream of the junctions with the connecting channel. The section in the connecting channel is at the midpoint along the channel between the two junctions. The 1D and 2D domains were defined such that the positive flow direction is from left to right in the parallel channels and from bottom to top for the connector channel as depicted by the flow arrows in Figure 3.7. Table 3.5 presents the steady test discharge and depth results for the 1D and 2D tests. Negative values at *CM*, shown in italics, indicate a flow reversal in the connector channel.

For all of the steady tests at the reported output sections, the maximum difference between the 1D and 2D discharge values is less than 2 m³/s and the maximum difference between the 1D and 2D depths is less than 0.03 m.

For the two unsteady tests, the boundary conditions were set according to Table 3.6. Boundary values were changed linearly from one value to another over a period of 10 hrs. Both unsteady tests were run with an implicitness of $\theta = 0.5$ at a time step of $\Delta t = 0.025$ hrs for a total of 30 hrs.

The unsteady tests results were evaluated using RMSE values for the water surface elevation and the volumetric discharge as presented in Table 3.7. For both tests, the RMSE for the discharge is below 1 m³/s at all output sections and the RMSE for the water surface elevation is maximum 0.021 m. The water surface elevation and discharge hydrographs for both unsteady tests at section *CM* in the connector channel are presented in Figure 3.8. The hydrographs show excellent agreement between the two models in terms of water surface elevation and discharge at this location throughout the simulations. They also demonstrate how well *River1D* is able to accurately simulate transient flow reversals.

3.4   Model Application

River1D was applied to a network of channels in the Mackenzie Delta (MD). The network model, developed for the upper delta with consideration for the most hydraulically significant channels and junctions, was calibrated and validated using three

open water events. The calibrated model was subsequently used to simulate flow

conditions during the 2008 breakup of the MD.

3.4.1   Study Site

The MD is the world's second largest Arctic delta with a vast and complex network of

interconnected channels and lakes, covering an area of over 13,000 km² (Emmerton et al.,

2007). Shown in Figure 3.9, it extends north from Point Separation, which is

approximately 25 km downstream of the community of Tsiigehtchic[1], and eventually

drains into the Beaufort Sea with flow contributions from both the Mackenzie and Peel

Rivers. The major channels in the upper Delta include the Middle, Peel and East

Channels. The "Turtle" (Beltaos et al., 2012; Morley, 2012) is the multi-branch reach of

the Middle Channel starting at Point Separation and extending nearly 40 km downstream.

The "Left Channel of the Turtle" or "Left Channel" (Beltaos et al., 2012) connects to the

Peel River system via the "Peel Mackenzie Connector" (Blackburn et al., 2015) and the

East Channel branches off from the Turtle approximately 23 km downstream of Point

Separation.

---

[1] The community of Tsiigehtchic was formerly known as 'Arctic Red River'. In 1994, the official name of
the community was changed from 'Artic Red River' to the designation traditionally used by the Gwichya
Gwich'in (Heine et al., 2007).

The complexity of this delta system can be partly attributed to low water surface

gradients coupled with variable river inflows and changes in sea level (due to the effects

of storm surges and tides). The flow regime is further complicated by ice and ice

jamming. Breakup ice jams can affect the flow distributions within the MD and in some

instances flow reversals in some channels can even occur (Terroux et al., 1981; Mackay,

1963). An understanding of how flow distributions are affected by ice jamming is

important because flooding and peak water levels in the MD are typically driven by

spring snowmelt runoff and ice jamming rather than by open water events (Goulding et

al. 2009; Morley, 2012).

3.4.2   Available Data and Model Geometry

The majority of data used in this study was collected as part of the Canadian International

Polar Year project entitled Study of the Canadian Artic River-delta Fluxes (IPY-SCARF).

These data include manual flow measurements, water levels, channel bathymetry, ice

thickness data, and radar satellite imagery. For the IPY-SCARF, the Canadian

Gravimetric Geoid 2005 (CGG05) was used as the vertical datum for water level

elevations and channel bathymetry elevations.

Water Survey of Canada (WSC) maintains gauges at a number of locations along

channels within the MD and two upstream on the Mackenzie and Peel Rivers. For those

used in this study, their locations (identified by station number) are shown in Figure 3.9.

WSC only publishes conversions to the Geodetic Survey of Canada Datum. Conversions

to the CGG05 datum used in this study were calculated and provided by the Water

Survey of Canada (WSC). Table 3.8 lists the stations according to their station number, station name, the type of data reported at the station, and the conversion of the published data to the CGG05 datum.

The model was developed for the most hydraulically significant or primary network of channels in the upper Delta as identified by Morley (2012) and shown in Figure 3.9. The model consists of seven channels and nine junctions with inflow boundaries (2) on the Mackenzie and Peel Rivers and outflow boundaries (3) on the West, Middle, and East Channels with model boundaries placed at the locations of WSC gauge stations. Available channel bathymetry to develop the network model included a total of only 36 cross sections. Because of this limited number of cross sections, the decision was made to employ a 'limited geometry approach' to develop the model. Hicks (1996) demonstrated that, in the absence of detailed channel bathymetry, a reliable hydraulic model can still be developed by approximating natural cross sections with equivalent rectangular cross sections. The model is defined using 933 rectangular cross sections that were developed from channel centerline locations and channel widths measured from georeferenced digital colour air photos (Nafziger et al., 2009) at 500 m intervals using a geographic information system (GIS). The extracted widths were then smoothed for input to the model using a 15 point moving average.

3.4.3   Open Water Calibration and Validation

The model was calibrated and validated for three open water periods. An unconventional approach was used to calibrate the model because of the lack of channel bathymetry data.

Typically model calibration is achieved by adjusting the channel roughness values until

simulated results and observed values are in agreement. In this case, the bed Manning's

roughness coefficient was set to an assumed value of n_b = 0.025 for each rectangular

cross section in the model, and channel bed slopes and elevations were adjusted, using

the mean bed elevations at the surveyed cross sections for guidance, until modelled water

surface elevations and flows were in good agreement with observed values. A single

value of roughness was used to represent the entire channel since the channel bathymetry

has been approximated using rectangular cross sections that neglect overbank flow. The

assumed bed Manning's coefficient was selected in accordance with hydraulic

computations along the Mackenzie River and in Delta channels in previous studies.

Parkinson and Holder (1982) performed a number of backwater calculations starting at

the Beaufort Sea and ending above Arctic Red River and found that n_b should range from

0.027 (at 7,800 m³/s) to 0.023 (at 30,000 m³/s). Beltaos (2012) performed 1D hydraulic

computations using *HEC-RAS* and determined that n_b = 0.025 was appropriate at

Mackenzie River at Arctic Red River (10LC014) for discharges that ranged between

20,000 m³/s to 30,000 m³/s. Beltaos et al. (2012) used local bathymetry and water level

data from loggers to calculate the flow at various locations in the MD using *HEC-RAS*.

For all calculations (which were used to estimate flows at Mackenzie River at Artic Red

River, the Head of the East Channel, the Peel Mackenzie Connector, in the Middle

Channel within and below the Turtle), n_b of 0.025 was employed. It should be noted that

the approach used in this study of setting the bed roughness and calibrating the model bed

elevations is unconventional and is not recommended for flood risk studies and

ecosystem sustainability assessments. In those instances it is recommended that comprehensive bathymetric surveys be conducted for modelling applications that consider both in channel and overbank flow.

The three open water periods were selected for calibration and validation of the model based on the time of the manual flow measurement campaigns during the IPY-SCARF study. The period with the most comprehensive manual flow measurements was selected as the calibration period (2-Aug-08 to 12-Aug-08) while the other two periods (14-Jun-07 to 21-Jun-07; 4-Sep-09 to 17-Sep-09) were selected for model validation. For each period boundary conditions were set based on the WSC gauge data. Discharge hydrographs were specified at inflow boundaries and water level hydrographs were specified at downstream boundaries. Reported discharge values at the upstream boundary on the Peel River were adjusted for input to the model to account for flow leaving the Peel to smaller distributary channels between the inflow boundary and the junction with the Peel Mackenzie Connector. Adjustments were based on the downstream manual flow measurements compared to the daily discharge values reported at the gauge on the same day as the manual measurement. The adjustments to the inflows on the Peel were as follows: 98% of reported inflows for the 2008 calibration period and the 2009 validation period; and 77% of reported inflows for the 2007 validation period. Model simulations were conducted with an additional one week lead up period to establish the initial conditions at the start of the calibration / validation periods. Model results were output at the time and location of all manual flow and water level measurements and are compared in Table 3.9. It should be noted that the significant

discrepancies between the simulated and measured values in the East Channel at Inuvik (10LC002) are attributed to omitting any distributaries along the East Channel between the head of the channel and the gauge.

The error relative to the total MD inflow at the time of manual discharge measurement (RE) was calculate as:

$$\mathrm{RE} = \frac{Q_{measured} - Q_{simulated}}{Q_{\text{total inflow}}} \times 100\% \qquad [3.16]$$

where $Q_{measured}$ is the water discharge measured in the field, $Q_{simulated}$ is the water discharge simulated by the model, and $Q_{total\ inflow}$ is the total inflow to the MD from gauge data (i.e. 10LC014 and 10MC002). The total inflow was used in the calculations in order to scale the error over the entire delta. Except for at the Middle Channel (10MC008) during the Validation Period #1, all of the RE values are 3.0% or less. The large error at this one particular location is not surprising. Model performance is expected to decrease in the downstream direction because of the omission of distributary channels, particularly with larger inflows to the MD when more flow is expected to drain into distributary channels away from the larger primary channels. During Validation Period #1, inflows to the MD were about 1.5 times higher compared to the other simulation periods.

Model results were also compared to WSC gauging locations within the domain that were not used to specify the model boundary conditions: Mackenzie River at Confluence East Channel (10LC015) and Peel River at Frog Creek (10MC022). Only water levels are available at these stations and are compared to model results in Figure 3.10. Water levels

simulated at Peel River at Frog Creek (10MC022) are consistently at least 2 m larger than those recorded during the manual flow measurement campaigns and those reported at the gauge. Although the model is not expected to accurately simulate water levels because of the rectangular channel approximation, discrepancies of this magnitude are excessive. At all other locations where water levels were recorded during the manual flow measurement campaign, the difference between observed and simulate water levels is less than 0.5 m. It is suspected that there could be an issue with the datum at this location. When the water levels at Peel River at Frog Creek (10MC022) are compared to those at the next upstream gauge on the Peel at Peel River Above Fort McPherson (10MC002), both corrected to CGG05, the water levels at the downstream gauge are higher than those at the upstream gauge, which is unlikely since this would suggest that the water is moving in the opposite or "uphill" direction. Overall, accounting for the possible reasons for why the model may not perform well with respect to discharge at downstream locations, in particular during larger flooding events, and the possible datum issue at Peel River at Frog Creek (10MC022), the model shows good agreement with the observed discharges and water levels for the open water calibration and validation periods.

3.4.4   2008 Breakup

In 2008, the MD experienced a dynamic breakup with large ice jams forming in the Middle and East Channels that resulted in extensive flooding. The progression of the breakup has been documented by others (Beltaos et al., 2012; Beltaos and Carter, 2009; Morley 2012) with relevant details summarized as follows. On May 16 an ice jam was reported on the Mackenzie River at Tsiigehtchic. On May 21 the ice in the larger

channels of the upper delta (Middle, East and Peel) was still relatively competent (intact but with open side strips and transverse cracks) while in the smaller channels ice cover decay was more advanced. On the same day, the ice jam at Tsiigehtchic released and an ice jam formed further downstream on the Middle Channel with the toe at 44 km downstream of Point Separation. By May 22 the head of this jam had reached Point Separation with rubble ice in all channels of the Turtle. Rubble from this jam had also moved into the East Channel forming a 12 km long jam with the jam toe approximately 22 km downstream of where the East Channel branches from the Middle Channel. A short jam also formed in the Peel Mackenzie Connector as a result of rubble ice moving in from the Left Channel; an indication that the jamming in the Turtle had caused a flow reversal in the Connector. The Middle Channel jam slowly deteriorated in place and became progressively shorter by thermal attrition at the head until it finally released on May 30.

3.4.5   Simulation of flow conditions during the 2008 breakup

The validated model was used to simulate flow conditions for two days during the 2008 breakup period representative of the pre-jam and ice jam conditions: May 19 (pre-jam conditions) and May 22 (ice jam conditions). The model was used to simulate the flow conditions assuming steady flow and static ice conditions. Model boundary conditions were based on the daily WSC gauge data but inflows were adjusted to account for differences between reported and actual flows. Inflows from the Peel were adjusted to 75% of the reported values at Peel River Above Fort McPherson (10MC002) to account for distributary channels diverting water away from the Peel upstream of the Peel

Mackenzie Connector. Based on open water measurements indicating that up to 23% is diverted upstream of the Peel Mackenzie Connector, a 25% diversion seemed reasonable during this breakup period when inflows from the Peel were much greater compared to the open water periods used for calibration and validation. Flows reported at Mackenzie River at Arctic Red River (10LC014) during the 2008 breakup are tagged with the 'ice conditions' flag and making them invalid or at least unreliable. Beltaos (2012) found that, for the 2008 breakup event, the gauge flows were inconsistent with i) past discharge measurements, ii) flows at the next upstream gauge, and iii) hydraulic calculations. Beltaos et al. (2012) estimated flows at Mackenzie River at Arctic Red River (10LC014) for May 19 and May 22 using *HEC-RAS* and these flow estimates were used in this study too. The boundary conditions used in the breakup simulations are listed in Table 3.10. Model ice conditions for these two dates were based on available ice thickness measurements and ice cover condition maps developed from satellite imagery showing the ice extents (van der Sanden and Drouin, 2011). A very limited number of ice thickness values were available to characterize the sheet ice conditions in 2008 prior to breakup. WSC recorded a thickness of 0.79 m at Aklavik (10MC003) on April 30 and a thickness of 1.11 m at Inuvik (10LC002) on April 24. Stranded ice blocks at Tsiigehtchic (10LC014) after the 2008 breakup ranged in thickness from 0.43 m to 1.40 m (Beltaos, et al. 2012). The height of shear walls left behind after the jam on the Middle Channel released were used to estimate the ice jam thickness. Shear wall heights collected downstream of Point Separation vary between 3.3 m and 5.3 m. The ice cover condition maps, shown in Figure 3.11, were used to estimate the sheet ice surface coverage due to

deterioration and the areal extents of the sheet ice and ice jams. No ice cover conditions map was available for May 19. May 16, which was the nearest day with an ice map with areal coverage of the model domain, was used to characterize the ice for the pre-jam conditions. The model ice thicknesses were specified according to Table 3.11.

For the May 19 pre-jam conditions, it was assumed that sheet ice was present at all cross sections in the model with a surface coverage of 75% to account for the thermal deterioration of the ice cover prior to breakup. A sheet ice Manning's roughness coefficient, n_s, of 0.02 was assumed based on the small roughness that Beltaos et al. (2012) observed on the bottom of upturned ice blocks stranded on the banks of the Mackenzie River and East Channel and the range of values given by Nezhikovskiy (1964) for smooth ice covers.

For the May 22 ice jam conditions, the model ice conditions in the Turtle region were configured as shown in Figure 3.12 using the May 22 ice cover conditions map as a guide for the spatial extents of the jamming. Portions of the Peel, Middle, and East Channels not shown in Figure 3.12 were assumed to have the same ice conditions as they did in the pre-jam configuration (75% surface ice coverage and sheet ice thickness according to Table 3.10). In channels that are included in the model (black lines in Figure 3.12) but no ice is defined, the channel is assumed to have open water conditions.

For cross sections affected by ice jamming, it was assumed that the ice jam occupied the entire cross section (surface coverage of 100%). For flow under ice jams, the hydraulic resistance was first estimated using the relationship developed by Beltaos (2001) for composite-flow Manning's roughness coefficient, n_c:

126

$$n_c \approx \left(0.063 \; to \; 0.075\right) t_j^{1/2} h^{-1/3} \tag{[3.17]}$$

where t_j is the thickness of the jam and h is the depth of water under the jam. Based on preliminary simulations, for jam thicknesses ranging from 3.3 m to 5.3 m and under jam depths ranging from about 9.4 m to 13.2 m, the values produced by this equation range from 0.05 to 0.08. This translates to under ice Manning's coefficients ranging from 0.07 to 0.12 (assuming $n_b = 0.025$). However, preliminary simulations with this range of roughness values and the observed range of jam thicknesses (from shear wall data) produced water levels that were far in excess of the observed water level data. For the 2008 ice jams Beltaos et al. (2012) observed "visibly moderate roughness" of the ice jam surfaces in the MD compared to ice jams in rivers. Additionally, in their modelling of the ice jamming in the Hay River Delta, De Coste et al. (2017) used values of 0.05 and 0.06 to calibrate the under ice roughness of the observed jams. For these reasons, a constant under ice jam Manning's coefficient, n_j, of 0.06 was selected here.

For the pre-jam and ice jam conditions the model results were compared to the water level data collected along the Middle Channel as shown in Figure 3.13. For both days water data from portable loggers are plotted for comparison with model water levels. For May 22, top of water and top of ice data, estimated from oblique photos of the jam in the Turtle area, are also plotted. For both cases additional runs were performed to provide a band of possible results by adjusting the various parameters in the model. For the pre-jam conditions, the model was run with a range of surface ice coverage values ranging from 50% to 100%. For the ice jam case the model was run with a range of values for the

ice jam thickness and roughness, to account for the range of shear wall height data collected after the jam release.

For the pre-jam conditions the results are not particularly sensitive to surface ice coverage and for the range of values the model results compare well with the observed logger data. For the ice jam conditions the results agree quite well with the observed logger data but seem to overestimate the jam measurements obtained from oblique photos. However, the accuracy of the photo-obtained levels is expected to be less compared to the logger levels. The case with the jam thickness of 4.3 m and a jam roughness of 0.06 agrees best with the observed logger levels. Model channel flows are compared for the pre-jam conditions (75% ice coverage) and ice jam conditions ($t_j = 4.3$ m; $n_j = 0.06$) in Table 3.12.

There are a number of interesting things to note between the simulated flows for these two dates:

- The change in flow within the modelled channels is significant compared to the 600 m³/s change in the total inflow to the MD (32300 m³/s to 32900 m³/s) that occurred between these two dates.
- The ice jam conditions forced more flow down the East and Left Channels and away from the Middle Channel. The increase in flow to the East Channel is consistent with observations at the gauge at Inuvik (10LC002). The increase in water level observed at the gauge was from 3.272 m to 3.992 m but the ice

conditions at the gauge were similar between those two days. Therefore the

increased water level suggests an increase in flow at the gauge.

- The flow reverses in the Peel Mackenzie Connector during the ice jam conditions

  which is consistent with observations in this channel during breakup.

3.5   *Conclusions and Recommendations*

This paper presents new network capabilities incorporated into the University of

Alberta's one dimensional hydrodynamic model, *River1D*. The approach used to

simulate junctions in the model takes into account the significant physical effects at

channel junctions (such as gravity and flow separation forces, and channel resistance)

rather than using the simpler assumption of equating water levels across the junction.

The model has also been equipped to automatically handle changes to junction

configuration due to flow reversals. The model's junction capabilities were assessed

using a series of steady and unsteady flow tests with two configurations: a diverging

channel (1 junction) and two parallel channels with a perpendicular connecting channel

(2 junctions). These configurations were also simulated using a 2D model, the University

of Alberta's *River2D*, for comparison. For all tests, the 1D model was able to simulate

the discharge exceptionally well compared to the 2D model. For some of the diverging

channel tests, the 1D model could not accurately simulate the depth / water surface

elevation immediately upstream of the junction but this could be partly attributable to 1D

model discretization and also may be due to neglecting some forces at the junction (e.g.

centrifugal forces acting on the main channel as the lateral channel branches off). The

unsteady flow tests for the two parallel channels with the perpendicular connecting

channel configuration demonstrated how well *River1D* is able to accurately simulate

transient flow reversals. Overall, the test results illustrate that the approach to simulating

junctions proposed in this paper, which includes some of the more important physical

effects at the junction but without the need to adjust model parameters, even in the event

of flow reversals, is quite robust.

Future development to the junction capabilities could involve the inclusion of other

forces acting on junctions included in Shabayek's junction formulations (e.g. centrifugal

pressure, interfacial shear, frictional shear). Although these inclusions may improve the

model accuracy they may come at the cost of operational practicality because of the

requirement for calibration of junction parameters. The absence of junction parameter

calibration made it relatively easy to apply *River1D* to a network of channels in the upper

MD.

The model of the upper MD was calibrated and validated for three open water periods.

For calibration and validation periods, the model showed good agreement with the

limited discharge and water level measurements. The validated model was used to

simulate flow conditions during the 2008 breakup in the MD. For the pre-jam and ice

jam conditions the modelled water surface profiles compared well with observed water

level data collected using data loggers but tended to overestimate the jam measurements

obtained from oblique photos. A comparison of the model flows for the pre-jam and ice

jam conditions suggests that ice jamming in the Turtle can significantly impact the

distribution of flow in the upper MD. For the ice jam conditions the flow reversed in the

Peel Mackenzie Connector. This reversal is consistent with observations in this channel during breakup. Future work could include using the available bathymetric information to input natural channel geometry within the reach of the Main Channel where ice jamming was observed in place of the approximated rectangular channel sections. This would allow for more accurate simulation of water surface elevations within the jamming reach with the available data. But in order to eliminate the need for the rectangular channel approximation, detailed bathymetric data throughout the MD is needed. This would also facilitate the inclusion of additional distributary channels that have not been considered in the current model. The work presented in this paper is expected to prove helpful towards the realization of *River1D* as a comprehensive public-domain river ice process model capable of simulating dynamic ice processes in complex natural river network systems.
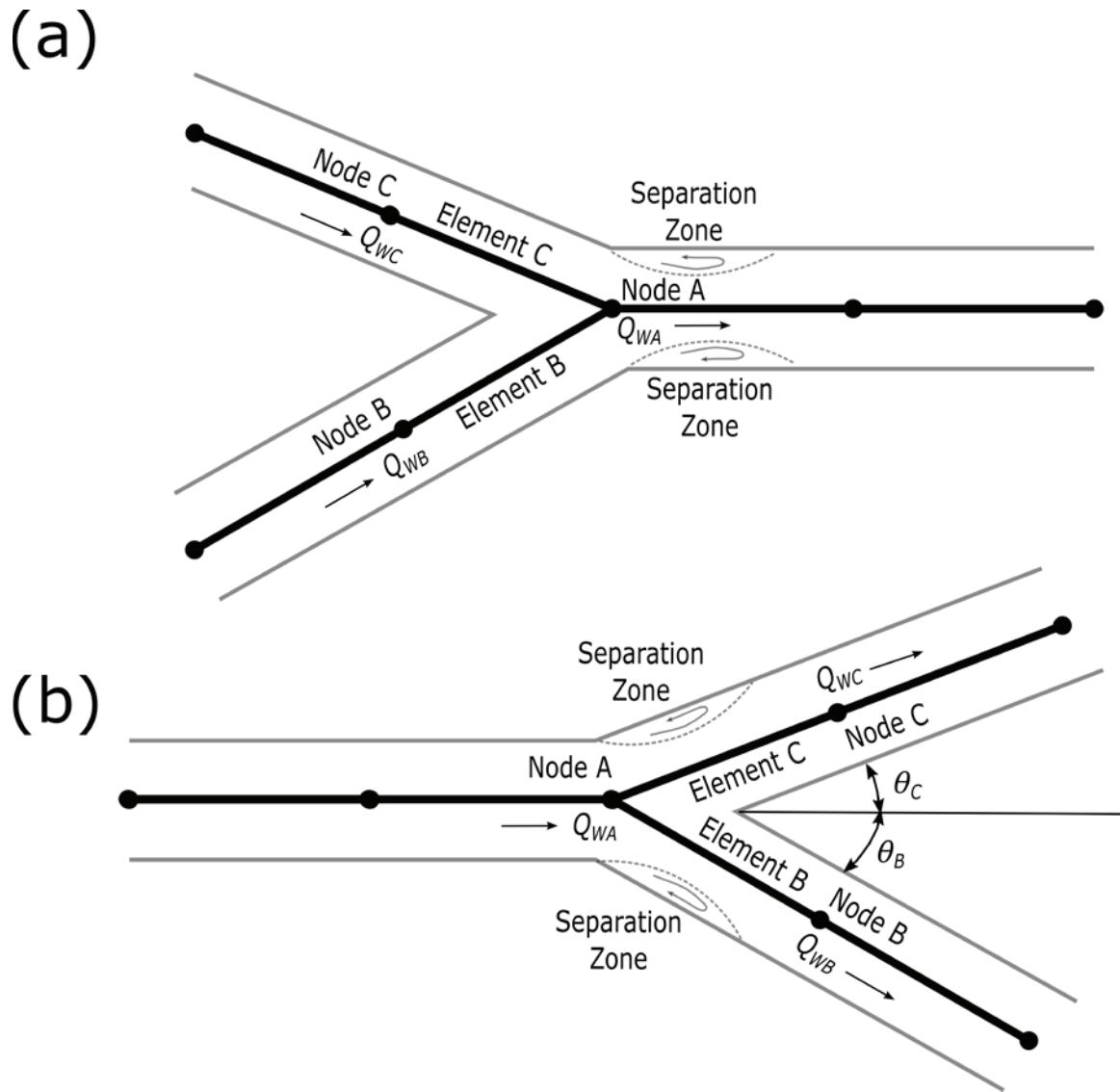
Figure 3.1: Plan view model junction configurations for (a) converging junctions and (b) diverging junctions.
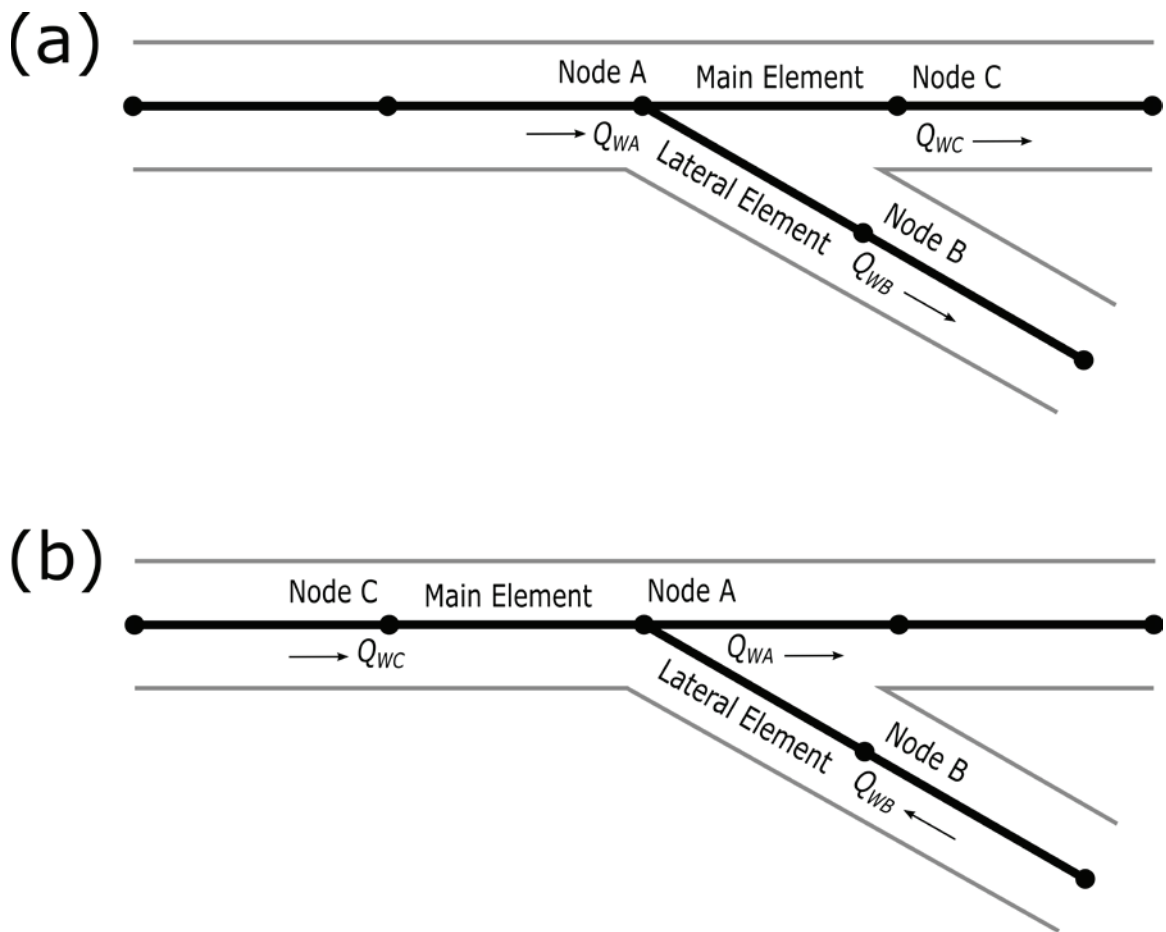
Figure 3.2: Model junction reconfiguration from a) diverging junction to b) converging junction when flow reverses at node B.
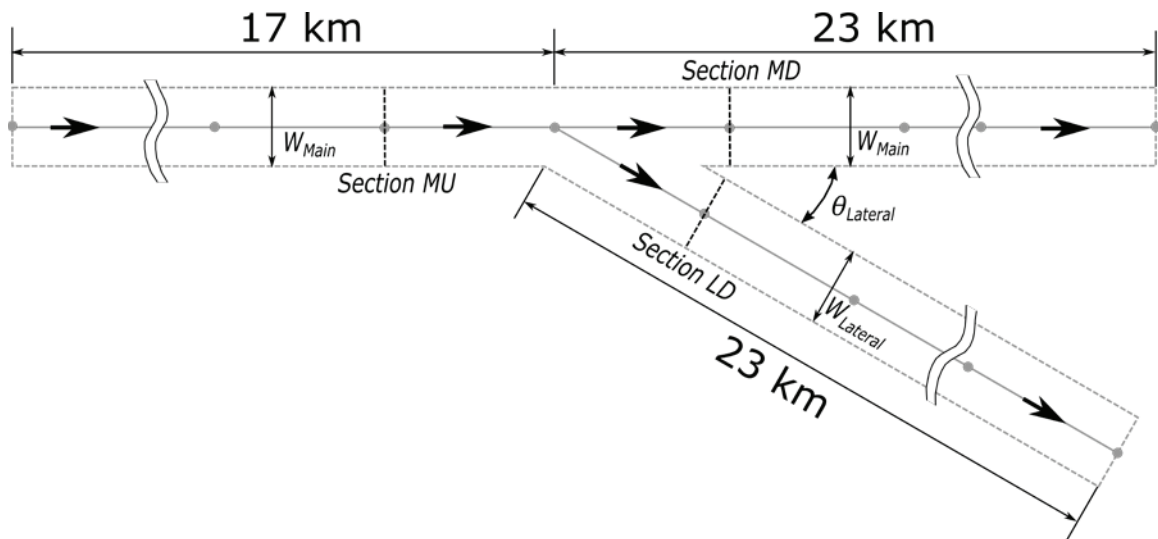
Figure 3.3: General plan view configuration for diverging junction tests.
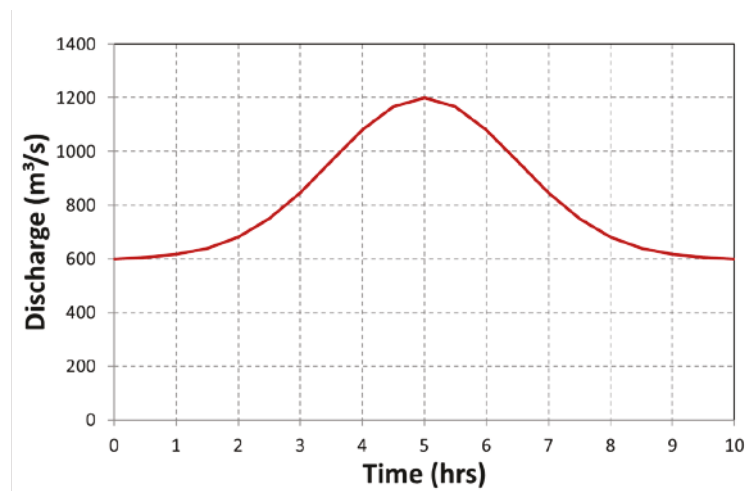
Figure 3.4: Inflow hydrograph for unsteady diverging junction tests.
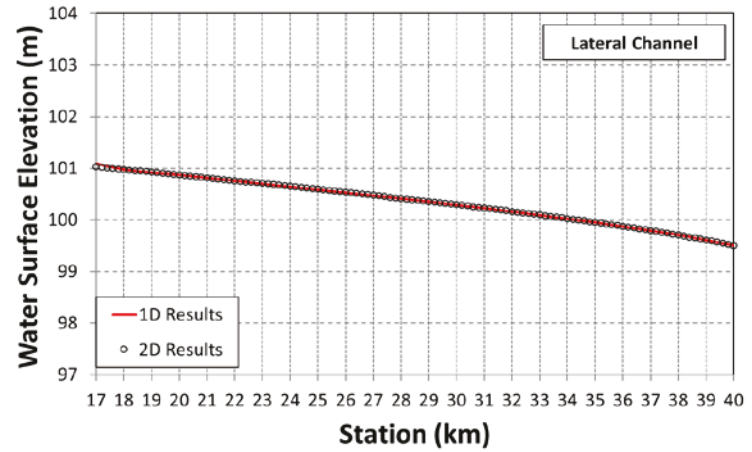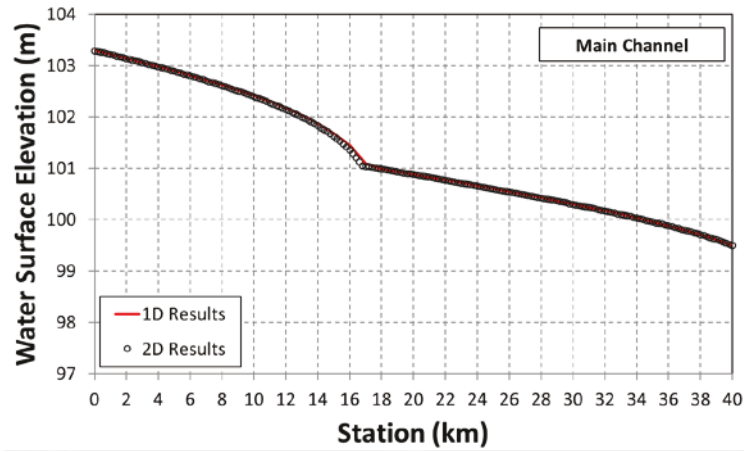
Figure 3.5: Steady water surface elevation profiles for the main and lateral channels for test DS15.
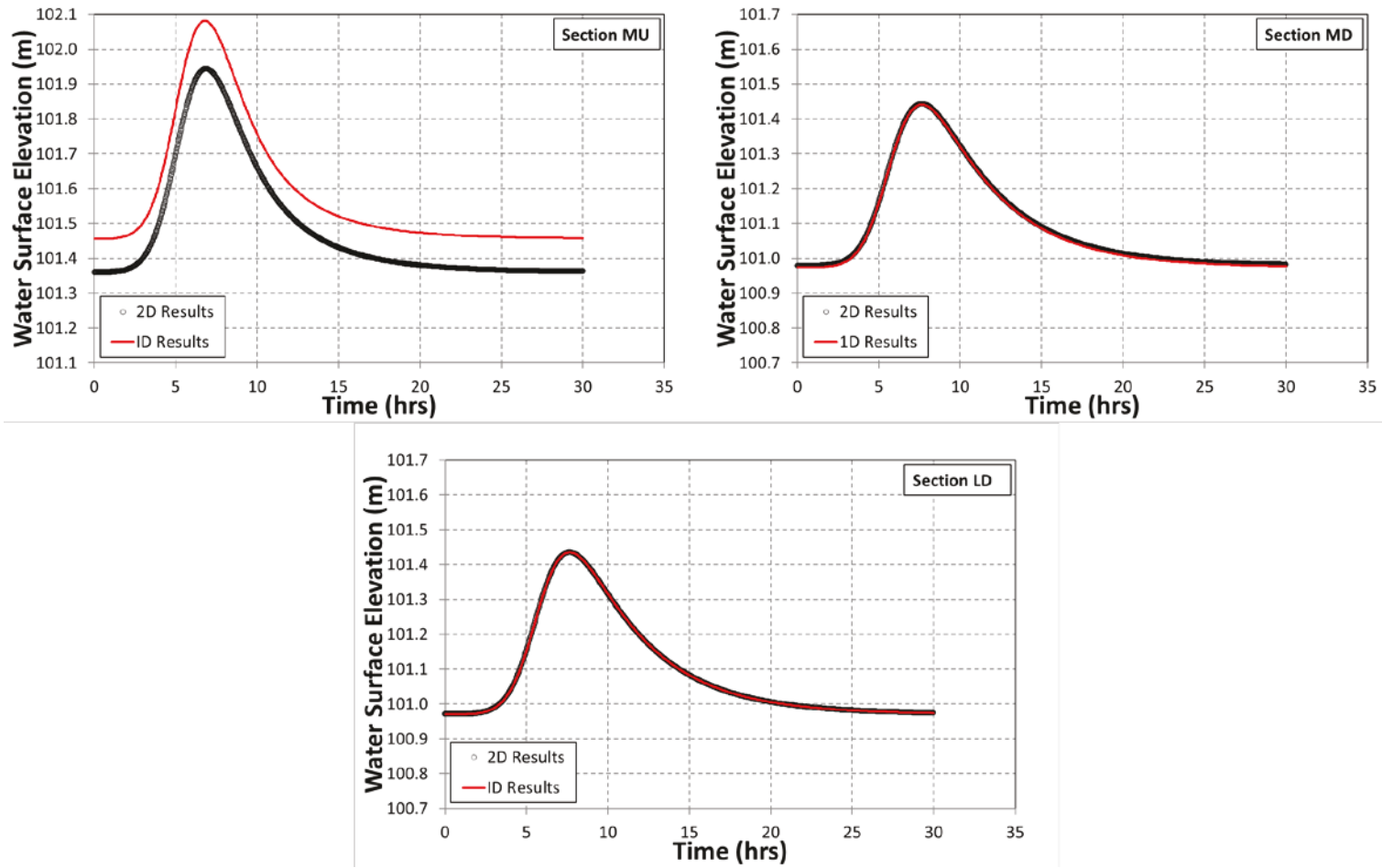
Figure 3.6: Water surface elevation hydrographs at output sections for test DT3.
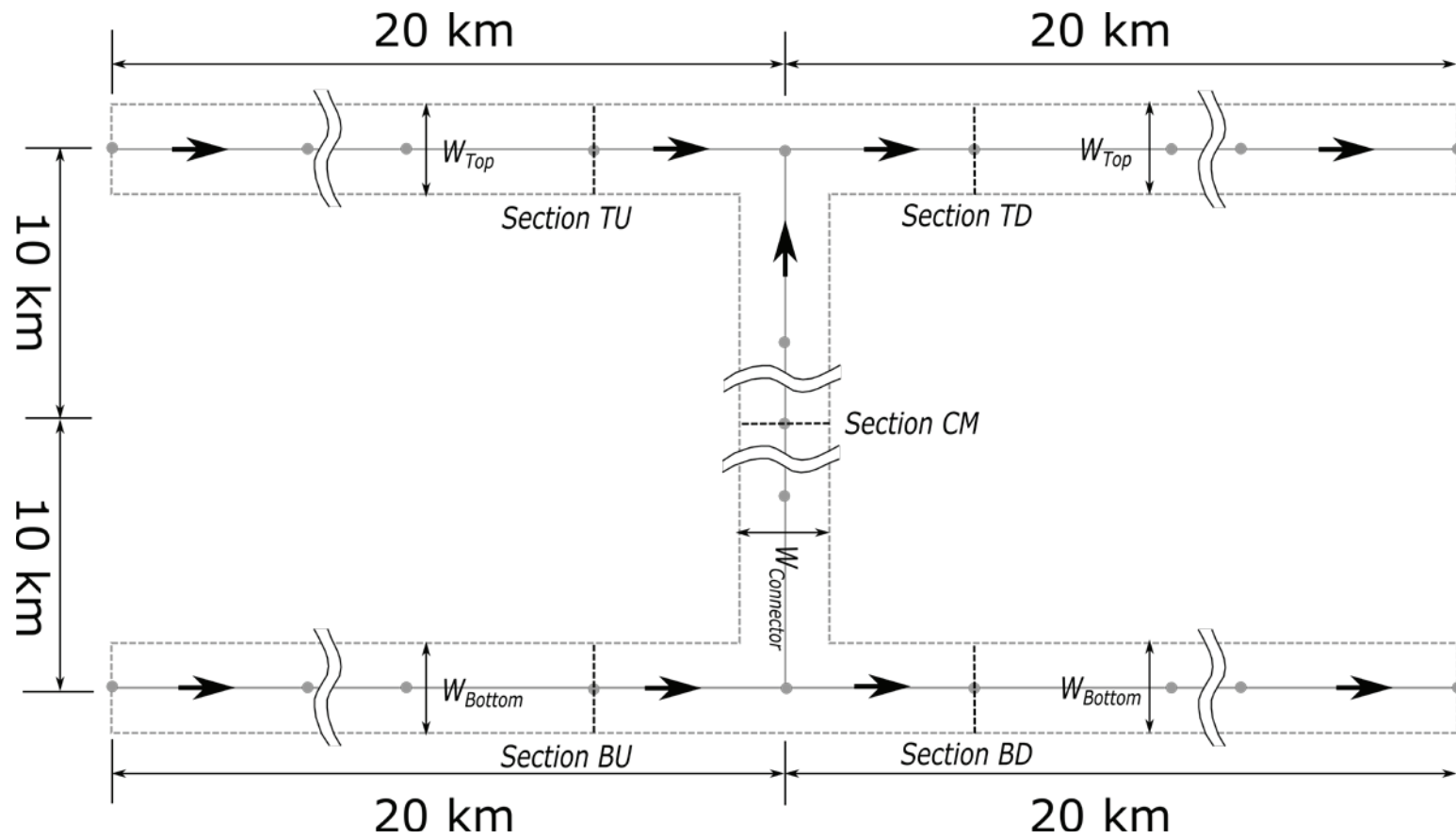
Figure 3.7: Plan view configuration for the two parallel channels with a perpendicular connecting channel test scenario.
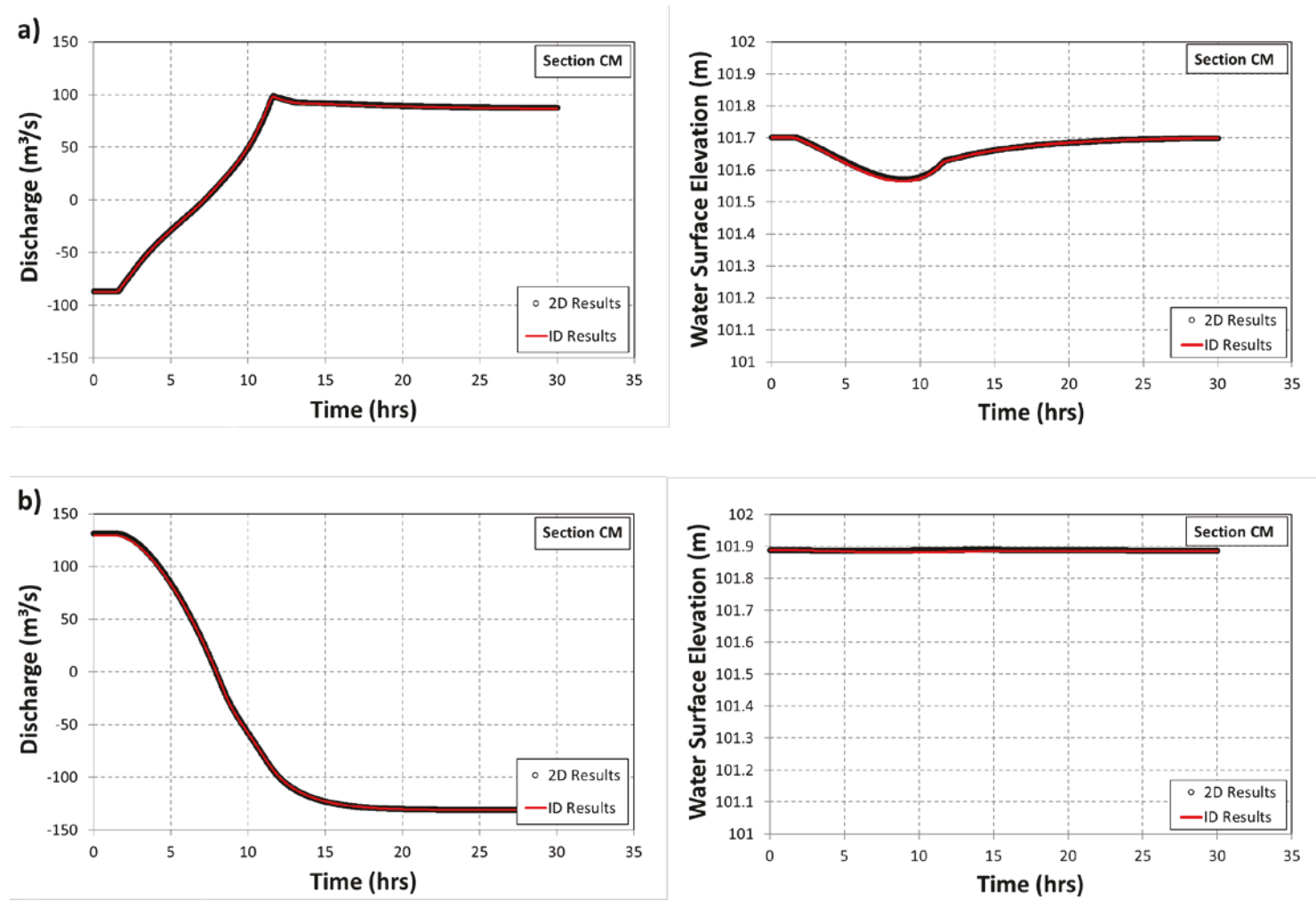
Figure 3.8: Two parallel channels with a perpendicular connecting channel discharge and water surface elevation hydrographs at section CM for unsteady tests: a) PPT1 and b) PPT2.

138
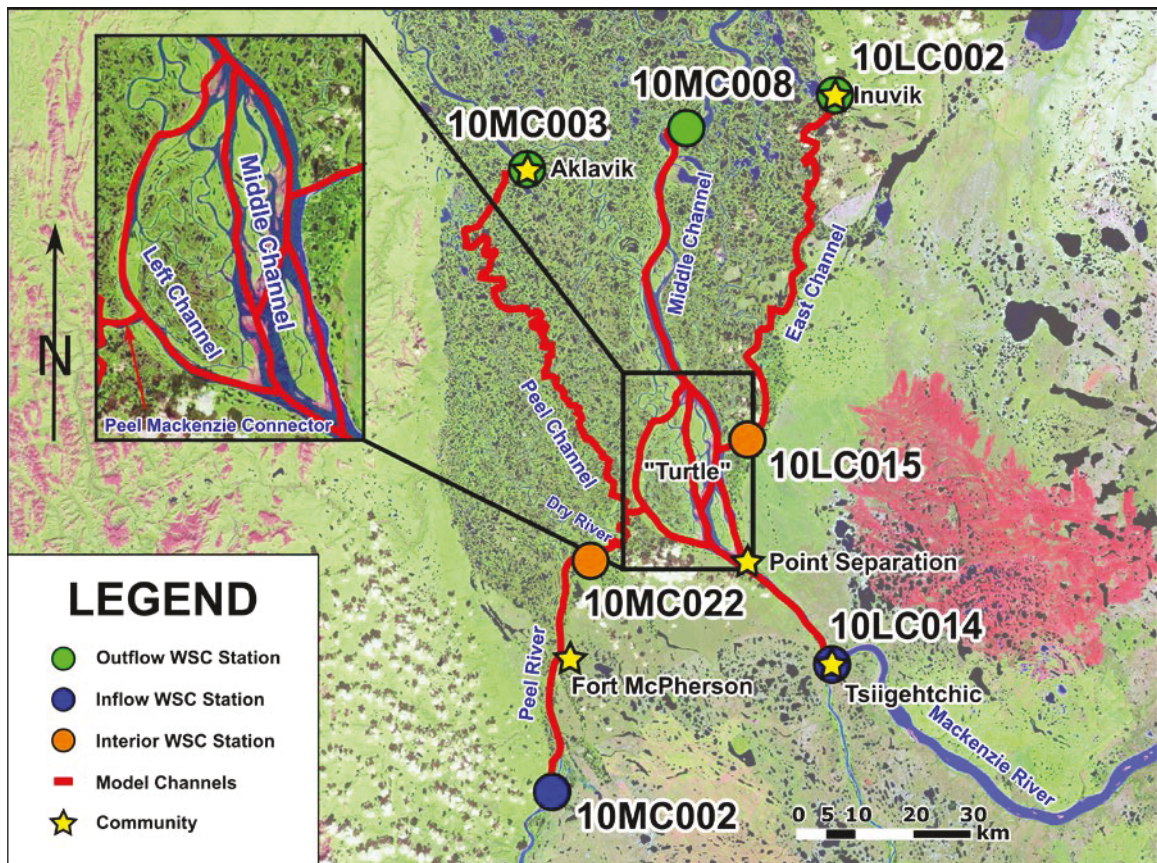
Figure 3.9: Location Map for the MD model with model channels, boundary locations and associated Water Survey of Canada gauging stations.
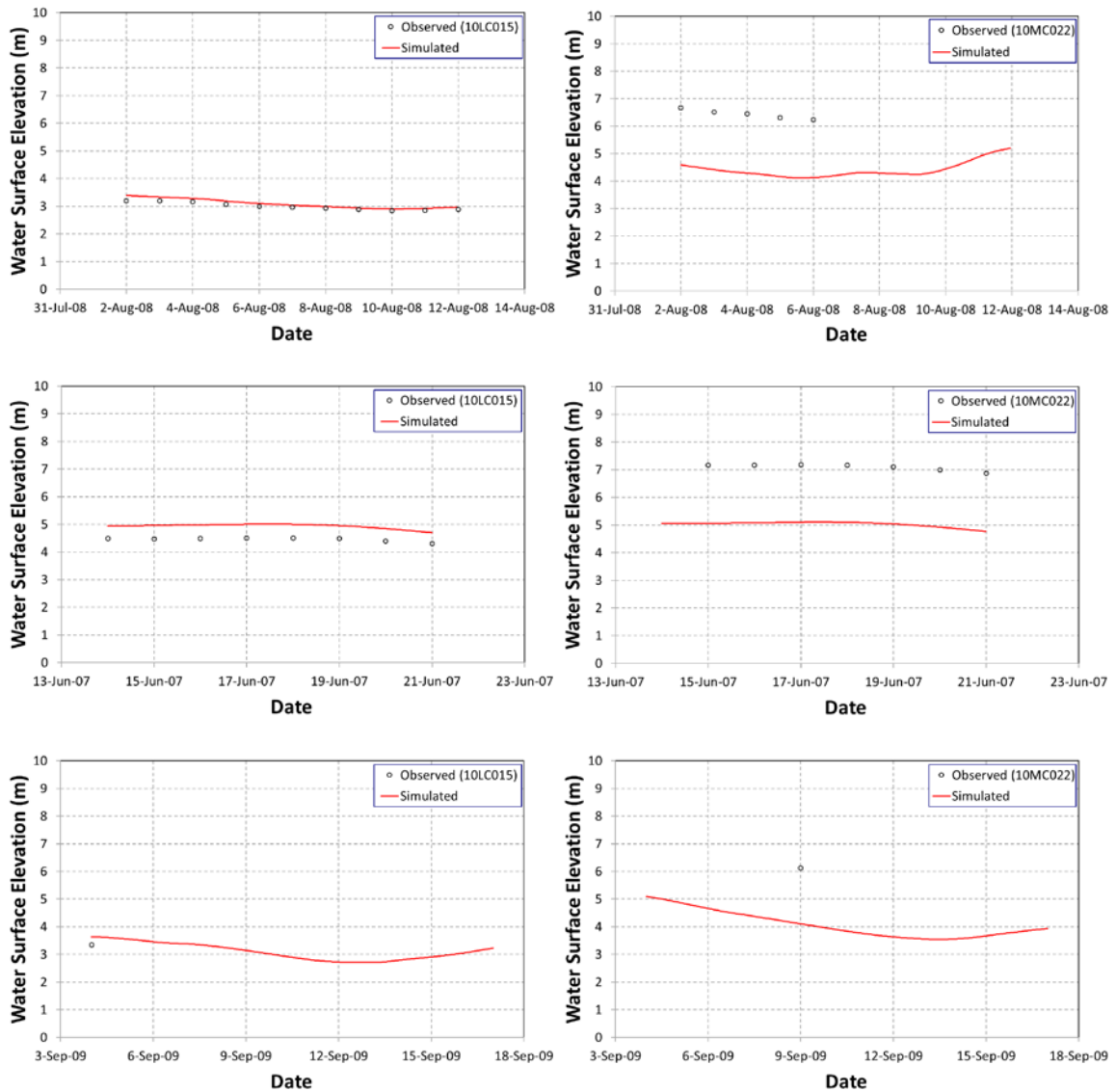
Figure 3.10: Simulated and observed water surface elevation hydrographs at 10LC015 and 10MC002 for the calibration and validation periods (with elevations referenced to CGG05).
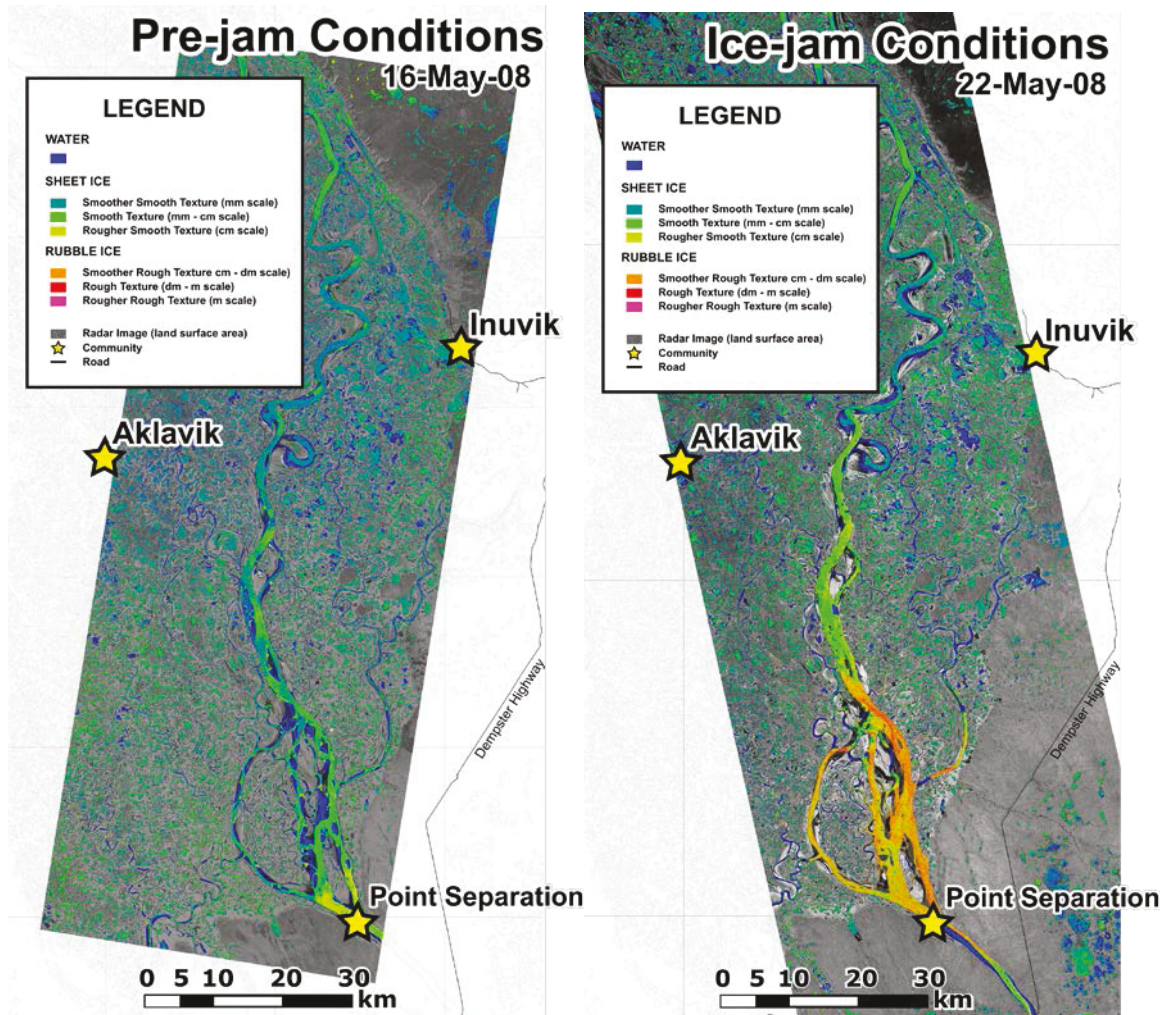
Figure 3.11: Ice cover condition maps for May 16 (Pre-jam Conditions) and May 22 (Ice jam Conditions) adapted from van der Sanden and Drouin (2011).
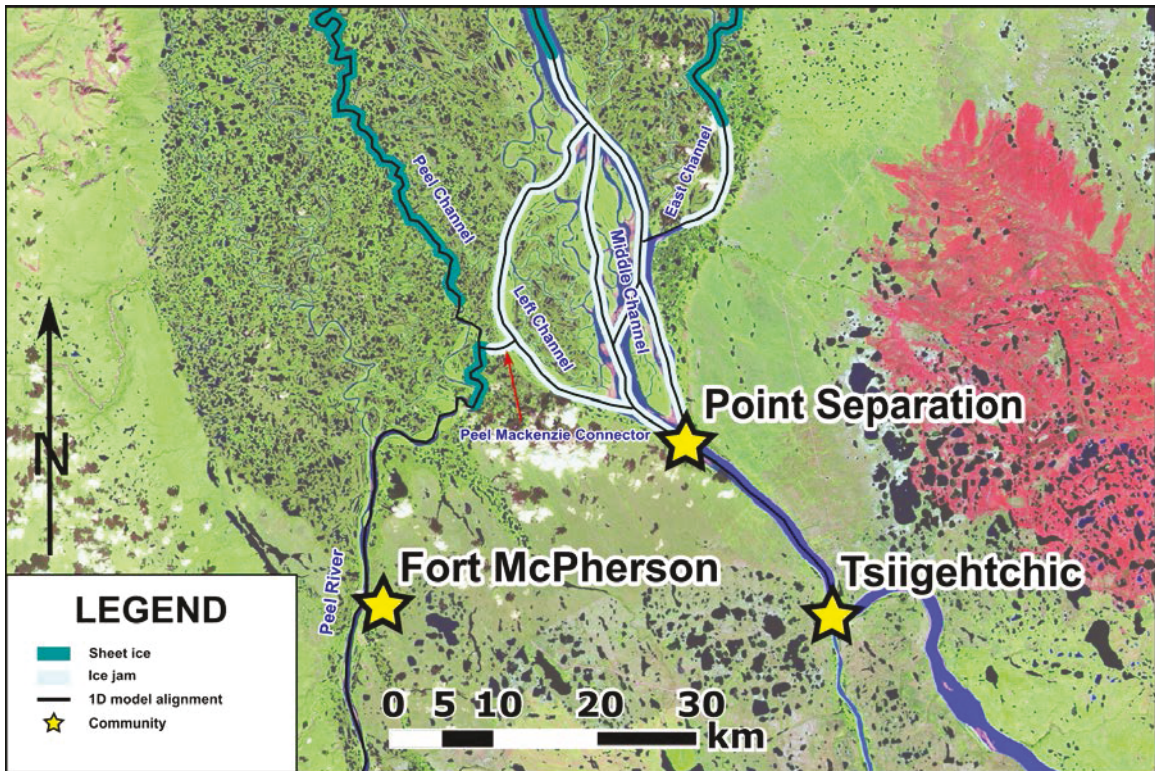
Figure 3.12: Model ice configuration in the Turtle area for the May 22 Ice jam conditions.
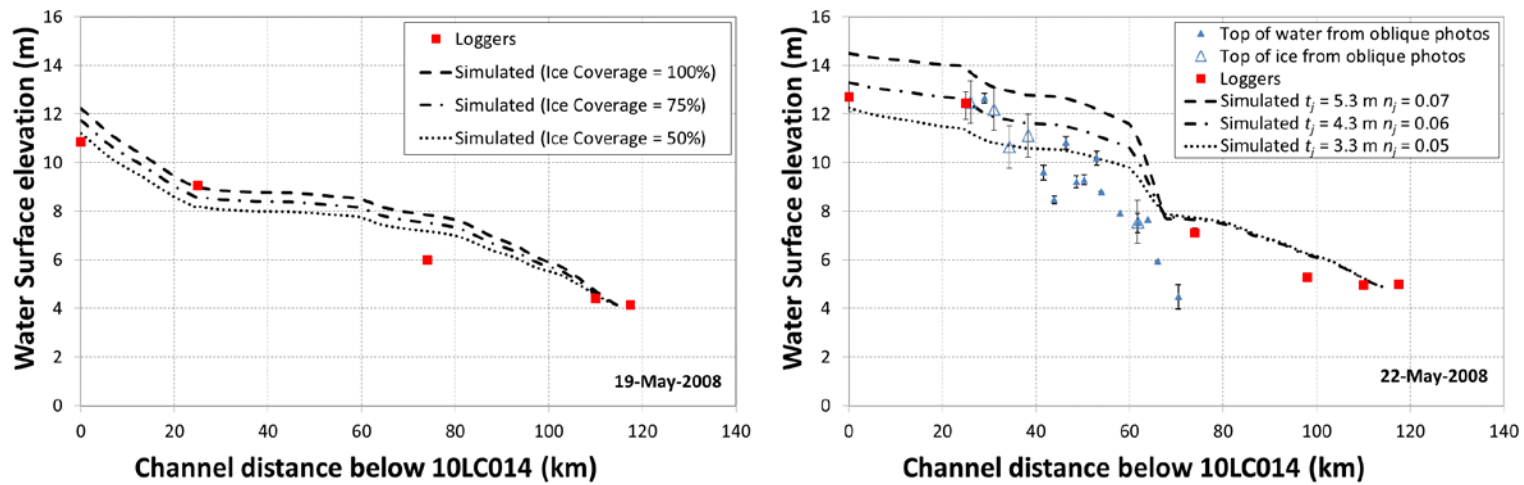
Figure 3.13: Water surface profiles of the Middle Channel for May 19 and May 22, 2008 with elevations referenced to CGG05.

Tables

Table 3.1: Test configurations for steady and unsteady diverging junction tests.

Test Configuration	Test Parameters				
	θ	W_{Main} (m)	$W_{Lateral}$ (m)	S_{oMain}	$S_{oLateral}$
1	30º	250	250	0.00005	0.00005
2	30º	250	250	0.00005	0.000025
3	30º	250	500	0.00005	0.00005
4	30º	250	500	0.00005	0.000025
5	45º	250	250	0.00005	0.00005
6	45º	250	250	0.00005	0.000025
7	45º	250	500	0.00005	0.00005
8	45º	250	500	0.00005	0.000025
9	60º	250	250	0.00005	0.00005
10	60º	250	250	0.00005	0.000025
11	60º	250	500	0.00005	0.00005
12	60º	250	500	0.00005	0.000025
13	75º	250	250	0.00005	0.00005
14	75º	250	250	0.00005	0.000025
15	75º	250	500	0.00005	0.00005
16	75º	250	500	0.00005	0.000025
17	90º	250	250	0.00005	0.00005
18	90º	250	250	0.00005	0.000025
19	90º	250	500	0.00005	0.00005
20	90º	250	500	0.00005	0.000025

Table 3.2: Diverging junction steady test results.

(*Continued on next page*).

Test	1D Results						2D Results					
	Q_{LD} (m³/s)	Q_{MD} (m³/s)	Q_{MU} (m³/s)	D_{LD} (m)	D_{MD} (m)	D_{MU} (m)	Q_{LD} (m³/s)	Q_{MD} (m³/s)	Q_{MU} (m³/s)	D_{LD} (m)	D_{MD} (m)	D_{MU} (m)
DS1	299.50	300.50	600.00	2.333	2.337	2.530	299.60	300.43	600.00	2.338	2.341	2.498
DS2	269.17	330.83	600.00	2.455	2.462	2.621	268.86	331.11	600.00	2.457	2.467	2.594
DS3	399.54	200.46	600.00	1.871	1.874	2.256	400.15	199.95	600.00	1.879	1.878	2.160
DS4	366.74	233.26	600.00	2.036	2.037	2.338	365.97	234.18	600.01	2.037	2.046	2.257
DS5	298.92	301.08	600.00	2.332	2.340	2.528	299.21	300.79	600.02	2.336	2.343	2.490
DS6	268.68	331.32	600.00	2.454	2.464	2.619	268.88	331.14	600.02	2.457	2.467	2.587
DS7	398.99	201.01	600.00	1.871	1.878	2.255	399.90	200.23	600.03	1.879	1.880	2.159
DS8	366.27	233.73	600.00	2.035	2.039	2.336	366.16	233.98	600.04	2.038	2.046	2.256
DS9	298.15	301.85	600.00	2.331	2.344	2.526	298.65	301.55	600.00	2.333	2.347	2.487
DS10	268.05	331.95	600.00	2.452	2.467	2.618	268.46	331.69	599.99	2.454	2.470	2.585
DS11	398.27	201.73	600.00	1.870	1.882	2.253	399.38	200.67	599.95	1.878	1.883	2.159
DS12	365.64	234.36	600.00	2.034	2.043	2.334	365.96	234.18	599.92	2.038	2.047	2.256

Table 3.2: Diverging junction steady test results (*continued*).

Test	1D Results						2D Results					
	Q_{LD} (m³/s)	Q_{MD} (m³/s)	Q_{MU} (m³/s)	D_{LD} (m)	D_{MD} (m)	D_{MU} (m)	Q_{LD} (m³/s)	Q_{MD} (m³/s)	Q_{MU} (m³/s)	D_{LD} (m)	D_{MD} (m)	D_{MU} (m)
DS13	297.26	302.74	600.00	2.329	2.349	2.524	298.19	301.82	599.90	2.332	2.348	2.483
DS14	267.32	332.68	600.00	2.450	2.471	2.616	268.14	331.84	599.89	2.453	2.470	2.582
DS15	397.42	202.58	600.00	1.869	1.887	2.250	398.74	201.20	599.95	1.876	1.887	2.153
DS16	364.91	235.09	600.00	2.033	2.047	2.332	365.53	234.42	599.97	2.037	2.049	2.252
DS17	296.31	303.69	600.00	2.326	2.354	2.522	297.48	302.38	599.89	2.327	2.351	2.480
DS18	266.53	333.47	600.00	2.448	2.475	2.614	267.68	332.14	599.88	2.451	2.472	2.578
DS19	396.51	203.49	600.00	1.868	1.893	2.247	397.20	202.92	599.96	1.872	1.895	2.155
DS20	364.12	235.88	600.00	2.032	2.052	2.330	364.33	235.95	599.96	2.033	2.056	2.256

Table 3.3: Diverging junction unsteady test results.

Test	Root Mean Square Error (RMSE)					
	RMSE for Water Surface Elevation (m)			RMSE for Discharge (m³/s)		
	Section LD	Section MD	Section MU	Section LD	Section MD	Section MU
DT1	0.004	0.004	0.033	0.77	0.81	1.36
DT2	0.002	0.005	0.028	0.74	0.87	1.34
DT3	0.008	0.004	0.101	1.15	0.86	1.45
DT4	0.001	0.010	0.085	1.09	0.98	1.41
DT5	0.004	0.003	0.039	0.86	1.02	1.31
DT6	0.003	0.003	0.034	0.76	1.05	1.27
DT7	0.008	0.003	0.100	1.53	1.25	1.47
DT8	0.003	0.006	0.084	1.05	0.91	1.42
DT9	0.003	0.003	0.039	1.09	0.94	1.30
DT10	0.003	0.003	0.034	0.97	0.99	1.27
DT11	0.007	0.003	0.097	1.76	1.52	1.43
DT12	0.003	0.004	0.081	1.25	1.09	1.38
DT13	0.004	0.004	0.040	1.35	1.48	1.26
DT14	0.003	0.004	0.034	1.20	1.48	1.22
DT15	0.006	0.003	0.099	2.00	1.67	1.40
DT16	0.004	0.003	0.082	1.55	1.22	1.34
DT17	0.003	0.006	0.042	1.58	1.91	1.25
DT18	0.004	0.006	0.036	1.51	2.00	1.22
DT19	0.004	0.003	0.092	1.96	0.81	1.34
DT20	0.004	0.004	0.074	1.74	0.66	1.29

Table 3.4: Two parallel channels with a perpendicular connecting channel steady test boundary conditions.

Test #	Inflow Boundary Conditions		Outflow Boundary Conditions	
	Q_{TOP} (m³/s)	Q_{BOTTOM} (m³/s)	D_{TOP} (m)	D_{BOTTOM} (m)
PPS1	300	300	1.5	1.5
PPS2	300	300	1.5	3.5
PPS3	300	300	3.5	1.5
PPS4	600	300	1.5	1.5
PPS5	300	600	1.5	1.5

Table 3.5: Two parallel channels with a perpendicular connecting channel steady test results.

| Test # | 1D Results |
	Q_{CM} (m³/s)	Q_{TU} (m³/s)	Q_{TD} (m³/s)	Q_{BU} (m³/s)	Q_{BD} (m³/s)	D_{CM} (m)	D_{TU} (m)	D_{TD} (m)	D_{BU} (m)	D_{BD} (m)
PPS1	0.00	300.00	300.00	300.00	300.00	2.322	2.331	2.312	2.331	2.312
PPS2	86.21	300.00	386.21	300.00	213.79	2.703	2.667	2.639	2.719	2.768
PPS3	-87.50	300.00	212.50	300.00	387.50	2.701	2.722	2.764	2.659	2.647
PPS4	-131.21	600.00	468.79	300.00	431.21	2.885	3.009	2.921	2.811	2.800
PPS5	129.53	300.00	429.53	600.00	470.47	2.888	2.820	2.790	3.001	2.930

| Test # | 2D Results |
	Q_{CM} (m³/s)	Q_{TU} (m³/s)	Q_{TD} (m³/s)	Q_{BU} (m³/s)	Q_{BD} (m³/s)	D_{CM} (m)	D_{TU} (m)	D_{TD} (m)	D_{BU} (m)	D_{BD} (m)
PPS1	0.10	299.99	300.07	300.00	299.91	2.330	2.331	2.313	2.331	2.312
PPS2	86.93	299.98	386.88	300.01	213.07	2.703	2.654	2.644	2.713	2.767
PPS3	-86.85	299.98	213.16	300.01	386.85	2.702	2.713	2.767	2.654	2.644
PPS4	-131.10	599.97	468.88	300.00	431.10	2.887	2.983	2.925	2.808	2.799
PPS5	131.33	299.98	431.29	600.01	468.65	2.889	2.808	2.799	2.982	2.924

Table 3.6: Two parallel channels with a perpendicular connecting channel unsteady test boundary conditions.

Test #	Inflow Boundary Conditions		Outflow Boundary Conditions	
	Q_{TOP} (m³/s)	Q_{BOTTOM} (m³/s)	D_{TOP} (m)	D_{BOTTOM} (m)
PPT1	300	300	3.5 to 1.5	1.5 to 3.5
PPT2	300 to 600	600 to 300	1.5	1.5

Table 3.7: Two parallel channels with a perpendicular connecting channel unsteady test results.

Test	Evaluation Statistic									
	RMSE for Water Surface Elevation (m)					RMSE for Discharge (m³/s)				
	Section CM	Section TU	Section TD	Section BU	Section BD	Section CM	Section TU	Section TD	Section BU	Section BD
PPT1	0.003	0.011	0.005	0.005	0.002	0.71	0.65	0.79	0.34	0.90
PPT2	0.003	0.021	0.005	0.008	0.003	0.79	0.66	0.93	0.26	0.91

Table 3.8: Water Survey of Canada gauging stations in the upper MD.

Station Number	Station Name	Type	Conversion to CGG05 datum (m)
10LC014	MACKENZIE RIVER AT ARCTIC RED RIVER	Flow & Level	-0.024
10MC002	PEEL RIVER ABOVE FORT MCPHERSON	Flow & Level	0.074
10LC015	MACKENZIE RIVER AT CONFLUENCE EAST CHANNEL	Level	-0.824
10MC022	PEEL RIVER AT FROG CREEK	Level	2.336
10MC003	MACKENZIE RIVER (PEEL CHANNEL) ABOVE AKLAVIK	Flow & Level	-10.056
10MC008	MACKENZIE RIVER (MIDDLE CHANNEL) BELOW RAYMOND CHANNEL	Flow & Level	-10.346
10LC002	MACKENZIE RIVER (EAST CHANNEL) AT INUVIK	Flow & Level	-10.856

Table 3.9: Simulated and measured values for the open water calibration and validation.

(*Continued on next page*).

Calibration Period (2-Aug-08 to 12-Aug-08)

Location	Time of Measurement	$Q_{measured}$ (m³/s)	$Q_{simulated}$ (m³/s)	$H_{measured}$ (m)	$H_{simulated}$ (m)	$Q_{total\ inflow}$ (m³/s)	RE (%)
Middle Channel below East Channel	2-Aug-08 19:30	7961	7741			15504	-1.4
Mackenzie River (Middle Channel) Below Raymond Channel (10MC008)[a]	12-Aug-08 15:00	13000	13454	1.349	1.355	14941	3.0
Mackenzie River at Confluence East Channel (10LC015) [a]	2-Aug-08 20:45	577	595	3.201	3.341	15504	0.1
Mackenzie River (East Channel) at Inuvik (10LC002) [a]	7-Aug-08 15:18	209	535	1.262	1.243	14485	2.2
Peel River at Frog Creek (10MC022) [a]	2-Aug-08 14:15	1443	1394	6.663	4.488	15504	-0.3
Peel River above Dry River	2-Aug-08 14:55	1415	1392			15504	-0.2
Peel River below Dry River	2-Aug-08 16:00	1384	1387			15504	0.0
Peel Channel below of Connector	2-Aug-08 16:30	652	780			15504	0.8
Mackenzie River (Peel Channel) above Aklavik (10MC003) [a]	12-Aug-08 12:00	973	865	1.204	1.202	14941	-0.7
Peel Mackenzie Connector	2-Aug-08 17:05	707	607			15504	-0.6
Left Channel	2-Aug-08 19:30	1019	1088			15504	0.4

Table 3.9: Simulated and measured values for the open water calibration and validation *(continued)***.**

Validation Period #1 (14-Jun-07 to 21-Jun-07)

Location	Time of Measurement	$Q_{measured}$ (m³/s)	$Q_{simulated}$ (m³/s)	$H_{measured}$ (m)	$H_{simulated}$ (m)	$Q_{total\ inflow}$ (m³/s)	RE (%)
Mackenzie River (Middle Channel) Below Raymond Channel (10MC008) [a]	14-Jun-07 13:09	16900	20995	2.629	2.619	23127	17.7
Mackenzie River at Confluence East Channel (10LC015) [a]	15-Jun-07 16:55	1110	1084	4.475	4.965	23424	-0.1
Mackenzie River (East Channel) at Inuvik (10LC002) [a]	21-Jun-07 17:07	409	1003	2.038	2.048	21452	2.8
Peel River at Frog Creek (10MC022) [a]	15-Jun-07 14:39	725	717	7.164	5.066	23424	0.0

Validation Period #2 (4-Sep-09 to 17-Sep-09)

Location	Time of Measurement	$Q_{measured}$ (m³/s)	$Q_{simulated}$ (m³/s)	$H_{measured}$ (m)	$H_{simulated}$ (m)	$Q_{total\ inflow}$ (m³/s)	RE (%)
Middle Channel below East Channel	8-Sep-09 14:55	7390	7535			14988	1.0
Mackenzie River at Confluence East Channel (10LC015) [a]	4-Sep-09 13:05	639	675			17068	0.2
Peel Mackenzie Connector	9-Sep-09 14:47	433	432			14400	0.0
Left Channel	9-Sep-09 13:45	1100	1063			14400	-0.3

[a] Location is coincident with gauge location but measured values were from the manual flow measurement campaign instead of gauge data.

Table 3.10: Boundary conditions for 2008 breakup simulations.

Boundary Location and Type	May 19 (pre-jam conditions) (m³/s or m)	May 22 (ice jam conditions) (m³/s or m)	Notes
Discharge at Mackenzie River at Artic Red River (10LC014)	28,600	29,000	mean daily flow from Beltaos et al. (2012)
Discharge at Peel River Above Fort McPherson (10MC002)	2775	2925	75% of reported mean daily gauge flow
Water level at Mackenzie River (Peel Channel) Above Aklavik (10MC003)	2.722	3.468	mean daily gauge level adjusted to CGG05
Water level at Mackenzie River (Middle Channel) Below Raymond Channel (10MC008)	4.140	4.863	mean daily gauge level adjusted to CGG05
Water Level at Mackenzie River (East Channel) at Inuvik (10LC002)	3.272	3.992	mean daily gauge level adjusted to CGG05

Table 3.11: Model ice thicknesses for 2008 breakup simulations.

Channel	Sheet ice thickness, t_s (m)	Ice jam thickness, t_j (m)
Middle and Turtle Channels	0.92[a]	4.3
East Channels	1.11	4.3
West / Peel	0.79	Not applicable
West Middle Connector	0.79	4.3

[a] average of 0.43 m and 1.40 m

Table 3.12: Model flows for pre-jam and ice jam conditions at various locations in the MD.

Location	Pre-jam conditions (May 19) (m³/s)	Ice-jam conditions (May 22) (m³/s)	Change in flow (m³/s)
East Channel (10LC015)	1583	2115	532
Peel Mackenzie Connector	1128	-24	-1152
Left Channel above Connector	2848	3534	686
Peel Channel below Connector	1647	2949	1302
Middle Channel below Turtle	28114	26861	-1253

References

Andrishak, R., Hicks, F. 2011. Ice effects on flow distributions within the Athabasca Delta, Canada. River Research and Applications 27: 1149-1158.

Beltaos, S. 2001. Hydraulic Roughness of Breakup Ice Jams. Journal of Hydraulic Engineering. 127 (8): 650-656.

Beltaos, S. 2012. Mackenzie Delta flow during spring breakup: uncertainties and potential improvements. Canadian Journal of Civil Engineering. 39 (5): 579-588

Beltaos, S., Carter, T. 2009. Field studies of ice breakup and jamming in the Mackenzie Delta. Proceedings of the 15th Workshop on River Ice, St. John's, NL, 266-283.

Beltaos, S., Carter, T., & Rowsell, R. 2012. Measurements and analysis of ice breakup and jamming characteristics in the Mackenzie Delta, Canada. Cold Regions Science and Technology, 82: 110-123.

Blackburn, J., She, Y., Hicks, F., Nafziger, J. 2015. Ice effects on flow distributions in the Mackenzie Delta. In: 18th CGU-HS Committee on River Ice Processes and the Environment Proc., 18th Workshop on the Hydraulics of Ice Covered Rivers, Quebec City, Quebec, August 18-20, 2015.

Blackburn, J., She, Y. 2019. A comprehensive public-domain river ice process model and its application to a complex natural river. Cold Regions Science and Technology. 163: 44-58.

Brayall, M., Hicks, F.E. 2012. Applicability of 2-D modeling for forecasting ice jam flood levels in the Hay River Delta, Canada. Canadian Journal of Civil Engineering, 39: 701-712.

Brunner, G.W. 2020b. HEC-RAS River Analysis System User's Manual Version 6.0 Beta. U.S. Army Corps of Engineers Hydrologic Engineering Center. 721 pp.

De Coste, M., She, Y., Blackburn, J. 2017. Incorporating the effects of upstream ice jam releases in the prediction of flood levels in the Hay River delta, Canada. Canadian Journal of Civil Engineering, 44: 643-651.

DHI, 2021. MIKE 11, A Modelling System for Rivers and Channels, Reference Manual, 500 pp.

Dow, K., Steffler, P.M., Zhu, D.Z. 2009. Case Study: Intermediate Field Mixing for a Bank Discharge in a Natural River. Journal of Hydraulic Engineering, 135(1): 1-12.

Emmerton, C.A., Lesack, L.F.W., Marsh, P. 2007. Lake abundance, potential water storage, and habitat distribution in the Mackenzie River Delta, western Canadian Arctic. Water Resources Research 43, W05419, 14 pp.

Ettema, R. Muste, M., Kruger, A. 1999. Ice jams in river confluences. US Army Corps of Engineering, Cold Regions Research and Engineering Laboratory, Report 99-06, 61 pp.

Fread, D.L. 1988. The NWS DAMBRK Model: Theoretical Background/User Documentation. Office of Hydrology, National Weather Service (NWS), Maryland, U.S.A.

Garcia-Navarro, M. P., Savirón, J. M. 1992. Numerical simulation of unsteady flow at open channel junctions. Journal of Hydraulic Research, 30(5): 595-609.

Ghostine, R., Kesserwani, G., Mose, R., Vazquez, J., Ghenaim, A., Gregoire, C. 2009. A confrontation of 1D and 2D RKDG numerical simulation of transitional flow at open-channel junction. International Journal for Numerical Methods in Fluids, 61: 752-767.

Ghostine, R., Vazquez, J., Nicolas, R., Terfous, A., Ghenaim, A., Mose, R. 2013. A comparative study of the 1D and 2D approaches for simulation of flows at right angled dividing junctions. Applied Mathematics and Computation, 219 (2013): 5070-5082.

Goulding, H., Prowse, T., Beltaos, S. 2009. Spatial and temporal patterns of breakup and ice jam flooding in the Mackenzie Delta, NWT. Hydrologic Processes, 23(18): 2555-2704.

Gurram, S.K., Karki, K.S., Hager, W.H. 1997. Subcritical junction flow. ASCE Journal of Hydraulic Engineering, 123(5): 447-455.

Heine, M., Andre, A., Kritsch, I., Cardinal, A. 2007. Gwichya Gwich'in Googwandak. The History and Stories of the Gwichya Gwich'in, 405 pp.

Hicks, F. E. 1996. Hydraulic flood routing with minimal channel data: Peace River, Canada. Canadian Journal of Civil Engineering, 23(2): 524-535.

Hicks, F.E., Steffler, P.M. 1990. Finite element modeling of open channel now. Water Resources Engineering Report No. 90-6. Department of Civil Engineering, University of Alberta, Edmonton, AB, 356 pp.

Hicks, F.E., Steffler, P.M. 1992. A Characteristic Dissipative Galerkin Scheme for Open Channel Flow. ASCE Journal of Hydraulic Engineering, 118: 337-352.

Holmquist, J.G., Waddle, T.J. 2013. Predicting macroinvertebrate response to water diversion from a mountain stream using two-dimensional hydrodynamic models and zero flow approximation. Ecological Indicators, 28: 115-124.

Hsu, C.C., Lee W.J., Chang C.H. 1998. Subcritical open-channel junction flow. ASCE Journal of Hydraulic Engineering, 124(8): 847-855.

Huang, J., Weber, L.J., Lai, Y.G. 2002. Three-dimensional numerical study of flows in open-channel junctions, ASCE Journal of Hydraulic Engineering, 128 (2002): 268-280.

Kesserwani, G., Ghostine, R., Vasquez, J., Mosé, R., Abdallah, M. Ghenaim, A. 2008. Simulation of subcritical flow at open-channel junction. Advances in Water

Resources, 31 (2008): 287-297.Mackay, J. R. 1963. The Mackenzie Delta Area, N.W.T. Miscellaneous Report 23. Geological Survey of Canada, Ottawa, Ontario, 202 pp.

Law, S.W. 1965. Dividing flow in an open channel. Thesis presented to McGill University, Montreal, Quebec, in partial fulfillment of the requirements for the degree of Masters of Engineering, 89 pp.

Morley, J. 2012. Observations of flow distributions and river breakup in the Mackenzie Delta, NWT. Master's Thesis, University of Alberta, Edmonton, Alberta, 288 pp.

Nafziger, J., Hicks, F., Andrishak, R., Marsh, P., Lesack, L. 2009. Hydraulic Model of River Flow and Storage Effects in the Mackenzie Delta, Canada. 17th International Northern Research Basins Symposium and Workshop, 1-10.

Nezhikhovskiy, R. A. 1964. Coefficients of roughness of bottom surface on slush-ice cover. Soviet Hydrology (American Geophysical Union), 127-150.

Pandey, A.K., Mohapatra, P.K., Jain, V., Bhatia, U. 2020. Studying subcritical opposing channel flows. Journal of Applied Water Engineering and Research, 8:4, 262-276.

Parkinson, F.E., Holder, G.K. 1982. Liard-Mackenzie winter regime study, final report. LHL 830. Prepared for British Columbia Hydro and Power Authority. Lasalle Hydraulic Laboratory Ltd., Montreal, Quebec.

Potok, A.J., Quinn, F.H. 1979. A Hydraulic Transient Model of the Upper St. Lawrence River for Water Resources Research, Water Resources Bulletin, American Water Resources Association, 15(6): 1538-1555.

Ramamurthy, A.S., Qu, J., Vo, D. 2007. Numerical and experimental study of dividing open-channel flows, ASCE Journal of Hydraulic Engineering, 133 (2007): 1135-1144.

Rivière, N., G. Travin, and R. J. Perkins. 2014. Transcritical Flows in Three and Four Branch Open-Channel Intersections. Journal of Hydraulic Engineering 140 (4): 04014003.

Shabayek, S. 2002. Conservation Equations for Subcritical Flow in Open Channel Junctions. PhD. thesis, University of Alberta, Edmonton, AB, 210 pp.

Shabayek, S., Steffler, P., Hicks, F. 2002. Dynamic model for subcritical combining flows in channel junctions. Journal of Hydraulic Engineering. 128(9): 821-828.

Shen, H.T. 2005. CRISSP1D programmer's manual. In CEATI Report No. T012700-0401. Department of Civil Engineering, Clarkson University, Potsdam, N.Y., 188 pp.

Taylor, E.H. 1944. Flow characteristics at rectangular open channel junctions. Trans. ASCE, 109: 893-902.

Terroux, A., Sherstone, D., Kent, T., Anderson, J., Bigras, S., & Kriwoken, L. 1981. Ice regime of the Lower Mackenzie River and Mackenzie Delta. The National Hydrology Research Institute, Environment Canada. Hull, Quebec, 115 pp.

Timalsina, N., Charmasson, J., Alfredsen, K.T. 2013. Simulation of the ice regime in a Norwegian regulated river. Cold Regions Science and Technology, 94: 61-73.

Turcotte, B., Morse, B. 2013. Ice jam mitigation at the St. Félicien Zoo. In: 17th CGU HS Committee on River Ice Processes and the Environment Proc., 17th Workshop on Hydraulics of Ice Covered Rivers, Edmonton, Alberta, July 21-24, 2013.

van der Sanden, J. J., Drouin, H. 2011. Spring 2008 Ice Cover Condition, Mackenzie River Delta, Northwest Territories, Canada. Remote sensing map set. Ottawa, ON.

Waddle, T. 2010. Field evaluation of a two-dimensional hydrologic model near boulders for habitat calculation. River Research and Applications, 26: 730-741.

Weber, L.J., Schumate, E.D., Mawer, N. 2001. Experiments on Flows at a 90° Open-Channel Junction. Journal of Hydraulic Engineering, 127(5): 340-350.

Yuan, S., Zhou, J., Hu, D., Zhu, S. 2020. An integral 1-D Eulerian-Lagrangian Method and Its Application to a Hydrodynamic River Network. Water 12, 542, 16 pp.

4. The Simulation of Ice Jam Profiles in Multi-channel Systems using a One-Dimensional Network Model

4.1 Introduction

For rivers in colder regions, ice jamming events can often pose a larger risk to flooding than open water events. This risk can come from both freeze-up and breakup ice jams though breakup jams tend to be more problematic because of the larger flows and large quantity and strength of ice during spring. A channel's capacity to convey ice is largely dependent on its morphology (Osada et al., 2020). Multi-channel networks, like river deltas, are particularly susceptible to ice jamming because of their low channel gradients, channel junctions, and the presence of mid-channel islands (Nafziger et al., 2019). In the Makenzie Delta, breakup jams can affect the flow distributions within the delta and in some instances flow reversals in some channels can even occur (Terroux et al., 1981; Mackay, 1963; Beltaos et al., 2012). Every spring the Town of Hay River in the Northwest Territories is faced with the risk of flooding due to ice jams forming in the channels of the Hay River Delta. Between 1984 and 2010, 34 ice jam flooding events were documented at the Town of Hay River (Kovachis, 2011). The most recent event in spring of 2022 was exceptionally severe with ice jam flooding requiring evacuation of the entire town and the neighbouring Kátł'odeeche First Nation. Peters et al. (2006) examined the flood hydrology of the Peace-Athabasca Delta and found that ice jamming was the most likely mechanism responsible for recharging some highly elevated areas in

the delta complex. In the Slave River Delta, ice jams play a role in the replenishment of moisture and sediment required for the ecological health of the delta (Zhang et al., 2017). And in Fort McMurray, flooding due to ice jamming at the Athabasca-Clearwater River confluence is an ongoing concern (Nafziger et al., 2021). Because of the prevalence of ice jams in multi-channel systems, the ability to simulate ice jams and the associated water levels in these settings can be helpful in flood forecasting and emergency preparedness and in the study of delta ecology.

Several researchers have simulated ice jams in multi-channel environments. These investigations have ranged in sophistication from simulating ice jams in single channels within multi-channel networks using one-dimensional (1D) approaches (Beltaos et al., 2012; De Coste et al., 2017; Blackburn and She, 2021) to using complex two-dimensional (2D) models with both hydrodynamic and ice dynamic capabilities (Kolerski and Shen, 2015; Oveisy and She, 2017). The 2D approach, although considered state-of-the-art for ice jam modelling in complex channel networks, can be a less practical option from an operational perspective as it requires costly 2D bathymetric data and also it can take much longer to obtain solutions (compared to 1D simulations). Ice jam profile models are easy-to-use and extremely useful tools for determining flood levels associated with ice jams. Ice jam profile models available include *RIVJAM* (Beltaos and Wong, 1986; Beltaos, 1988, 1993); *ICEJAM* (Flato and Gerard, 1986; Flato, 1988), and *HEC-RAS* (Hydrologic Engineering Center's River Analysis System). These models solve the ice jam stability equation (Pariset et al., 1966; Uzuner and Kennedy, 1976) in conjunction with a 1D gradually varied flow equation. *ICEJAM* and *RIVJAM* consider only single

163

channels. *HEC-RAS* does have network modelling capabilities but there are no explicit provisions for how an ice jam is calculated if it extends through a channel junction. Very few 1D studies have looked at how channel junctions and islands impact ice jam physics and ice jam thickness. Jasek (1995) recognized that 1D ice jam profile models tend to over predict ice jam thickness in channels with islands because they combine the channel widths on either side of the island when calculating the thickness profile. As a result, he developed an approach for modelling ice jam profiles in channels with islands by separately simulating single channel segments of a multi-channel system using the *ICEJAM* model and then linked them together using appropriate boundary conditions. Although Jasek (1995) was able to estimate the likely effect of islands on the ice jam profile and the associated water levels, the approach required that the flow split around the island was known and it could not be easily applied to more complex channel networks where flow hydraulics need to be solved. To estimate the discharge in the Yukon River during an ice jam, Jasek et al. (2001) modelled an island-laden reach of the river using *ICEJAM*. The effect of islands was incorporated into the simulations using an 'island-compensation' technique. This approach involves modifying cross sections to simulate the reduction of ice jam thickness due to islands. Specifically, cross sections with islands were adjusted by excluding the smaller channel and lowering the bed of the larger channel to account for the smaller channel's flow area. Jasek et al. (2001) found that, by using this approach, they were able to yield similar discharge estimates compared to those obtained through large-scale particle image velocimetry. The 'island-compensation' technique, although it accounts for the effect of islands on ice jam stage, is

quite laborious and also is not applicable to river deltas where channels split but do not rejoin. Beltaos (2003) applied the *RIVJAM* model to simulate ice jam profiles in the Peace-Athabasca delta to determine threshold flows for significant flooding and replenishment of the delta's ecosystem to occur. Since *RIVJAM* considers single channels only, the study was divided into several sub-reaches of constant flow and the model was applied sequentially between sub-reaches. Lindenschmidt et al. (2012) used a one-dimensional modelling approach to simulate ice jams in the Red River delta. To simulate more realistic ice jam flooding using the 1D approach, a diffuse lateral abstraction was included to account for flow from the main channel into side channels and diversions.

This paper presents a new 1D approach for simulating ice jams and the associated water surface profiles in complex natural river systems. It is built upon the University of Alberta's public-domain hydrodynamic and river ice processes model, *River1D*. It is unique in that it considers the effect of the junction discharge ratio on channel junction elements when solving the ice jam stability equation and can simulate ice jam profiles that extend through complex channel networks with multiple junctions and islands. The model was first compared to a series of simulations from Jasek (1995). The model was then validated with simulations of ice jam profiles in the Hay River Delta during the 2009 breakup.

4.2 Model Description

The model for simulating ice jam profiles in channel networks is built on the University of Alberta's public-domain 1D model, *River1D*, which solves the Saint-Venant equations using the characteristic-dissipative-Galerkin (CDG) finite element scheme (Hicks and Steffler, 1990, 1992). This model was recently reformulated to accommodate natural channel cross sections (Blackburn and She, 2019) and more recently the model's channel network capabilities were enhanced to use a momentum conservation approach at junctions (rather than assuming equal water levels through junctions) and allow for dynamically changing junction configurations as a result of flow reversals (Blackburn and She, 2021). She and Hicks (2006) adapted *River1D* to calculate wide channel jam profiles in single rectangular channels by solving the ice jam stability equation (Pariset et al., 1966; Uzuner and Kennedy, 1976). In this new version, the solution algorithm has been adapted for solving the ice jam stability equation within channel networks with special provisions for handling junctions.

4.2.1 Hydrodynamic equations

The model solves for the conservation of mass and momentum in the streamwise direction, accounting for the presence of floating ice and anchor ice on the river bed:

$$\frac{\partial A}{\partial t} + \frac{\partial Q_w}{\partial x} = \frac{\rho_i}{\rho_w}\frac{\partial A_i}{\partial t} + (1-p_a)\frac{\partial A_{an}}{\partial t} \qquad [4.1]$$

$$\frac{\partial Q_w}{\partial t}+\frac{\partial(\beta Q_w U_w)}{\partial x}+gA_w\frac{\partial H}{\partial x}+gA_w S_f=0 \qquad [4.2]$$

where A is the cross sectional area to the water surface; Q_w is discharge of water under and through the ice; A_w is the flow cross sectional area; U_w is the average flow velocity (Q_w/A_w); H is the water surface elevation above a specified datum; β is the momentum flux correction coefficient (1 for rectangular channels, 1.06 for natural channels, and calculated based on Fread (1988) for compound channels); S_f is the boundary friction slope; A_i is the cross sectional area of the surface ice; A_{an} is the cross sectional areas of the anchor ice; ρ_i and ρ_w are the densities of the ice and water, respectively; p_a is the porosity of the anchor ice; t represents time; and x represents the streamwise path of the river.

4.2.2   Ice jam stability equation and solution algorithm (single channel)

The model calculates wide channel jams by solving the following form of the ice jam stability equation (adapted from Ashton (1986)):

$$\frac{dt_j}{dx}=\frac{\rho_i g S_w}{2K_v\gamma_e}-\frac{\tau_c}{B_{wi}K_v\gamma_e}+\frac{\rho_w g R_i S_f}{2K_v\gamma_e t_j}-\frac{\mu}{B_{wi}K_v\left(1-p_j\right)}t_j \qquad [4.3]$$

where t_j is the ice jam thickness; S_w is the slope of the water surface; K_v is the passive pressure coefficient; $\gamma_e=0.5\left(1-\rho_i/\rho_w\right)\left(1-p_j\right)\rho_i g$; p_j is the ice jam porosity; τ_c is the cohesion of the ice in the jam; B_{wi} is the width of the underside of the jam; R_i is the hydraulic radius of the ice affected portion of the flow cross sectional area; and μ is the

167

composite jam stress parameter defined according to Flato and Gerard (1986). Erosion

under the jam is controlled by an erosion velocity V_{max}. If the water velocity exceeds

V_{max}, the depth below the jam is increased until the water velocity is equal to V_{max}.

To solve for a steady state ice jam profile in a single channel, the model solves equation

[4.3] using the following algorithm that has been adapted from the *ICEJAM* model.

1. Start with an initial user input ice thickness profile.

2. Solve the ice jam stability equation by stepping from the head (upstream)
to the toe (downstream) of the jam, using the current hydrodynamic solution as
input.

3. Using the new ice jam profile solution, solve the hydrodynamic equations.
(Although the hydrodynamic equations are for transient flow, if solved iteratively
with constant boundary conditions, the solution will converge to a steady state
solution). Continue to solve the hydrodynamic equations iteratively until the
difference in water discharge between iterations, Q_{diff}, is below a user specified
threshold, $Q_{tolerance}$ at all nodes.

4. Repeat steps 2 and 3 until the hydrodynamic solution and the ice jam
profile converge to a steady state solution.

For the case when the flow exceeds the banks of the channel, the model assumes the ice

jam remains in the main channel and does not spill over into the overbank area.

4.2.3   Ice jam stability equation and solution algorithm (channel networks)

For the single channel case, the solution of the ice jam stability equation is straight forward. Start at the head (upstream) and step through the domain to the toe (downstream). But for the channel network case, although the solution must still step from upstream to downstream, it is imperative that the solution is being calculated from known values of ice thickness. For this to be true, the calculations must step through the domain in a particular way depending on the configuration of the channel network. Consider the case where an ice jam extends through a river reach with an island, as shown in Figure 4.1.

The solution must first step to the upstream end of the island (red line), then through both reaches around the island (blue and green lines) before the solution can progress through the reach downstream of the island (yellow line). In complex channel networks, with many junctions and reaches, the order in which the solution must progress can be quite complicated. Although this could be automated, in the current version of the model the user must specify the order in which the reaches of a network are solved.

With the reach order specified, the solution algorithm as previously described for a single channel is followed with one exception. Once the solution encounters a junction, the model steps through the elements in the junction with special considerations to the ice jam stability equation for the junction elements. Figure 4.2 illustrates the plan view for junction elements for both converging and diverging junctions.

The solution of the ice jam stability equation in junction Elements B and C is assumed to be a function of the portions of the water discharge at Node A flowing in Element B and Element C. The discharge ratio, ξ, is defined as:

$$\xi = \frac{Q_{wA(\text{Element B})}}{Q_{wA}}$$ [4.4]

where Q_{wA} is the discharge at node A and $Q_{wA(\text{Element B})}$ is the portion of Q_{wA} flowing in Element B. Applying mass conservation at Node A:

$$Q_{wA(\text{Element C})} = (1-\xi)Q_{wA}$$ [4.5]

and $Q_{wA(\text{Element C})}$ is the portion of Q_{wA} flowing in Element C.

For the converging case, the ice jam stability equation is solved at Node A for both Elements B and C. For each junction element, the water surface slope and the width of the underside of the ice jam must be calculated at Node A. For Element B, the water surface slope at Node A is calculated as the average water slope for Elements B and D, S_{wBAD}, and the width of the underside of the ice jam at Node A is:

$$B_{wiA(\text{Element B})} = \xi B_{wiA}$$ [4.6]

Similarly for Element C, the water surface slope at Node A is calculated as the average water slope for Elements C and D, S_{wCAD}, and the width of the underside of the ice jam at Node A is:

170

$$B_{wi\text{A(Element C)}} = (1-\xi)B_{wi\text{A}} \tag{4.7}$$

Additionally, bank resistance is halved at Node A in Elements B and C to account for the fact that resistance is only acting on one side of each junction element.

Once the ice jam stability equation is solved at Node A for both junction elements, the ice jam thickness at Node A is calculated as:

$$t_{j\text{A}} = \xi t_{j\text{A(Element B)}} + (1-\xi)t_{j\text{A(Element C)}} \tag{4.8}$$

With ice jam thickness solved at Node A, the solution can continue to progress downstream. To solve for the ice jam thickness at Node D, the water surface slope at Node A in the solution for Element D is weighted based on ξ:

$$S_{w\text{A(Converging Junction)}} = \xi S_{w\text{BAD}} + (1-\xi)S_{w\text{CAD}} \tag{4.9}$$

For the diverging case, the ice jam stability equation is first solved at Node A for Element D using the following equation to weight the water surface slope at node A:

$$S_{w\text{A(Diverging Junction)}} = \xi S_{w\text{DAB}} + (1-\xi)S_{w\text{DAC}} \tag{4.10}$$

Since there is only one solution for the ice jam thickness at Node A for diverging junctions, no weighting of the thickness is required. The ice jam stability equation is then solved at Nodes B and C for Elements B and C with discharge weighted values of B_{wi} at Node A based on equations [4.6] and [4.7].

4.3   *Model Comparison*

River1D's ability to model ice jam profiles in channel networks was compared to numerical tests performed by Jasek (1995) for investigating the theoretical effect of islands on ice jam profiles. The tests were performed in rectangular channels with islands of different length. Channels on either side of the island were set to be geometrically identical so that a 50/50 flow split to either side of the island could be assumed. Since no model was available for simulating ice jams in multi-channel environments, Jasek (1995) used the *ICEJAM* model to solve for each channel segment separately and linked them together using appropriate boundary conditions. Global parameters for the tests are specified in Table 4.1.

The tests were performed for various channel slopes (S_{bed}), island lengths (L_{is}), and inflow discharges. Jasek (1995) assessed the effect of the island for each simulation by comparing the minimum stage along the island (Y_{min}) to the equilibrium stage generated by an equivalent single channel (Y_{eq}). Simulations from the current study are presented along with the results from Jasek (1995) in Table 4.2. For each test the thickness at the jam head and toe were set to 1 m and the water level at the downstream boundary was set to the normal stage (Y_{normal}) for an equivalent single channel with a specified ice thickness of 1m.

The results from the present study agree very favourable with the results from Jasek (1995). Although the values of Y_{eq} and Y_{min} vary slightly between the two models, the

stage reduction ratios (Y_{min} / Y_{eq}) are very similar for both models. The relative difference

(RD) of the stage reduction ratio was calculated as:

$$RD = \frac{\left(\dfrac{Y_{min}}{Y_{eq}}\right)_{\text{Present Study}} - \left(\dfrac{Y_{min}}{Y_{eq}}\right)_{\text{Jasek (1995)}}}{\left(\dfrac{Y_{min}}{Y_{eq}}\right)_{\text{Jasek (1995)}}}$$

[4.11]

For all tests, the relative difference is 0.77% or lower. Jasek (1995) presented ice jam

profiles for Test 8 through 14. The same profiles are presented here in Figure 4.3.

The profiles traverse through one side of the island but represent either side since the

results are identical on both sides of the island. These profiles compare visually very

well with the same ice jam profiles presented in Jasek (1995). All profiles exhibit the

same toe-like thickening and minimum depth at the upstream end of the island and the

same stage reduction and thinner ice in the channels on either side of the island. The

profiles also exhibit the same reduction in thickness at the downstream end of the island.

A bottom and top of ice comparison profile plot for Test 14 is presented in Figure 4.4.

Although the relative differences presented in Table 4.2 show that Test 14 has the largest

difference compared to the other profiles in Figure 4.3 (RD = 0.51%), Figure 4.4

illustrates that visually the results are very similar to those from Jasek (1995). The minor

differences between the model results for Y_{eq} and Y_{min} in Table 4.2 could be the result of a

number of factors including model discretization, boundary conditions, and differences in

the modelling approaches. Tests in the present study were conducted with a model

discretization of 100 m. Model discretization was not reported in Jasek (1995). Similarly the boundary conditions for the head and toe configuration and the downstream water surface elevation were not explicitly specified in Jasek (1995) and were inferred from the test result ice jam profiles for use in the present study. Therefore, the boundary conditions used in this study may not in fact be identical to those used in Jasek (1995). Differences in the modelling approaches could also contribute to the differences in the results from the two studies. For example, both studies take different approaches to handle junctions. In Jasek (1995), ice thicknesses were forced to be equal on either side of the junction as a boundary condition whereas in the current study, ice jam thickness is solved across junctions. This is a possible reason why the relative difference tends to increase as the island length decreases. For the longer islands, the ice jam on either side of the island approaches an equilibrium thickness where the minimum stage occurs, but for the shorter islands, the impacts of the junctions are still felt at the minimum stage location.

Although the results from these two studies agree well it is important to note that Jasek's approach requires additional computation routines be set up to link separate segments together and it also requires that junction hydraulics be known. In *River1D*, both these limitations are eliminated. Therefore, it would be easier to use *River1D* conduct tests with ice jams around islands where the channels on either side of the island are not identical and junction hydraulics are not known.

4.4   *Model Application and Validation*

4.4.1   Study Site

The model was applied to the Hay River Delta (HRD), located in the Northwest

Territories of Canada. The study reach, shown in Figure 4.5, extends from the Water

Survey of Canada gauge (Hay River near Hay River (07OB001)) to the mouth of the Hay

River at Great Slave Lake. The numbers along the channels in Figure 4.5 are the

distances in kilometres from the Hay River's headwaters. The HRD starts at the Forks

(km 1108) where the river splits into the West and East Channels. The river splits again

along the West channel forming the Rudd Channel and Fishing Village Channel. Before

draining into Great Slave Lake, the Fishing Village Channel splits again forming the

Island Channel. The East Channel contains two islands labelled "A" and "B".

4.4.2   Model bathymetry

The model consists of 311 cross sections with an average spacing of 90 m. The model

bathymetry was developed from two separate data sets. The single channel upstream of

the Forks from km 1095.6 to km 1107.4 was developed from cross sections surveyed by

the University of Alberta in 1987 and the Department of Indian and Northern

Development (DIAND) in 2002. These sections are for in-channel flow only and do not

include the overbank region. Additional sections were interpolated between the surveyed

sections for a total of 137 cross sections (11 surveyed and 126 interpolated). The HRD

portion starting just upstream of the Forks at km 1107.4 was developed from the 2D

bathymetry survey of the HRD presented in Brayall and Hicks (2012). The 2D survey

175

data were supplemented with elevations extracted from Google Earth to better define the overbank region. The 2D data was used to generate a digital elevation model (DEM) of the HRD. A total of 174 cross sections were extracted from the DEM. With the 311 cross sections, the model was assembled using 13 channel reaches, 7 junctions, 1 inflow boundary and 4 outflow boundaries as shown in Figure 4.5.

4.4.3   Open water validation

For the main channel portion of the cross section, a bed Manning's roughness of $n_b =$ 0.025 was selected for all cross sections, based on previous modelling efforts in the Hay River and the HRD (Brayall and Hicks, 2012; De Coste et al., 2017). In the HRD portion of the model, where cross sections include overbank area, the overbank roughness was set to 0.15 based on engineering judgement (where the floodplain is mostly vegetated with trees but is also developed with buildings). The 1D model's open water performance was validated using surveyed water surface profiles, Acoustic Doppler Current Profiler (ADCP) measurements, and 2D modelling results from Brayall (2011). In Brayall (2011), discharges were simulated to develop a relationship between the total discharge and the flow split at the Forks. In this study, four of these discharges were simulated and compared to Brayall's 2D model results. The model was only compared to these four discharges because all simulated breakup scenarios fall within the range of these four discharges. Plus, the bathymetric survey data used to develop the 2D model did not have the overbank area well defined so the results from both models are not expected to be in agreement for higher discharges. The inflow discharges and the corresponding downstream lake levels (applied to all four downstream boundaries) are

176

based on discharges reported at Hay River Near Hay River (07OB001) and the corresponding lake levels reported at Great Slave Lake at Hay River (07OB002) (shown in Figure 4.5). These boundary conditions are presented in Table 4.3.

Figure 4.6 compares the flow split to the East Channel (%) versus total inflow to the HRD (m³/s) for the 1D model to the 2D results from Brayall (2011). A single point from ADCP measurements conducted in July 2007 is also presented in Figure 4.6. The 1D results compare well with the 2D curve and the ADCP point. The 1D model does not match perfectly with the 2D results but this is not surprising since the 1D model does not handle all of the 2D effects at junctions (e.g. centrifugal pressure, interfacial shear, and frictional shear).

Model calibration in Brayall (2011) was conducted using water surface elevation data that were collected during August 2005. The survey was conducted over a seven-day period where the discharge at the WSC station (07OB001) decreased from 258 m³/s to 160 m³/s. Brayall (2011) simulated both discharges using the boundary conditions presented in Table 4.3 and compared the results to the surveyed data. Figures 4.7 and 4.8 present water surface profiles from the 1D model compared with the 2D results and the surveyed data. The 1D model results are almost identical to the 2D results except in the West Channel (Hay River Terminating at the Rudd Channel) between km 1108 and km 1108.5 where the 2D model water levels (and survey data) are greater than the 1D model levels. This is likely due to the fact that the 2D model accounted for the bridge pier of the West Channel Bridge (Figure 4.5) while the current 1D model does not.

4.4.4 Simulation of the 2009 Breakup Ice Jam Profiles

The validated model was used to simulate ice jam profiles documented during the 2009 breakup of the Hay River. In 2009, ice started moving on May 3rd which resulted in small jams forming in the HRD with the head upstream of the Forks. Early on May 4th, an upstream wave arrived in town resulting in consolidation events in both the East and West Channels. The jam in the West Channel was pushed downstream and all the way down past the split of the Rudd and Fishing Village Channels. The East Channel jam remained in place but the head of the jam moved downstream to the Forks. During that day, a large jam formed approximately 50 kilometres upstream of the WSC station (07OB001). By the morning of May 5th, incoming ice had moved the head of the jam to upstream of the Forks. No additional ice movement was observed that day. Early on May 6th, the upstream jam released, sending a wave downstream to the HRD. The ice jams in the East and West Channels were pushed down to Great Slave Lake. Water levels peaked that night causing considerable flooding along the East Channel. By the morning of May 7th, water levels were dropping and the resulting jams were receding by thermal attrition.

Observations of the 2009 breakup were collected by the University of Alberta in collaboration with DIAND and the Town of Hay River. Data included water levels collected with a Real Time Kinetic Global Positioning System (RTK-GPS), late winter intact ice thicknesses, photos taken during water level data collection, and photos taken during flights to track the breakup progression. During breakup, elevation profiles were collected on four days: May 3rd, May 4th, May 5th, and May 7th. To simulate these

178

profiles, the required model inputs include the inflow discharge, water levels at downstream boundaries, jam head and toe locations, and intact ice thickness downstream of jam toe(s). The inflow discharges were set according to the daily discharge reported at WSC 07OB001 (Hay River near Hay River) and downstream boundary water levels were based on the water levels from elevation profile data, presented in Brayall (2011). Table 4.4 presents the boundary conditions for the ice jam profile simulations.

Intact ice thicknesses downstream of the jam(s) were based on late winter ice thickness measurements taken at the downstream ends of the East, Rudd, and Fishing Village Channels. The average thickness from these measurements is 1.0 m. This value was also used to set the jam head ice thickness in the model since it is assumed that at the head ice floes would be juxtaposed and not consolidated and therefore the late winter thickness should be representative of the thickness of unconsolidated ice floes at the head. Jam head locations were determined from profile data and confirmed with photo evidence. Toe locations were based on those presented in Brayall and Hicks (2012) for 2D simulations of the same profiles but also confirmed with photo evidence. Head and toe locations are presented in Table 4.5. For May 7th, where the jam had pushed passed the downstream boundary, the toe of the jam was set at the boundary. Global parameters for the ice jam stability equation were set according to Table 4.6. Where applicable, the acceptable range for the parameter is also provided. For all scenarios the jam extended fully between the jam head and jam toes except for May 7th where the channel on the east side of Island A was free of ice.

A sheet ice Manning's roughness coefficient, n_s, of 0.02 was used for all intact ice downstream of the toe. The ice jam Manning's roughness, n_j, was set to 0.055 for all scenarios and is close to the value of 0.05 used by De Coste et al. (2017) in their modelling of the 2009 breakup ice jamming in the HRD. Ice jam profiles for each of the four days are presented in Figures 4.9 through 4.12. For the East Channel, the profile passes to the east of Island B and to the west of Island A. For each day, profile data were collected along the Hay River (upstream of the Forks), the East Channel, the Rudd Channel, and the Fishing Village Channel using RTK-GPS. Surveyed data were labelled with two different tags: EOW (edge of water) or TOI (top of ice). However, some TOI data were excessively high. For those values, photos taken during measurements were examined to determine what the measurement actually represented. In some cases they represented top of ice for stranded pieces of ice like in Figure 4.13. Stranded ice levels were collected by the field team to document the maximum ice levels that were achieved on May 6th when the ice jam release wave from upstream reached the HRD. Where evidence was available, outliers that could be identified as stranded ice were removed from the data set since they are not representative of the ice jam profile at the time of the profile measurement. In total, 19 survey points were excluded from the ice profile plots because they could be identified as representative of stranded ice. These were all collected on May 7th. There was one additional outlier collected on May 5th that was also excluded. In this case, two measurements were taken on the same piece of ice but the measurements differed by over 2 m. Since the lower value is consistent with upstream

and downstream values, the higher value was excluded. Some outliers still remain in the data set because there was no evidence to support their exclusion.

Overall the model ice jam profiles agreed favourably with the surveyed profiles using just one ice jam roughness value for all four days. However, the model slightly underestimated the top elevations of the jam in the East Channel on May 7th (Figure 4.12). This is likely because the jam consolidated when the ice jam release wave from upstream moved through the HRD on May 6th. De Coste et al. (2017) reported that, at the entrance to the HRD, the flow from this wave peaked at 895 m³/s. By applying this May 6th peak discharge at the inflow boundary of the model to calculate the jam configuration but then reducing the inflow discharge to the May 7th value when the survey was conducted to calculate the water surface profile (without changing the jam configuration), the results are in better agreement with the observations, as shown in Figure 14. When the profile is modelled in this manner the average difference between the simulated and observed top of ice is reduced by 50%, from 0.4 m (with reported daily discharge) to 0.2 m (with peak discharge). Figure 4.14 also shows the locations of islands B and A in the East Channel profile to illustrate how the islands affect the shape of the jam in a similar manner to the test cases with the idealized rectangular channel. At Island B, the jam exhibits the same thickening at the upstream end and a reduction in thickness at the downstream end compared to the idealized cases. The changes in thickness are less pronounced at Island A. The reason for this is unclear but is possibly due to the island's proximity to the jam toe and/or the absence of ice in the channel to the east of Island A. The model also slightly underestimated the profile in the East Channel

on May 4th (just upstream of the jam toe between km 1110 and km 1111 in Figure 4.10) and the results would likely be improved by using the same peak discharge approach to calculating the jam configuration but the peak discharge due to the jam release wave is not available for this day.

4.5   *Conclusions and Recommendations*

Ice jamming frequently occurs in complex river networks. A new modelling approach for simulating ice jam profiles in 1D channel network models has been developed. The model simulates ice jam profiles that extend through complex channel networks with multiple junctions and islands by considering the effect of the junction discharge ratio on channel junction elements when solving the ice jam stability equation. The model was used to simulate idealized cases for ice jamming in a channel with a single island and agreed well with results from a previous study. The model was then used to simulate ice jam profiles in the HRD. The open water validation illustrated the model's capability to simulate the flow split at the Forks compared to surveyed discharge data and 2D model flow split results. Using a single under ice jam roughness of 0.055, the model was able to simulate surveyed ice jam profiles quite well in the HRD except the model did have a tendency to under predict water and ice levels in the East Channel downstream of the Forks for profile data collected after an ice jam release wave had passed through the HRD. When the peak discharge was used to calculate the ice jam configuration rather than the daily discharge reported on the day the ice jam profile data were collected, the

model was able to more accurately simulate the surveyed levels and the difference between the observed and simulated top of ice levels was reduced by 50%.

Future work could include applying the model to other channel networks for additional model validation. Also the model could be automated so that the user is not required to provide the reach and junction order for the solution progression of the ice jam stability equation. Additional future work could consider the simulation of dynamic ice jam formation in channel networks by solving ice mass and momentum equations in place of the jam stability equation.
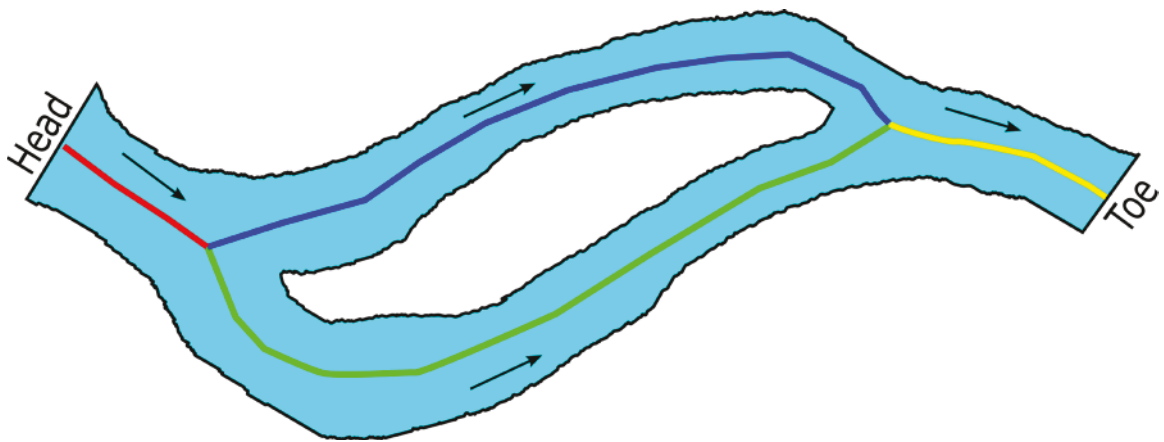
Figure 4.1: Plan view of reach with island and ice jam stability equation solution reaches (arrows indicate flow direction).
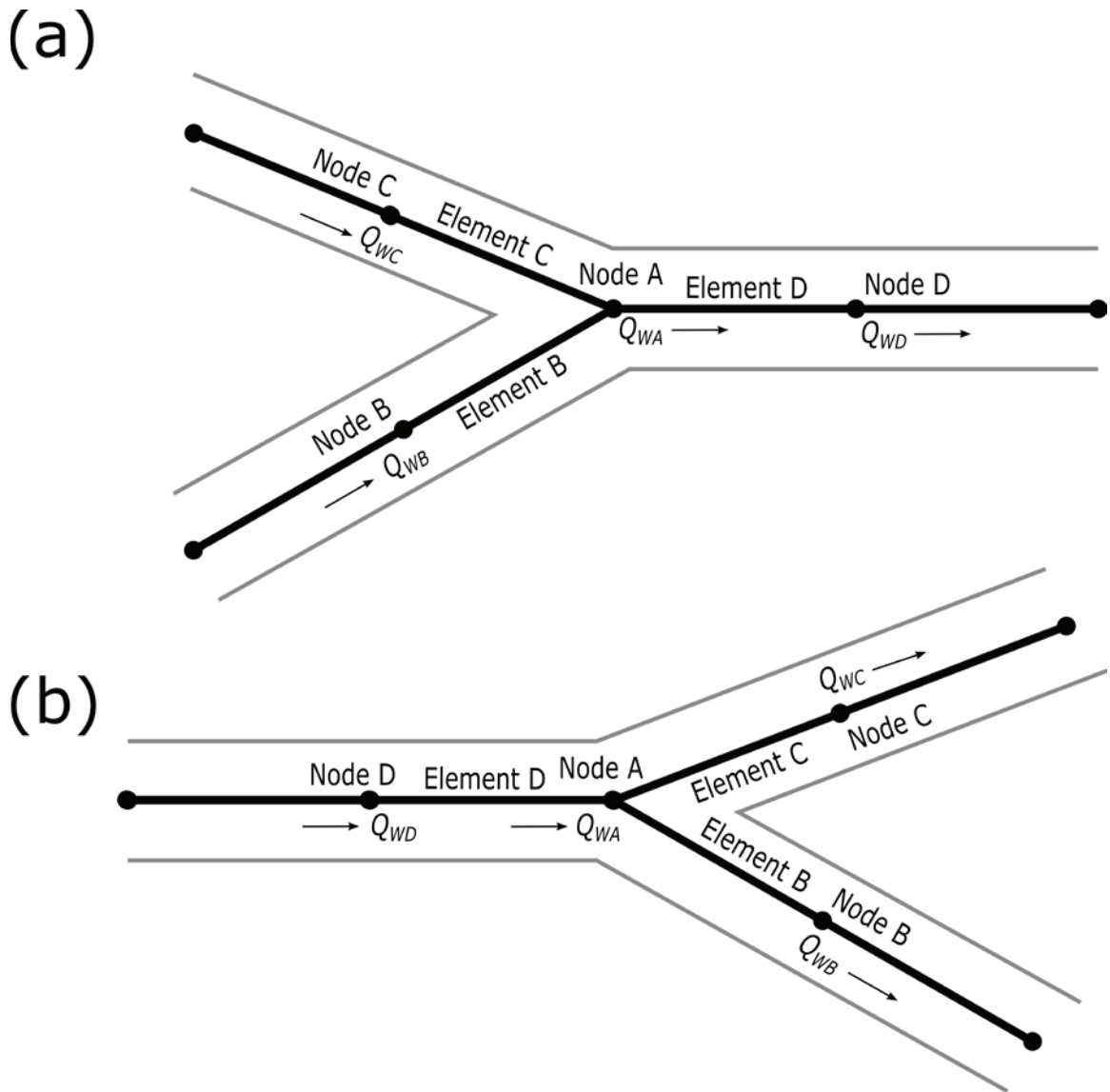
Figure 4.2: Plan view model configurations for (a) converging and (b) diverging junctions.
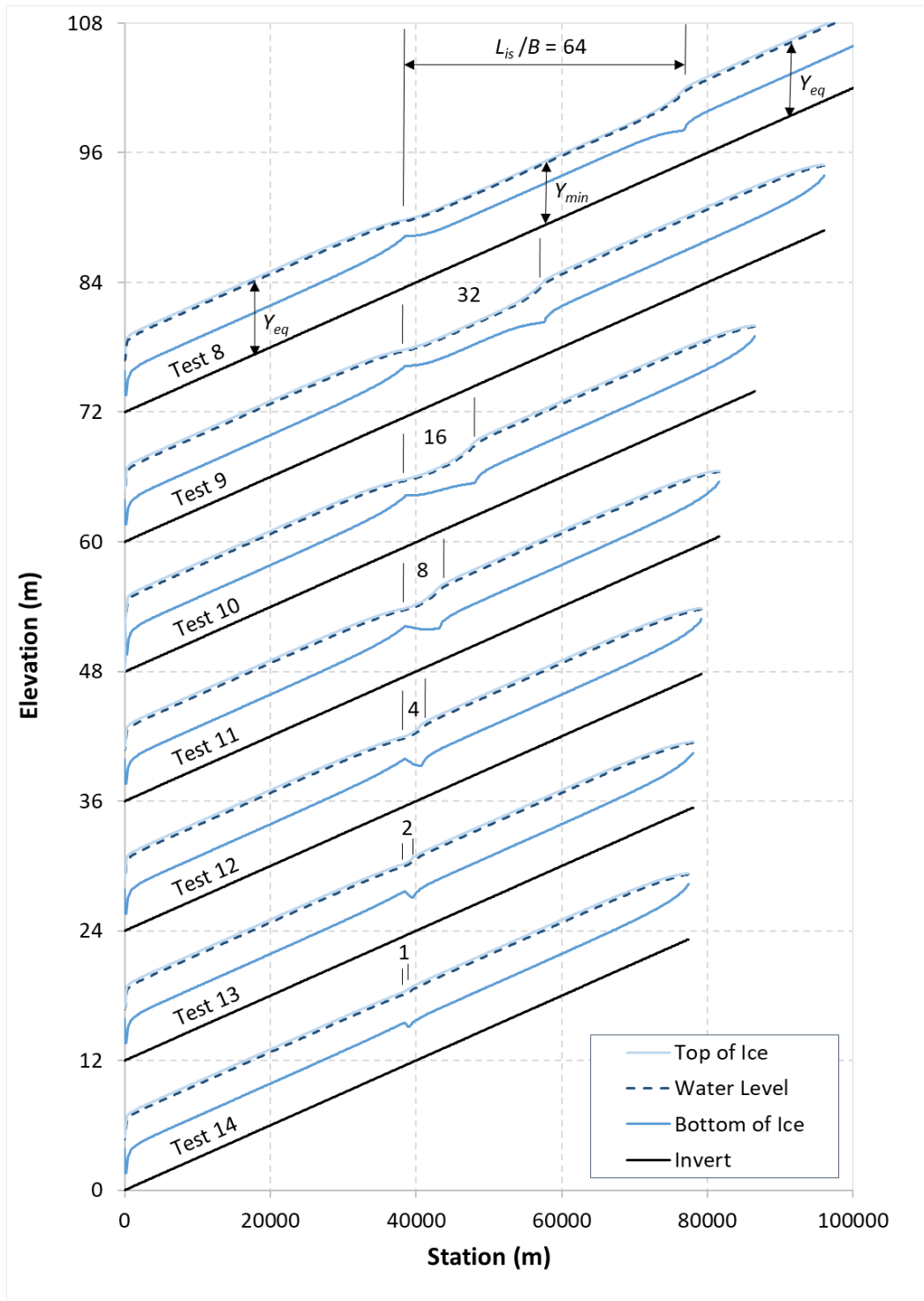
Figure 4.3: Ice jam profiles for Tests 8 through 14 (vertical scale adjusted for presentation).
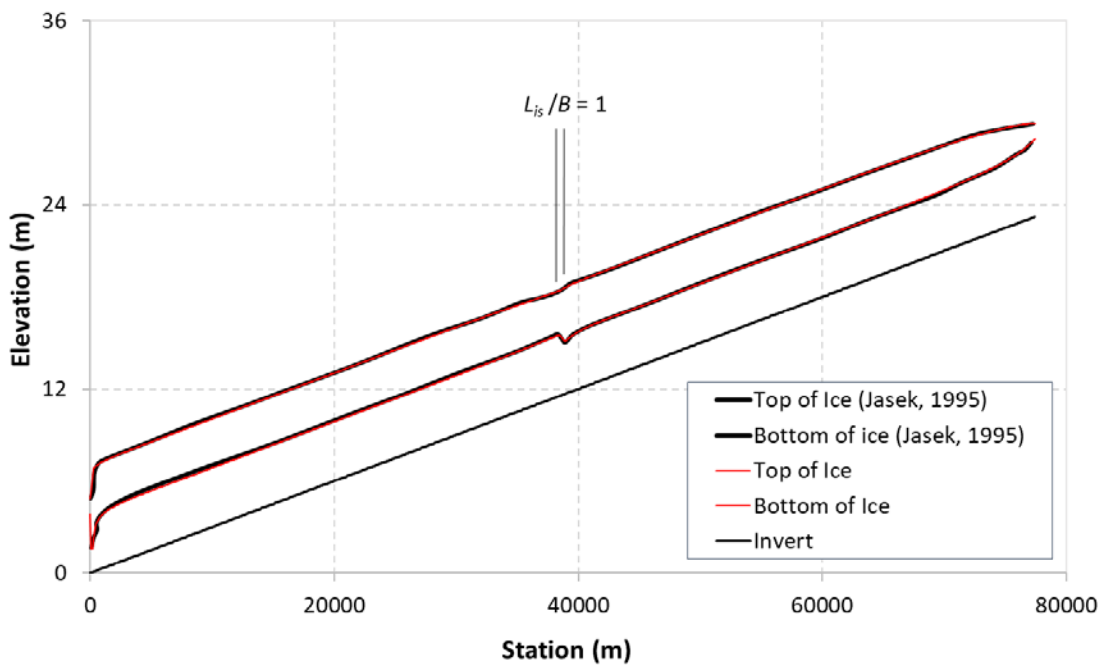
Figure 4.4: Test 14 top and bottom of ice comparison with digitized data from Jasek (1995).
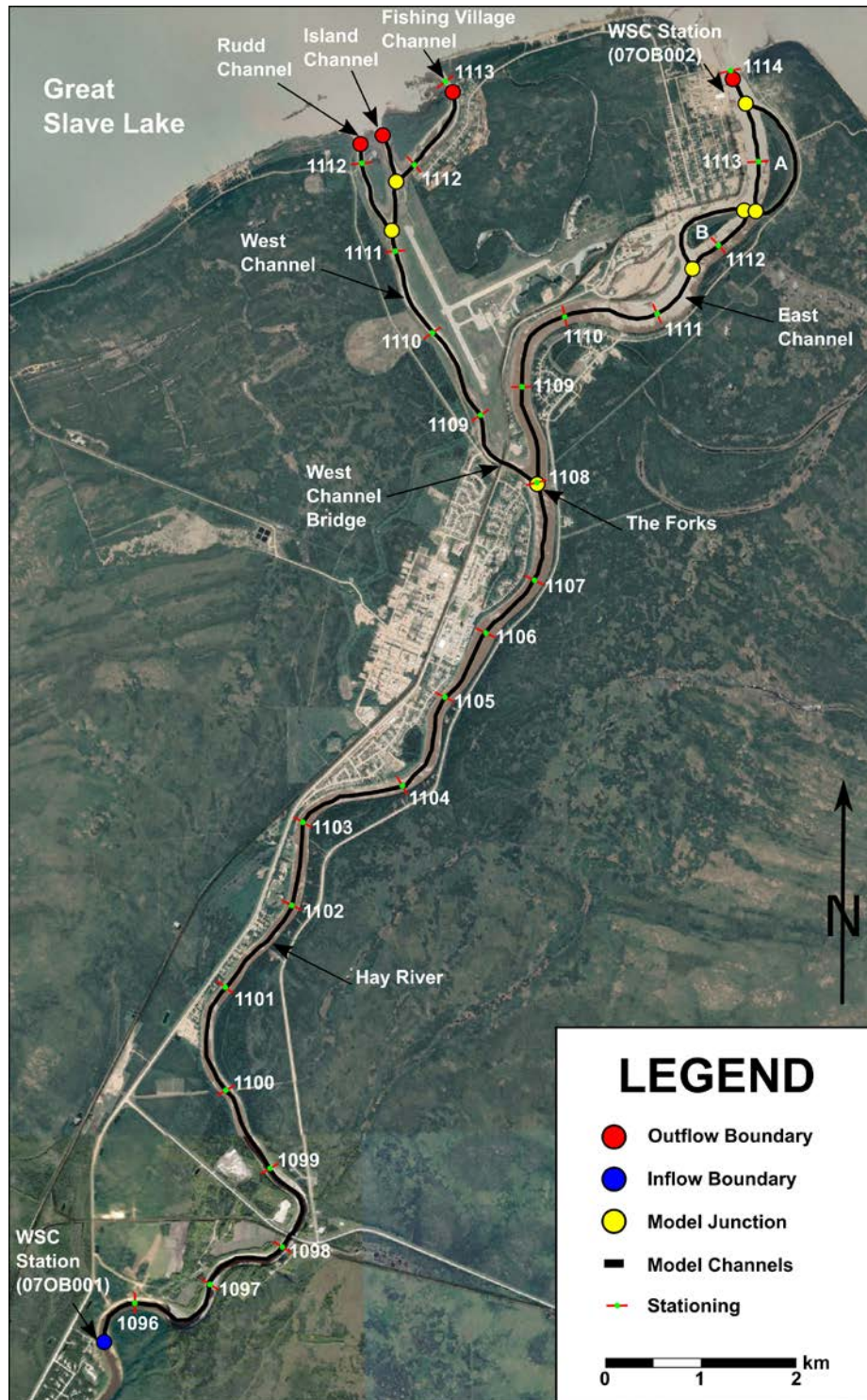
Figure 4.5: Map view and model plan view with satellite imagery from Google Earth (Image data: © 2022 CNES / Airbus).
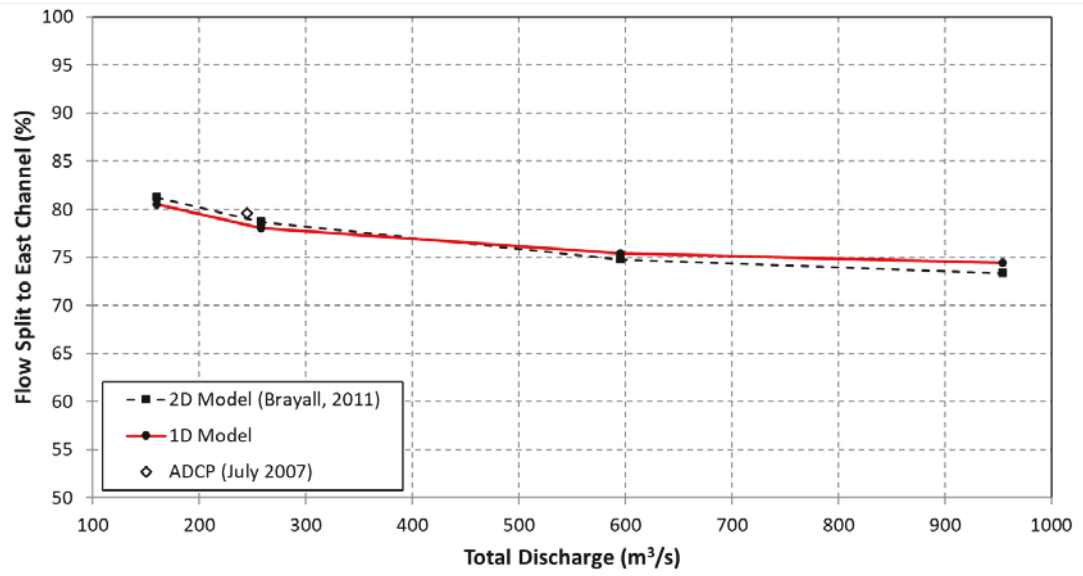
Figure 4.6: Comparison of flow split curves generated by Brayall (2011) and the current 1D model.
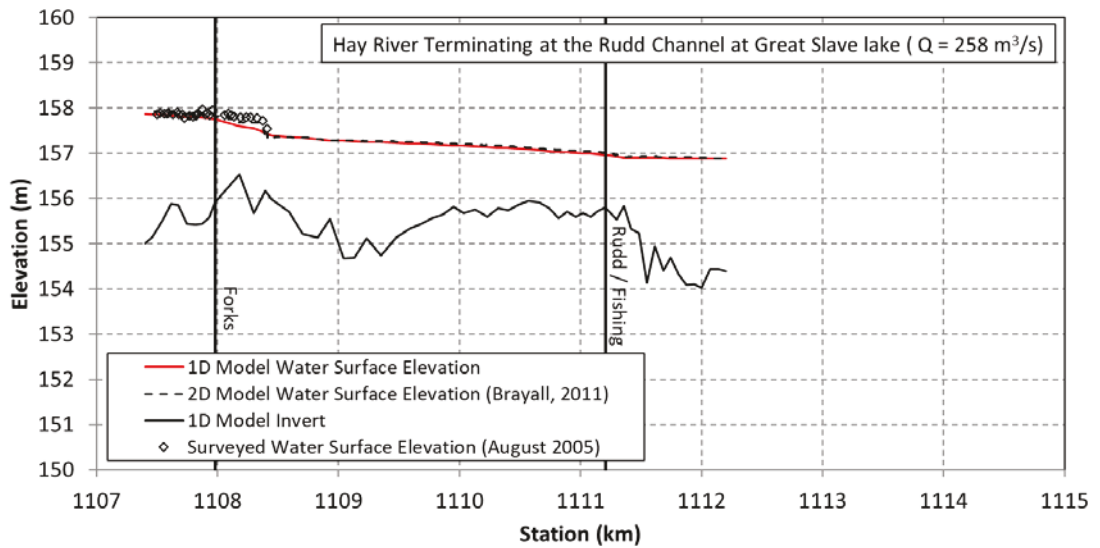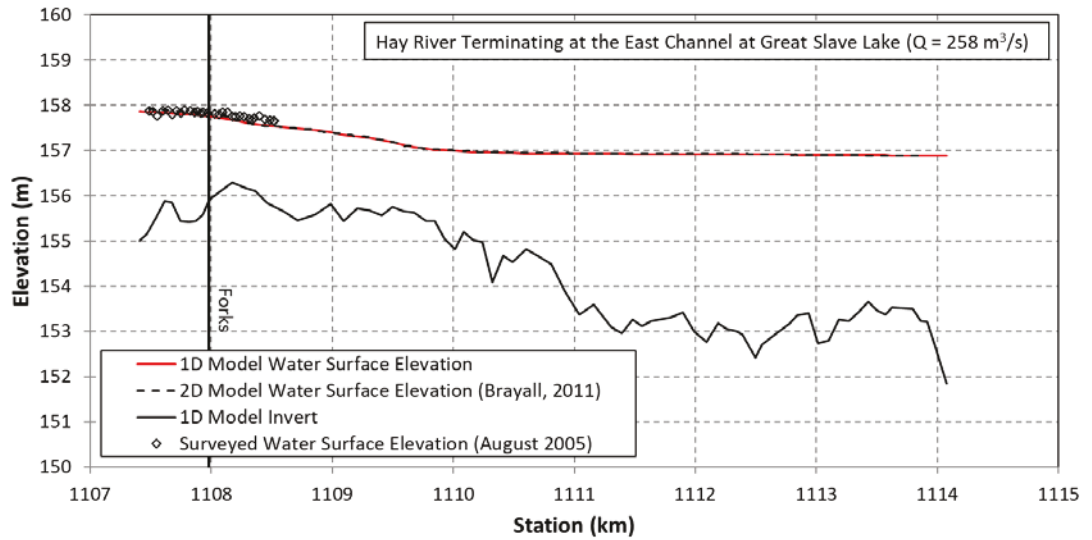
Figure 4.7: Comparison of water surface profiles generated with the current model with those generated by Brayall (2011) and surveyed water levels attributed to Q = 258 m³/s.
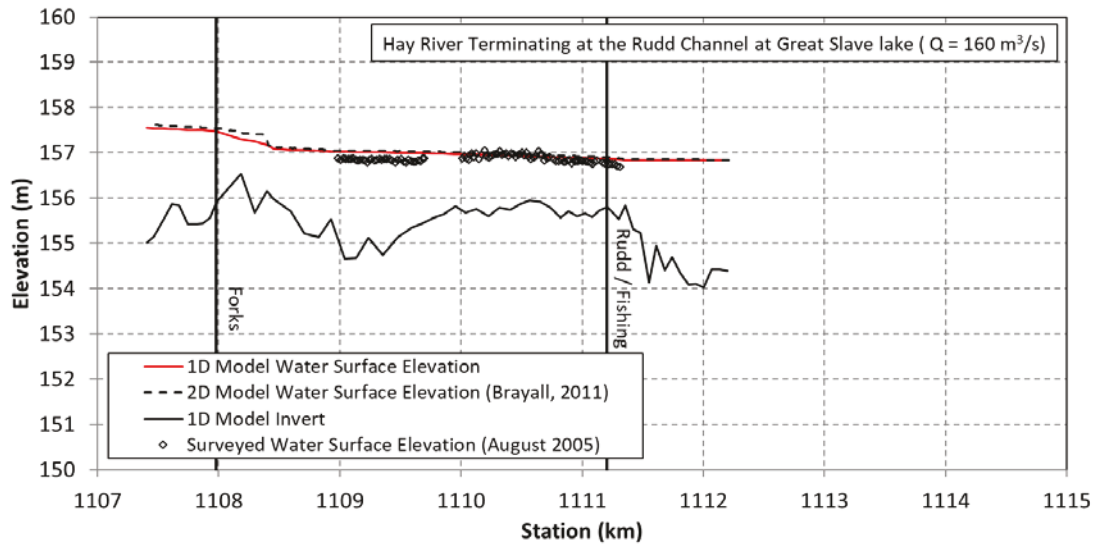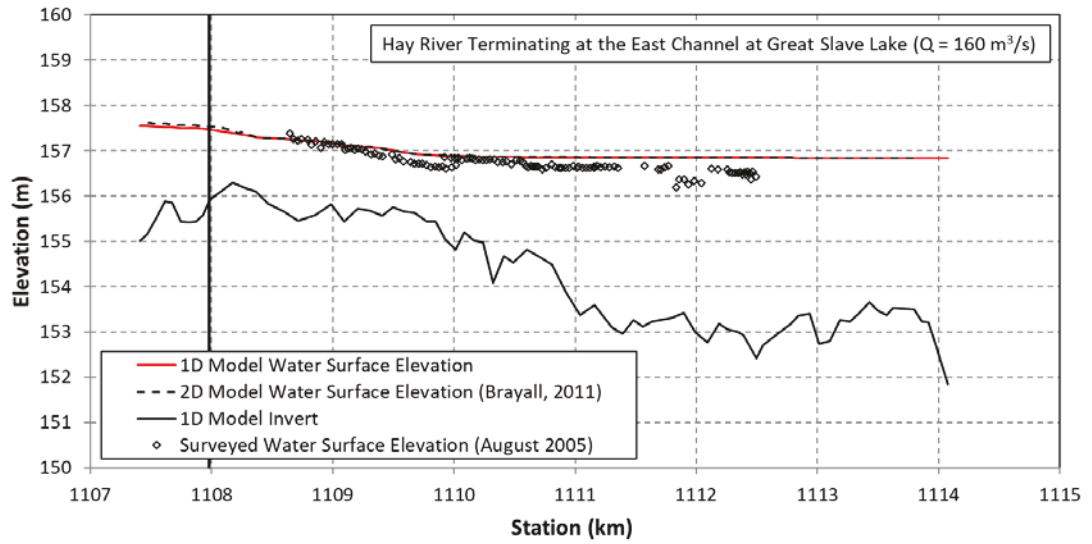
Figure 4.8: Comparison of water surface profiles generated with the current model with those generated by Brayall (2011) and surveyed water levels attributed to Q = 160 m³/s.
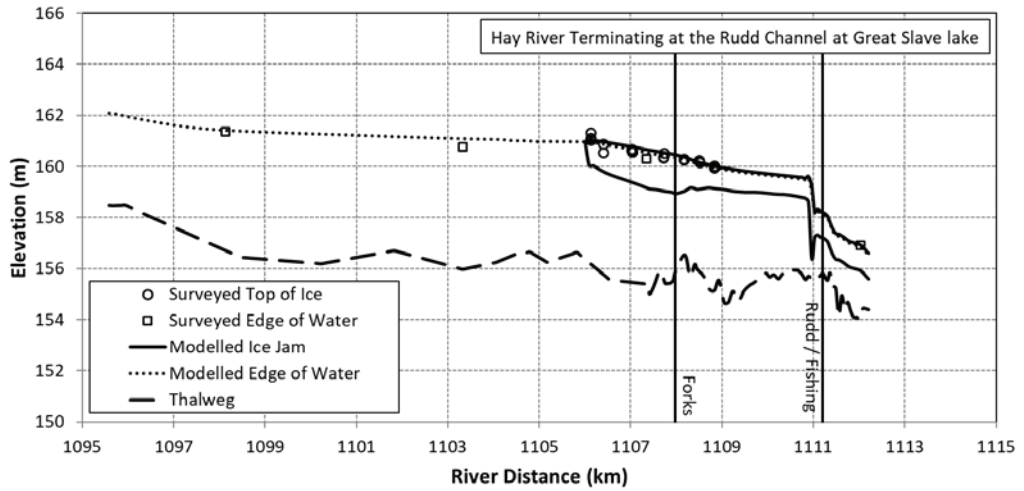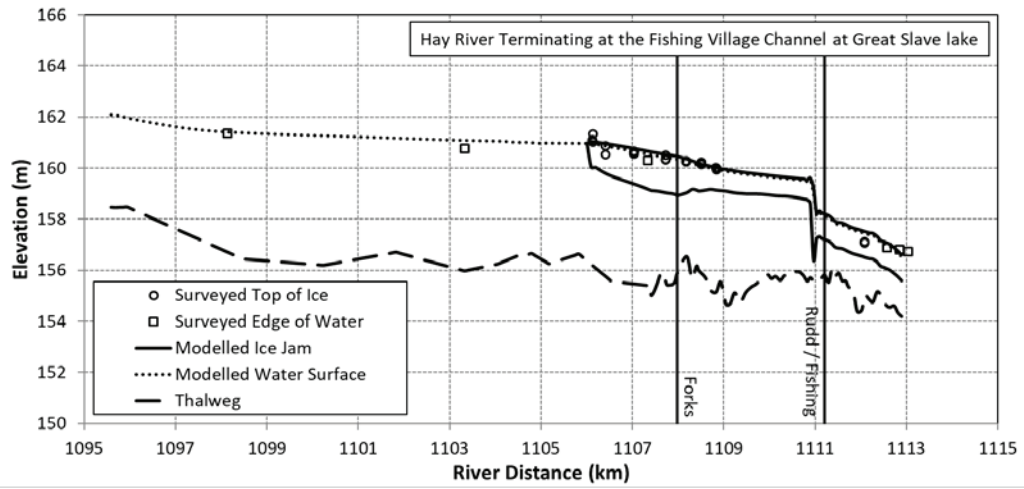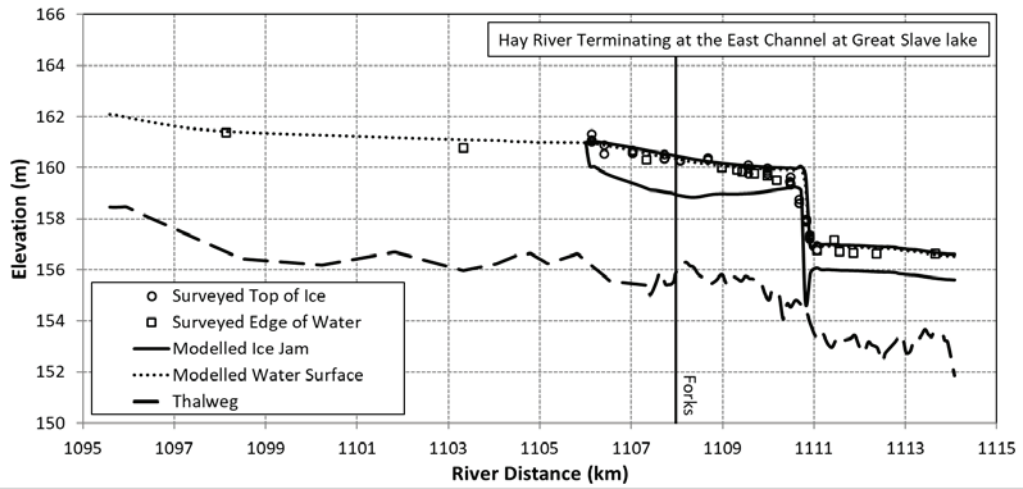
Figure 4.9: Ice jam profiles for May 3rd, 2009.

192
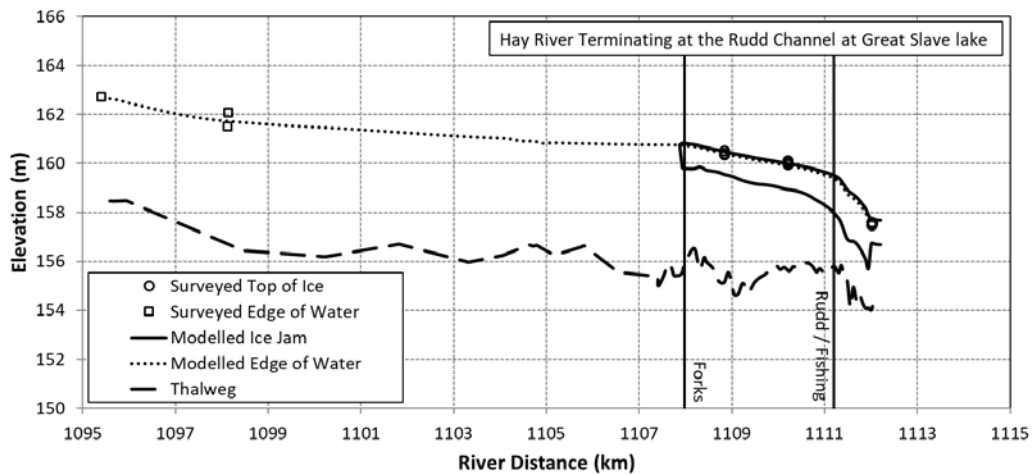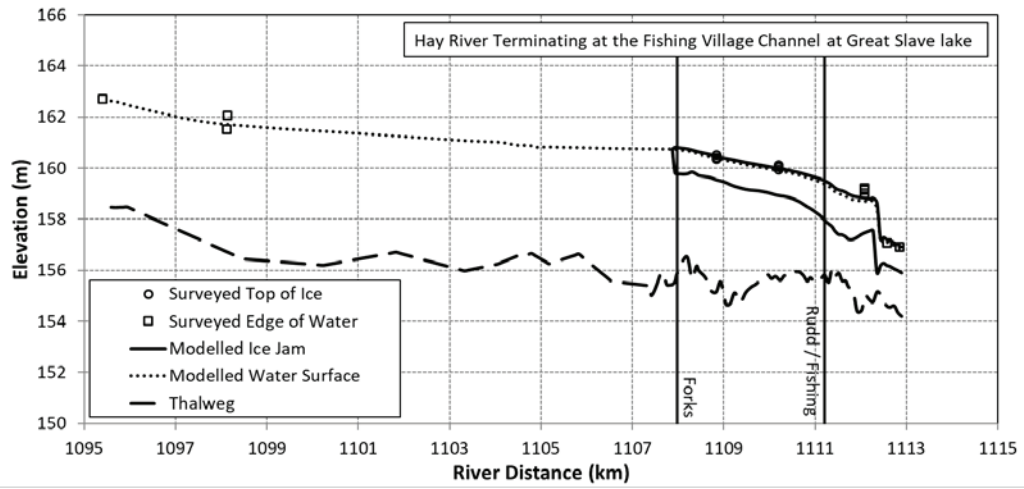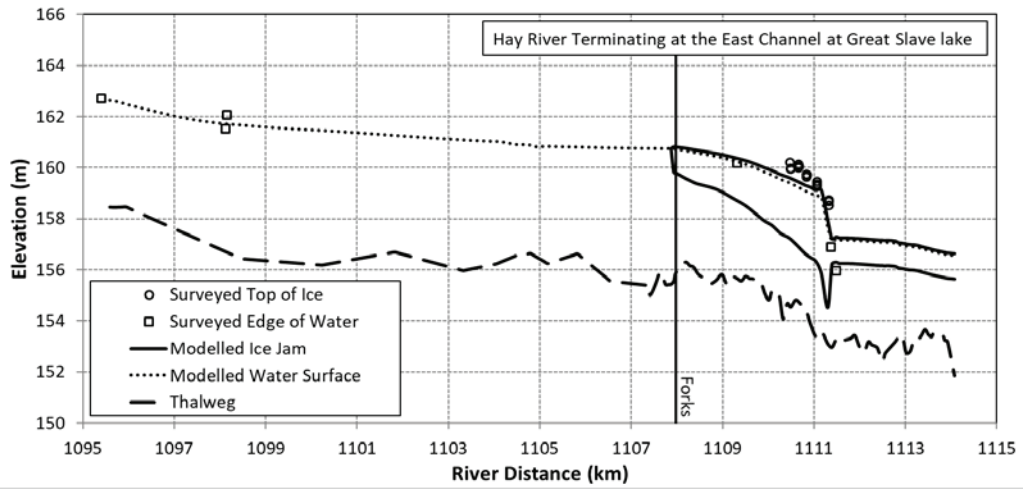
Figure 4.10: Ice jam profiles for May 4th, 2009.

193
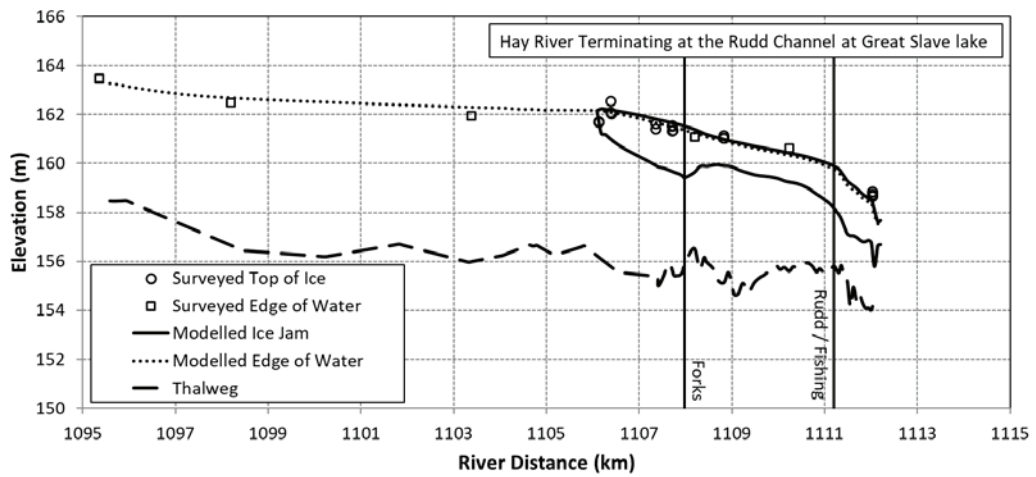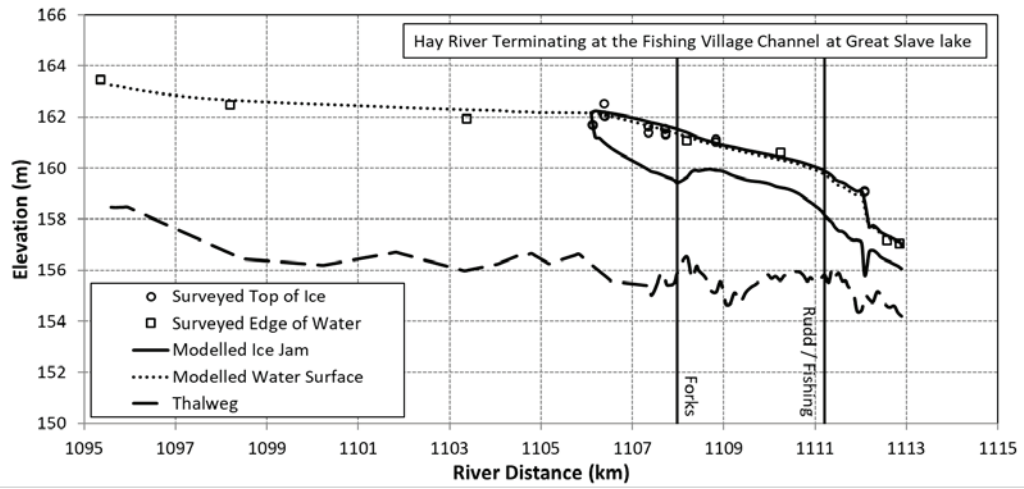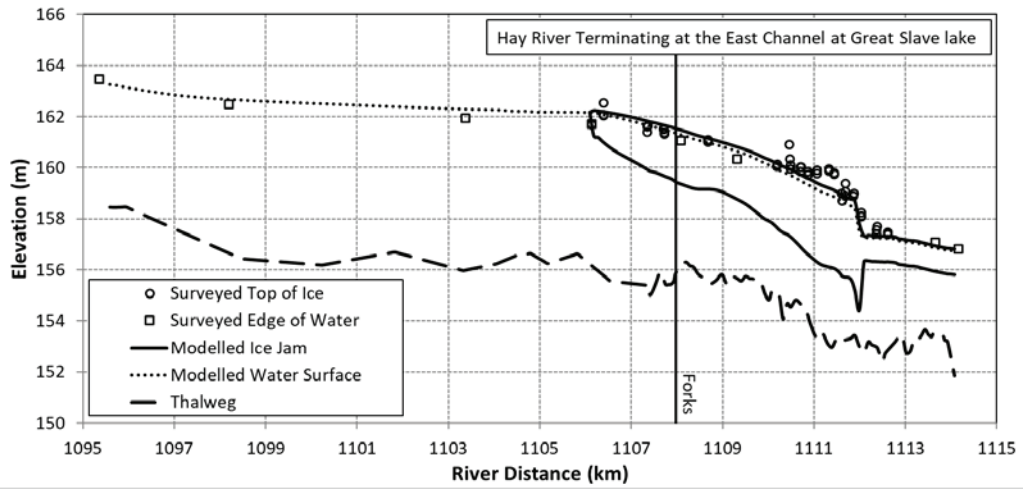
Figure 4.11: Ice jam profiles for May 5th, 2009.

194
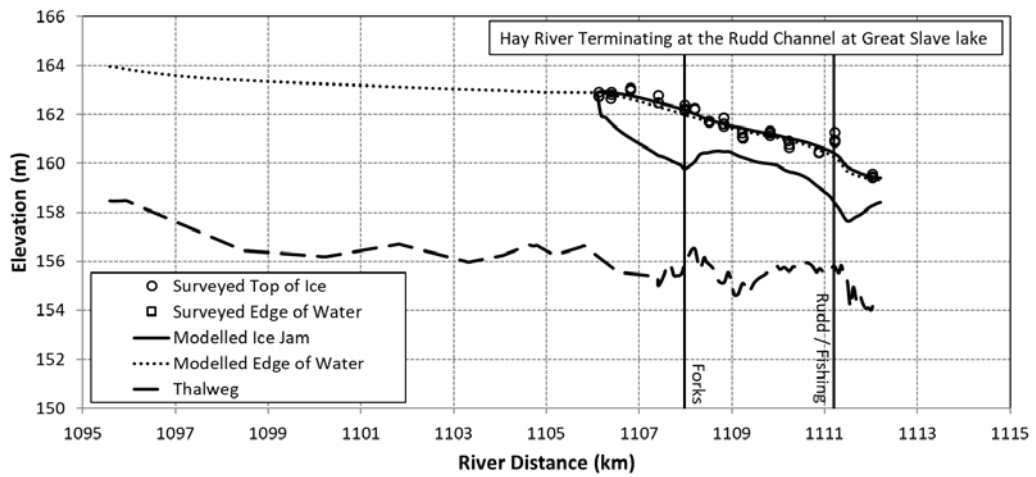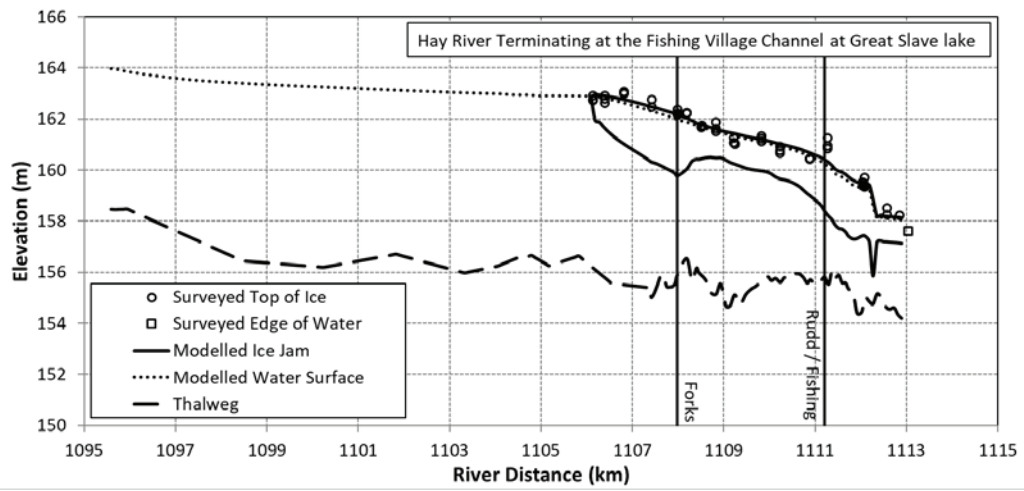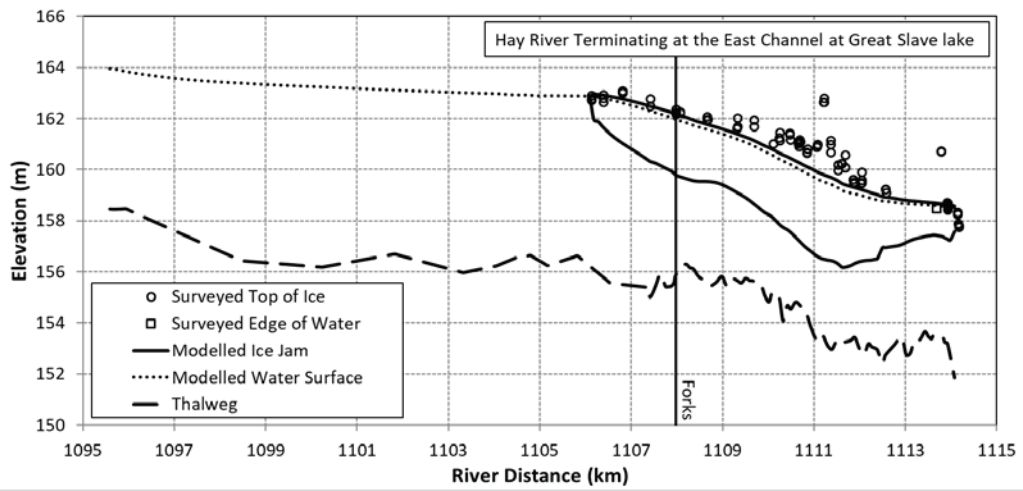
Figure 4.12: Ice jam profiles for May 7th, 2009.

Figure 4.13: Example of stranded ice block recorded using TOI label.
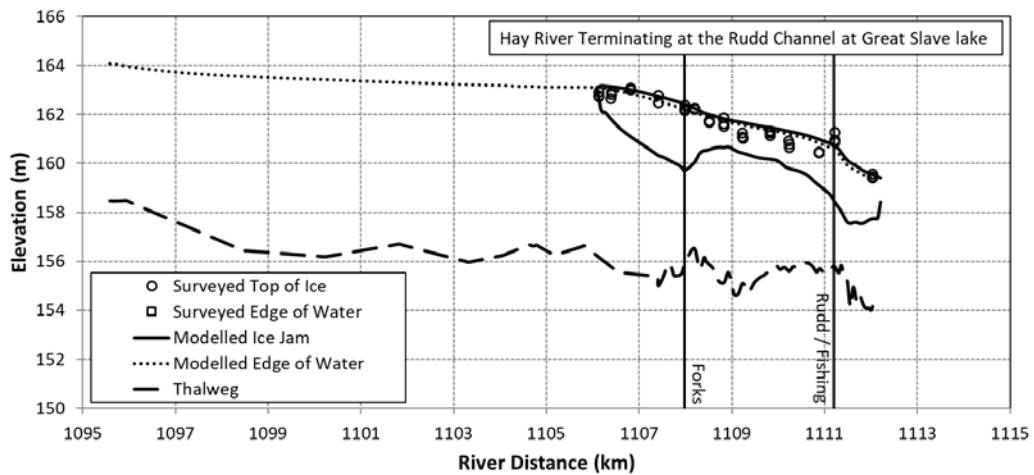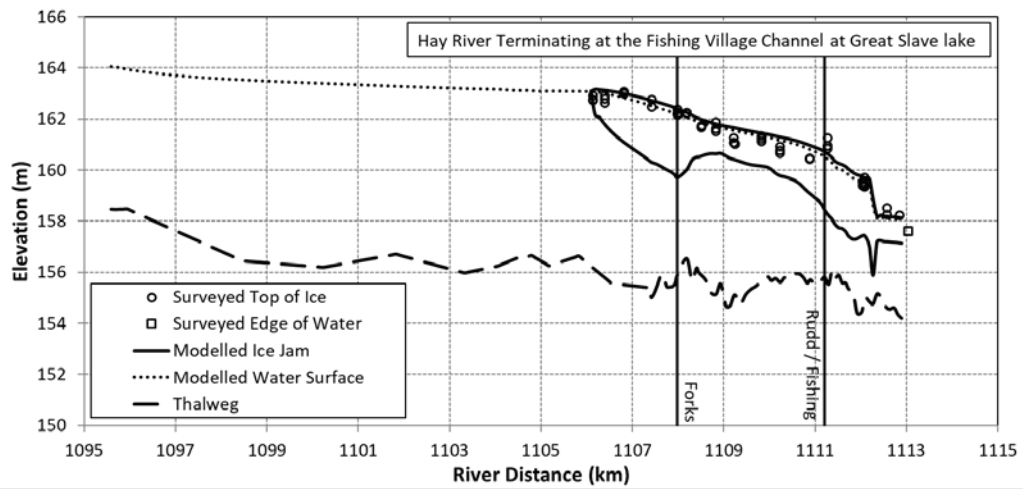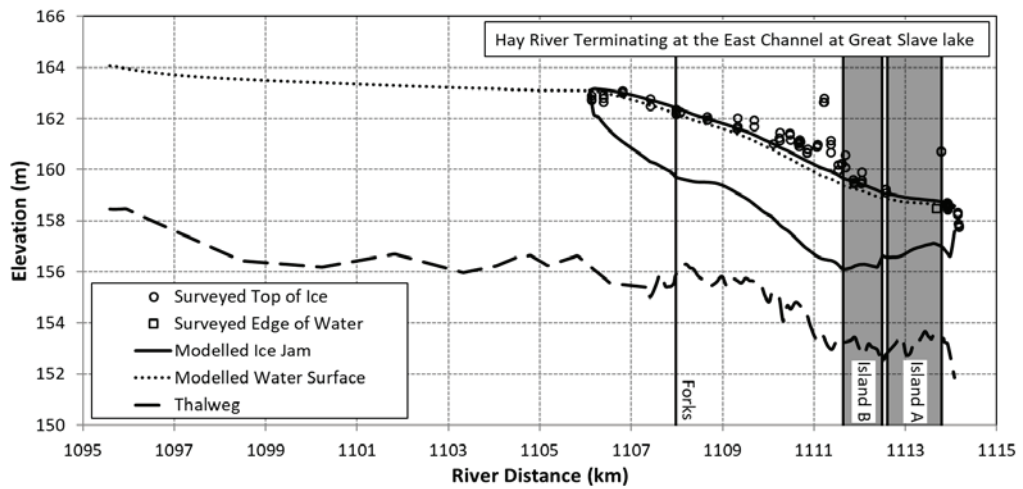
Figure 4.14: Jam profiles for May 7ᵗʰ with peak discharge used in jam calculation.

Tables

Table 4.1: Global parameters for ice jam simulations with islands.

Parameter	Value
Channel width, B (m)	600
Bed roughness height, k_b (m)	0.08
Density of ice, ρ_i (kg/m³)	916
Ice jam roughness height, k_i (m)	3.0
Composite jam strength parameter, μ	1.3
Ice cohesion, τ_c (Pa)	0
Ice jam porosity, p_j	0.4
Erosion velocity, V_{max} (m/s)	1.6
Passive pressure coefficient, K_v	7.55
Maximum allowable difference in discharge, $Q_{tolerance}$ (m³/s)	0.01

Table 4.2: Model parameters and test results for ice jam simulations with islands.

Test	Parameter				Present Study			Jasek (1995)			RD
	Q_w	S_{bed}	Y_{normal}	L_{is}/B	Y_{eq}	Y_{min}	Y_{min}/Y_{eq}	Y_{eq}	Y_{min}	Y_{min}/Y_{eq}	
	(m³/s)	(m/m)	(m)		(m)	(m)		(m)	(m)		(%)
1	1500	0.001	3.677	64	9.29	6.57	0.706	9.33	6.59	0.706	0.00
2	1500	0.001	3.677	32	9.29	6.57	0.707	9.33	6.6	0.707	0.00
3	1500	0.001	3.677	16	9.29	6.69	0.720	9.33	6.72	0.720	0.00
4	1500	0.001	3.677	8	9.29	7.17	0.772	9.33	7.18	0.770	0.26
5	1500	0.001	3.677	4	9.29	7.87	0.847	9.33	7.87	0.843	0.47
6	1500	0.001	3.677	2	9.29	8.49	0.914	9.33	8.47	0.907	0.77
7	1500	0.001	3.677	1	9.29	8.89	0.957	9.33	8.86	0.950	0.74
8	1500	0.0003	4.774	64	6.77	5.72	0.845	6.79	5.73	0.844	0.12
9	1500	0.0003	4.774	32	6.77	5.72	0.845	6.79	5.73	0.844	0.12
10	1500	0.0003	4.774	16	6.77	5.79	0.856	6.79	5.8	0.855	0.12
11	1500	0.0003	4.774	8	6.77	6.00	0.885	6.79	6	0.884	0.11
12	1500	0.0003	4.774	4	6.77	6.24	0.921	6.79	6.24	0.919	0.22
13	1500	0.0003	4.774	2	6.77	6.46	0.954	6.79	6.45	0.950	0.42
14	1500	0.0003	4.774	1	6.77	6.61	0.977	6.79	6.6	0.972	0.51
15	4000	0.00005	12.231	64	12.66	12.51	0.988	12.68	12.56	0.990	-0.20
16	4000	0.00005	12.231	16	12.60	12.55	0.996	12.67	12.63	0.996	0.00
17	4000	0.00005	12.231	1	12.57	12.57	0.999	12.66	12.66	1.000	-0.10

Table 4.3: Boundary conditions for open water simulations.

Inflow Discharge from 07OB001 (m³/s)	Downstream Lake Levels from 07OB002 (m)
160	156.834
258	156.885
595	156.991
954	156.912

Table 4.4: Boundary conditions for ice jam profile simulations.

Date	Inflow Discharge (m³/s)	Downstream Boundary Water Level (m)		
		East Channel	**Rudd Channel[1]**	**Fishing Village Channel**
May 3	317	156.52	156.52	156.52
May 4	463	156.56	157.6	156.82
May 5	540	156.73	157.6[2]	156.97
May 7	700	158.5	159.32	158.06

[1] Island Channel boundary condition assumed to be the same as the Rudd Channel
[2] No data available for May 5th, assumed to be equal to water level from May 4th

Table 4.5: Jam head and toe locations for ice jam profile simulations.

Date	Head Location (km)	Toe Location (km)		
		East Channel	**Rudd Channel**	**Fishing Village Channel**
May 3	1106.09	1111.00	1111.00	1111.00
May 4	1107.93	1111.36	1111.94	1112.43
May 5	1106.18	1111.94	1111.97	1112.21
May 7	1106.18	1114.08[3]	1112.20[3]	1112.46

[3] Toe of jam set at downstream boundary

Table 4.6: Global parameters for the ice jam profile simulations.

Parameter	Value	Values in Literature
Density of ice, ρ_i (kg/m³)	916	916 (Jasek, 1995) 917 (Lal and Shen, 1991)
Composite jam strength parameter, μ	1.3	1.28 (Pariset and Hausser, 1961; Pariset et al., 1966) 0.8 -1.2 (Healy and Hicks, 1999) 0.98 – 1.99 (Flato and Gerard, 1986)
Ice cohesion, τ_c (Pa)	0	0 for breakup jams
Ice jam porosity, ja	0.4	0.4 (Jasek, 1995; Beltaos, 2003)
Erosion velocity, V_{max} (m/s)	1.5	1.6 (Jasek, 1995) 1.25 (Flato, 1988)
Passive pressure coefficient, K_v	10	7.55 (Jasek, 1995) 10 – 12 (Beltaos, 2003)
Maximum allowable difference in discharge, $Q_{tolerance}$ (m³/s)	0.01	

References

Beltaos, S. 1988. Configuration and properties of a breakup jam. Canadian Journal of Civil Engineering, Ottawa, 15(4): 685-697.

Beltaos, S. 1993. Numerical computation of river ice jams. Canadian Journal of Civil Engineering, Ottawa, 20(1): 88-99.

Beltaos, S. 2003. Numerical modelling of ice-jam flooding on the Peace-Athabasca delta. Hydrological Processes, 17, 3685-3702 (2003).

Beltaos, S., Carter, T., & Rowsell, R. 2012. Measurements and analysis of ice breakup and jamming characteristics in the Mackenzie Delta, Canada. Cold Regions Science and Technology, 82: 110-123.

Beltaos, S., Wong, J. 1986. Downstream transition of river ice jams. Journal of Hydraulic Engineering, ASCE, 112(2): 91-110.

Blackburn, J., She, Y. 2019. A comprehensive public-domain river ice process model and its application to a complex natural river. Cold Reg. Sci. Technol. 163, 44-58.

Blackburn, J., She. Y. 2021. One-dimensional channel network modelling and simulation of flow conditions during the 2008 ice breakup in the Mackenzie Delta, Canada. Cold Reg. Sci. Technol. 189 (2021) 103339.

Brayall, M. G. 2011. 2-D Hydraulic and Ice Process Modeling at Hay River, NWT. M.Sc. thesis, Department of Civil and Environmental Engineering, University of Alberta, Edmonton, AB.

Brayall, M. Hicks, F.E. 2012. Applicability of 2-D modeling for forecasting ice jam flood levels in the Hay River Delta, Canada. Canadian Journal of Civil Engineering, 39: 701-712.

De Coste, M., She, Y., Blackburn, J. 2017. Incorporating the effects of upstream ice jam releases in the prediction of flood levels in the Hay River delta, Canada. Canadian Journal of Civil Engineering, 44: 643-651.

Flato, G. 1988. Calculation of ice jam profiles. Master's Thesis, University of Alberta, Edmonton, Alberta, 177 pp.

Flato, G., and Gerard, R. 1986. Calculation of ice jam thickness profiles. Proc., 4th Workshop on Hydraulics of River Ice, Subcommittee of Hydraulics of Ice Covered Rivers, National Research Council of Canada, Montreal, C-3.1-18.

Fread, D.L. 1988. The NWS DAMBRK Model: Theoretical Background/User Documentation. Office of Hydrology, National Weather Service (NWS), Maryland, U.S.A.

Healy, D., Hicks, F. 1999. Comparison of ICEJAM and RIVJAM Ice Jam Profile Models. Journal of Cold Regions Engineering, 13(4): 180-198.

Hicks, F.E., Steffler, P.M. 1990. Finite element modeling of open channel now. Water Resources Engineering Report No. 90-6. Department of Civil Engineering, University of Alberta, Edmonton, AB, 356 pp.

Hicks, F.E., Steffler, P.M. 1992. A Characteristic Dissipative Galerkin Scheme for Open Channel Flow. ASCE Journal of Hydraulic Engineering 118: 337-352.

Jasek, M. 1995. Ice jam simulations in rivers with islands. Proceedings of the 8th Workshop on the Hydraulics of Ice Covered Rivers, Kamloops, BC, 421-441.

Jasek, M., Muste, M., Ettema, R. 2001. Estimation of Yukon River discharge during an ice jam near Dawson City. Canadian Journal of Civil Engineering, 28: 856-864.

Kolerski, T., Shen, H.T. 2015. Possible effects of the 1984 St. Clair River ice jam on bed changes. Canadian Journal of Civil Engineering, 42: 696-703.

Kovachis, N. 2011. Patterns of river breakup timing and sequencing, Hay River, NWT. Master's Thesis. University of Alberta, Edmonton, Canada, 459 pp.

Lindenschmidt, K.-E., Sydor, M., Carson, R., Harrison, R. 2012. Ice Jam Modelling of the Lower Red River. Journal of Water Resource and Protection, 2012, 4, 1-11.

Mackay, J. R. 1963. The Mackenzie Delta Area, N.W.T. Miscellaneous Report 23. Geological Survey of Canada, Ottawa, Ontario, 202 pp.

Nafziger, J., She, Y., Hicks, F. 2019. Dynamic river ice processes in a river delta network. Cold Regions Science and Technology, 158: 275-287.

Nafziger, J., Kovachis, N., Emmer, S. 2021. A Tale of Two Basins: The 2020 river ice breakup in northern Alberta, part I: The Athabasca River. In: CGU-HS Committee on River Ice Processes and the Environment Workshop on the Hydraulics of Ice Covered Rivers. August 29-September 1, 2021, Saskatoon, SK.

Osada, K., Ettema, R., Shimizu, Y., Wakai, A. 2020. ASCE Journal of Cold Regions Engineering, 34(1): 0401917.

Oveisy, A., She, Y. 2017. Modelling Ice Jam Formation in the Hay River Delta during 2009 Breakup. Proceedings on the 19th Workshop on the Hydraulics of Ice Covered Rivers, Whitehorse, Yukon, Canada.

Pariset, E., Hausser, R. 1961. Formation and evolution of ice covers on rivers. Transactions of the Engineering Institute of Canada 5: 41-49.

Pariset, E., Hausser, R., Gagnon, A. 1966. Formation of ice covers and ice jams in rivers. ASCE Journal of the Hydraulics Division 92(HY6): 1-24.

Peters, D.L., Prowse, T.D., Pietroniro, A. Leconte, R. 2006. Flood hydrology of the Peace-Athabasca Delta, northern Canada. Hydrological Processes. 20: 4073-4096.

She, Y., Hicks. F. 2006. Modeling ice jam release waves with consideration for ice effects. Cold Regions Science and Technology, 45: 137-147.

Terroux, A., Sherstone, D., Kent, T., Anderson, J., Bigras, S., & Kriwoken, L. 1981. Ice regime of the Lower Mackenzie River and Mackenzie Delta. The National Hydrology Research Institute, Environment Canada. Hull, Quebec, 115 pp.

Uzuner, M.S., Kennedy, J.F. 1976. Theoretical Model of River Ice Jams. ASCE Journal of the Hydraulics Division 102 (HY9): 1365-1383.

Zhang, F., Mosaffa, M. Chu, T., Lindenschmidt, K-E. 2017. Using Remote Sensing Data to Parameterize Ice Jam Modeling for a Northern Inland Delta. Water, 9, 306.

5.   Summary and Conclusions

The work in this thesis improves on the state-of-the-art in 1D river ice modelling capabilities. River ice models are important tools for both engineers and researchers because they provide an efficient and cost effective means of analyzing the impacts of ice on a river's regime (e.g. impacts to channel geomorphology, river ecology) and on human infrastructure (e.g. impacts on hydropower operations, impacts due to ice jam flooding). They are also paramount for studying how river ice impacts have and will continue to change due to one of humanity's biggest challenges: climate change. Although many 1D river ice models exist, none are without limitations in their application. The objective of this thesis was to improve upon the open water and river ice modelling capabilities in the University of Alberta's *River1D* model as part of a long-term goal to develop a public-domain comprehensive river ice process model that is capable of handling complex natural river systems from compound single channels to river deltas with multiple junctions and islands. New features added to the model include natural channel cross section modelling capabilities, new and enhanced river ice process modelling capabilities, dynamic junction and channel network modelling capabilities, and ice jam profile modelling capabilities within complex natural channel networks. This study offers three new and novel contributions to 1D river ice modelling.

1. A comprehensive ice processes model with natural channel modelling capabilities, using the robust CDG finite element scheme, has been developed. An unprecedentedly comprehensive calibration and validation of the model were

207

conducted with survey data, including water levels, flows, water temperature, surface ice concentrations, border ice widths, ice cover progression rates, and ice thicknesses.

2. A new momentum-based approach to modelling channel junctions and 1D networks has been developed. The new approach takes into account the significant physical effects at channel junctions (such as gravity and flow separation forces, and channel resistance) rather than using the simpler, more commonly adapted assumption of equating water levels across the junction. The approach is also equipped with the ability to dynamically change junction configurations (i.e. diverging to converging or vice versa) as a result of flow reversals.

3. A new modelling approach for simulating ice jam profiles in 1D channel network models has been developed. The model simulates ice jam profiles that extend through complex channel networks with multiple junctions and islands by considering the effect of the junction discharge ratio on channel junction elements when solving the ice jam stability equation.

These contributions are discussed below and recommendations for future research are presented at the end.

5.1   *Natural channel and ice processes modelling*

River1D was enhanced with the ability to simulate natural channel geometry, water supercooling, anchor ice formation and release, border ice formation, under-cover

transport of frazil, and ice cover progression based on leading edge stability criteria. Previous versions of the model employed an equation formulation that required a rectangular channel approximation to natural cross sections. Although the rectangular channel approximation is helpful when bathymetric data is scare, the rectangular channel formulation limits the application of the model since water levels cannot be modelled accurately without natural channel bathymetry. The new natural channel capabilities were validated with simulation of water levels on the Susitna River, Alaska, for both open water and ice covered scenarios. This is an important enhancement to the model since accurate water level modelling is paramount in the forecasting of flood levels. The new ice process enhancements to the model, although available in other models, are novel here because they are being simulated using a FEM solution approach. Additionally, these new ice process enhancements raise the level of sophistication of *River1D* which is an important step towards the long-term goal of developing a public-domain comprehensive river ice process model capable of simulating complex real-world river ice problems. Freeze-up and winter data collected along the Susitna River allowed for a comprehensive calibration and validation of many of the new model enhancements. Model results agreed favourably with observed water levels, flows, water temperatures, surface ice concentrations, border ice widths, ice cover progression rates, and river ice thicknesses.

5.2   *Junction and network modelling*

Because ice jams tend to occur where river geometry is complicated by junctions (e.g. at confluences, and in reaches with islands), the ability to model junction hydraulics effectively was recognized as an important feature for any river ice model. Although the most common approach to modelling junctions in 1D models is to assume equal water levels across the junction, this approach is limited to applications where water surface slopes are flat and flows are relatively steady and not dynamic. A new momentum based approach to modelling channel junctions and networks has been developed and validated. The model was compared to a 2D model for a number of steady and unsteady tests. For the steady tests, the model performed exceptionally well with respect to discharge split, but model accuracy for water level simulation upstream of the flow splits could be improved. Water level discrepancies between the 1D and 2D models could be partly attributed the omission of forces at the junction (e.g. centrifugal force). For the unsteady tests, the model was able to simulate transient flows in the test network, including flow reversals.

The new model was then applied to a network of channels in the MD. The model was calibrated and validated using three open water events. The calibrated model was then used to simulate flow conditions during the 2008 breakup of the MD. Model results agreed well with observed water level data collected using data loggers and also indicated a flow reversal in the Peel Mackenzie Connector; a reversal that is consistent with observations in this channel during the 2008 breakup. This new momentum based

approach to junctions will be key for future applications of the model to dynamic ice jam formation and/or ice jam release in complex channel networks.

5.3   *Ice jam profile modelling in channel networks*

After developing the new junction hydraulics capabilities in *River1D*, the model was expanded to include ice jam profile modelling through channel junctions. This is a unique contribution because existing ice jam profile models are either limited to simulating a single channel or they do not explicitly provide details as to how or whether they can accurately simulate ice jam profiles in channels with junctions. This new capability was compared to test results from a previous modelling study for a number of idealized cases of ice jamming in a channel with a single island. Not only did the model perform well with the idealized case results, it was also able to calculate the flow split around the island, which had to be specified in the previous study.

The ice jam profile modelling capabilities were used to simulate ice jam profiles in the HRD. The model was able to simulate a series of surveyed ice profiles from the 2009 breakup quite well using a single under ice jam roughness value except for the profile data collected after an ice jam release wave had passed through the HRD, causing the ice jam to collapse and consolidate. When the peak discharge was used to calculate the ice jam configuration rather than the daily discharge reported on the day the ice jam profile data were collected, the model was able to more accurately simulate the surveyed levels and the difference between the observed and simulated top of ice levels was reduced by 50%.

5.4   *Future Recommendations*

To continue to improve upon the river ice modelling capabilities in *River1D*, the author recommends the following:

- The capability to simulate bridging based on bridging criterion in addition to the current option which requires a user specified location and time of bridging.

- Inclusion of other forces acting on junctions (e.g. centrifugal pressure, interfacial shear, frictions shear). This inclusion may improve the junction modelling accuracy.

- Automation of the ice jam profile calculations in networks to eliminate the need for the user specified reach order when solving the ice jam stability equation.

- Combination of the junction modelling capabilities with ice dynamic equations for the simulation of dynamic ice jam formation in channel networks.

- Inclusion of a means of evaluating the stability of an ice cover as it forms. This could either be done using a discrete approach of evaluating the ice stability at every element or it could be accomplished by solving a momentum equation for the floating ice.

- Extension of the junction modelling capabilities in *River1D* to include the other ice processes presently in the model.

References

Andrishak, R., Hicks, F.E. 2005. Impact of Climate Change on the Peace River Thermal Ice Regime. In: CGU HS Committee on River Ice Processes and the Environment Proc., 13th Workshop on Hydraulics of Ice Covered Rivers, September 15-16, 2005, Hanover, NH, 21–40.

Andrishak, R., Hicks, F. 2008. Simulating the effects of climate change on the ice regime of the Peace River. Canadian Journal of Civil Engineering 35: 461-472.

Andrishak, R., Hicks, F. 2011. Ice effects on flow distributions within the Athabasca Delta, Canada. River Research and Applications 27: 1149-1158.

Ashton, G.D. 1973. Heat transfer to river ice covers. In Proceedings of the 30th Eastern Snow Conference, Amherst, Mass., 8-9 February 1973. Eastern Snow Conference, Monmouth, Maine, 125-135.

Ashton, G.D. 1974. Froude criterion for ice-block stability. Journal of Glaciology 13: 307-313.

Ashton, G.D. (Ed.) 1986. River and Lake Ice Engineering. Water Resources Publications, Littleton, Colorado, 485 pp.

Ashton, G., Beltaos, S. 2013. Chapter 8: Thermal Growth of Ice Cover. In: Beltaos, S. (ed) River Ice Formation. CGU HS Committee on River Ice Processes and the Environment, 257-296.

Beltaos, S. 1988. Configuration and properties of a breakup jam. Canadian Journal of Civil Engineering, Ottawa, 15(4): 685-697.

Beltaos, S. 1993. Numerical computation of river ice jams. Canadian Journal of Civil Engineering, Ottawa, 20(1): 88-99.

Beltaos, S. 2001. Hydraulic Roughness of Breakup Ice Jams. Journal of Hydraulic Engineering. 127 (8): 650-656.

Beltaos, S. 2003. Numerical modelling of ice-jam flooding on the Peace-Athabasca delta. Hydrological Processes, 17, 3685-3702 (2003).

Beltaos, S. 2012. Mackenzie Delta flow during spring breakup: uncertainties and potential improvements. Canadian Journal of Civil Engineering. 39 (5): 579-588

Beltaos, S. 2013. Chapter 7: Freezeup Jamming and Formation of Ice Cover. In: Beltaos, S. (ed) River Ice Formation. CGU HS Committee on River Ice Processes and the Environment, 181-255.

Beltaos, S., Carter, T. 2009. Field studies of ice breakup and jamming in the Mackenzie Delta. Proceedings of the 15th Workshop on River Ice, St. John's, NL, 266-283.

Beltaos, S., Carter, T., & Rowsell, R. 2012. Measurements and analysis of ice breakup and jamming characteristics in the Mackenzie Delta, Canada. Cold Regions Science and Technology, 82: 110-123.

Beltaos, S., Prowse, T. 2001. Climate impacts on extreme ice-jam events in Canadian rivers, Hydrological Sciences Journal, 46(1): 157-181.

Beltaos, S., Wong, J. 1986. Downstream transition of river ice jams. Journal of Hydraulic Engineering, ASCE, 112(2): 91-110.

Blackburn, J., She, Y., Hicks, F., Nafziger, J. 2015. Ice effects on flow distributions in the Mackenzie Delta. In: 18th CGU-HS Committee on River Ice Processes and the Environment Proc., 18th Workshop on the Hydraulics of Ice Covered Rivers, Quebec City, Quebec, August 18-20, 2015.

Blackburn, J., She, Y. 2019. A comprehensive public-domain river ice process model and its application to a complex natural river. Cold Regions Science and Technology. 163: 44-58.

Blackburn, J., She. Y. 2021. One-dimensional channel network modelling and simulation of flow conditions during the 2008 ice breakup in the Mackenzie Delta, Canada. Cold Reg. Sci. Technol. 189 (2021) 103339.

Brayall, M. G. 2011. 2-D Hydraulic and Ice Process Modeling at Hay River, NWT. M.Sc. thesis, Department of Civil and Environmental Engineering, University of Alberta, Edmonton, AB.

Brayall, M., Hicks, F.E. 2012. Applicability of 2-D modeling for forecasting ice jam flood levels in the Hay River Delta, Canada. Canadian Journal of Civil Engineering, 39: 701-712.

Brooks, A.N., Hughes, T.J.R. 1982. Streamline Upwind Petrov-Galerkin Formulations for Convection Dominated Flows with Particular Emphasis on the Incompressible Navier-Stokes Equations. Computer Methods in Applied Mechanics and Engineering. 32(1-3): 199-259.

Brown, R.S., Mackay, W.C. 1995. Fall and winter movements and habitat use by cutthroat trout in the Ram River, Alberta. Transactions of the American Fisheries Society 124: 873-885.

Brown, R.S., Power, G., Beltaos, S., Beddow, T.A. 2000. Effects of hanging ice dams on winter movements and swimming activity of fish. Journal of Fish Biology 57: 1150-1159.

Brunner, G.W. 2020a. HEC-RAS, River Analysis System Hydraulic Reference Manual Version 6.0 Beta. U.S. Army Corps of Engineers Hydrologic Engineering Center. 466 pp.

Brunner, G.W. 2020b. HEC-RAS River Analysis System User's Manual Version 6.0 Beta. U.S. Army Corps of Engineers Hydrologic Engineering Center. 721 pp.

Calkins, D.J. 1984. Instream Ice Calibration of Computer Model. Alaska Power Authority Document no. 1122. 111 pp.

Carson, R., Beltaos, S., Groeneveld, J., Healy, D., She, Y., Malenchak, J., Morris, M. Saucet, J. Kolerski, T., Shen, H. T. 2011. Comparative testing of numerical models of river ice jams. Canadian Journal of Civil Engineering, 38(6): 669-678.

Carson, R., Groeneveld, J. L. 1997. Evolution of the ICESIM Model. In: CGU HS Committee on River Ice Processes and the Environment Proc., 9th Workshop on River Ice, September 24-26, 1997, Fredericton, NB, 289-302.

Clark, S. 2013. Chapter 3: Border and Skim Ice. In: Beltaos, S. (ed) River Ice Formation. CGU HS Committee on River Ice Processes and the Environment, 77-106.

Clark, S., Doering, J. 2006. Laboratory experiments on frazil-size characteristics in a counterrotating flume. Journal of Hydraulic Engineering, 132: 94-101.

Daly, S.F. 1984. Frazil ice dynamics. U.S. Army Cold Regions Research and Engineering Laboratory, Hanover, N. H., 46 pp.

Daly, S.F. 1991. Frazil ice blockage of intake trash racks. CRREL Technical Digest 91-1. Army Corps of Engineers Cold Regions Research and Engineering Laboratory. Hanover, New Hampshire, 12 pp.

Daly, S.F. 2013. Chapter 4: Frazil Ice. In: Beltaos, S. (ed) River Ice Formation. CGU HS Committee on River Ice Processes and the Environment, 107-134.

Daly, S.F. and Axelson, K.D. 1990. Stability of floating and submerged blocks. Journal of Hydraulic Research 28: 737-752.

De Coste, M., She, Y., Blackburn, J. 2017. Incorporating the effects of upstream ice jam releases in the prediction of flood levels in the Hay River delta, Canada. Canadian Journal of Civil Engineering, 44: 643-651.

DHI, 2021. MIKE 11, A Modelling System for Rivers and Channels, Reference Manual, 500 pp.

Dow Ambtman, K. E., Hicks, F. E., & Steffler, P. M. 2011a. Experimental Investigation of the Pressure Distribution beneath a Floating Ice Block. Journal of Hydraulic Engineering, 137: 399-411.

Dow Ambtman, K. E., Steffler, P. M., & Hicks, F. E. 2011b. Analysis of the Stability of Floating Ice Blocks. Journal of Hydraulic Engineering, 137: 412-422.

Dow, K., Steffler, P.M., Zhu, D.Z. 2009. Case Study: Intermediate Field Mixing for a Bank Discharge in a Natural River. Journal of Hydraulic Engineering, 135(1): 1-12.

Emmerton, C.A., Lesack, L.F.W., Marsh, P. 2007. Lake abundance, potential water storage, and habitat distribution in the Mackenzie River Delta, western Canadian Arctic. Water Resources Research 43, W05419, 14 pp.

Environment Canada, 2013. RIVICE Model - User's Manual. RIVICE Steering Committee, Environment Canada, January 2013, 185 pp.

Ettema, R. Muste, M., Kruger, A. 1999. Ice jams in river confluences. US Army Corps of Engineering, Cold Regions Research and Engineering Laboratory, Report 99-06, 61 pp.

Flato, G. 1988. Calculation of ice jam profiles. Master's Thesis, University of Alberta, Edmonton, Alberta, 177 pp.

Flato, G., and Gerard, R. 1986. Calculation of ice jam thickness profiles. Proc., 4th
Workshop on Hydraulics of River Ice, Subcommittee of Hydraulics of Ice Covered
Rivers, National Research Council of Canada, Montreal, C-3.1-18.

Fread, D.L. 1988. The NWS DAMBRK Model: Theoretical Background/User
Documentation. Office of Hydrology, National Weather Service (NWS), Maryland,
U.S.A.

Fread, D.L., Jin, M., Lewis, J. M., 1996. An LPI Numerical Solution for Unsteady Mixed
Flow Simulation, North American Water Congress, Anaheim, CA June 22-28, 1996,
American Society of Civil Engineers, 1-7.

Garcia-Navarro, M. P., Savirón, J. M. 1992. Numerical simulation of unsteady flow at
open channel junctions. Journal of Hydraulic Research, 30(5): 595-609.

Ghareh Aghaji Zare, S., Ansari, S., Rennie, C.D., Seidou, O., Groenveld, R., Ahsan, R.,
Malenchak, J., Ahmari, H. 2015. Simulation of river ice processes in a regulated ice
covered river. In: CGU HS Committee on River Ice Processes and the Environment
Proc., 18th Workshop on Hydraulics of Ice Covered Rivers, Quebec City, Quebec.

Ghostine, R., Kesserwani, G., Mose, R., Vazquez, J., Ghenaim, A., Gregoire, C. 2009. A
confrontation of 1D and 2D RKDG numerical simulation of transitional flow at open-
channel junction. International Journal for Numerical Methods in Fluids, 61: 752-767.

Ghostine, R., Vazquez, J., Nicolas, R., Terfous, A., Ghenaim, A., Mose, R. 2013. A
comparative study of the 1D and 2D approaches for simulation of flows at right
angled dividing junctions. Applied Mathematics and Computation, 219 (2013): 5070-
5082.

Girling, W.C., Groeneveld, J. 1999. Anchor Ice Formation Below Limestone Generating
Station. In: CGU HS Committee on River Ice Processes and the Environment Proc.,

10th Workshop on Hydraulics of Ice Covered Rivers, Winnipeg, Manitoba, Canada, pp. 160-173.

Gosink, J.P., Osterkamp, T.E. 1983. Measurements and analyses of velocity profiles and frazil ice-crystal rise velocities during periods of frazil-ice formation in rivers. Annals of Glaciology, 4: 79-84.

Goulding, H., Prowse, T., Beltaos, S. 2009. Spatial and temporal patterns of breakup and ice jam flooding in the Mackenzie Delta, NWT. Hydrologic Processes, 23(18): 2555-2704.

Gurram, S.K., Karki, K.S., Hager, W.H. 1997. Subcritical junction flow. ASCE Journal of Hydraulic Engineering, 123(5): 447-455.

Haresign, M., Toews, J.S., Clark, S. 2011. Comparative testing of border ice growth prediction models. In: CGU HS Committee on River Ice Processes and the Environment Proc., 16th Workshop on River Ice, September 18-22, 2011, Winnipeg, MB, 400-412.

HDR, Alaska Inc. 2014. Ice processes in the Susitna River study, Study plan Section 7.6, Initial Study Report. Prepared for Alaska Energy Authority. 51 pp.

Healy, D., Hicks, F. 1999. Comparison of ICEJAM and RIVJAM Ice Jam Profile Models. Journal of Cold Regions Engineering, 13(4): 180-198.

Healy, D., Hicks, F.E. 2006. Experimental Study of Ice Jam Formation Dynamics, Journal of Cold Regions Engineering, 30(4): 117-139.

Heine, M., Andre, A., Kritsch, I., Cardinal, A. 2007. Gwichya Gwich'in Googwandak. The History and Stories of the Gwichya Gwich'in, 405 pp.

Hicks, F.E. 1996. Hydraulic Flood Routing with Minimal Channel Data: Peace River, Canada. Canadian Journal of Civil Engineering 23(2): 524-535.

Hicks, F. 2016. An introduction to River Ice Engineering for Civil Engineers and Geoscientists, 159 pp.

Hicks, F. E., McKay, K., Shabayek, S. 1997. Modelling an ice jam release surge on the St. John River, New Brunswick. In: CGU HS Committee on River Ice Processes and the Environment Proc., 9th Workshop on River Ice, September 24-26, 1997, Fredericton, NB, 303-314.

Hicks, F.E., Steffler, P.M. 1990. Finite element modeling of open channel now. Water Resources Engineering Report No. 90-6. Department of Civil Engineering, University of Alberta, Edmonton, AB, 356 pp.

Hicks, F.E., Steffler, P.M. 1992. A Characteristic Dissipative Galerkin Scheme for Open Channel Flow. ASCE Journal of Hydraulic Engineering 118: 337-352.

Hicks, F.E., Steffler, P.M., Gerard, R. 1992. Finite element modeling of surges propagation and an application to the Hay River, N.W.T. Canadian Journal of Civil Engineering 19 (3): 454-462.

Holmquist, J.G., Waddle, T.J. 2013. Predicting macroinvertebrate response to water diversion from a mountain stream using two-dimensional hydrodynamic models and zero flow approximation. Ecological Indicators, 28: 115-124.

Hsu, C.C., Lee W.J., Chang C.H. 1998. Subcritical open-channel junction flow. ASCE Journal of Hydraulic Engineering, 124(8): 847-855.

Huang, J., Weber, L.J., Lai, Y.G. 2002. Three-dimensional numerical study of flows in open-channel junctions, ASCE Journal of Hydraulic Engineering, 128 (2002): 268-280.

Huokuna, M. 1990. The Finnish River Ice Research Project – the Numerical River Ice Model in Use. In: Proceedings of 10th IAHR International Symposium on Ice, Espoo, Finland. Volume 3: 215-230.

Hutchison, T.K., Hicks, F. 2007. Observations of ice jam release events on the Athabasca River, AB. Canadian Journal of Civil Engineering 34(4): 473-484.

Jasek, M. 1995. Ice jam simulations in rivers with islands. Proceedings of the 8th Workshop on the Hydraulics of Ice Covered Rivers, Kamloops, BC, 421-441.

Jasek, M., Ghobrial, T., Loewen, M., Hicks, F. 2011. Comparison of CRISSP modeled and SWIPS measured ice concentrations on the Peace River. In: CGU HS Committee on River Ice Processes and the Environment Proc., 16th Workshop on River Ice, September 18-22, 2001, Winnipeg, MB, 249-273.

Jasek, M., Muste, M., Ettema, R. 2001. Estimation of Yukon River discharge during an ice jam near Dawson City. Canadian Journal of Civil Engineering, 28: 856-864.

Jasek, M., Shen, H.T., Pan, J, Paslawski, K. 2015. Anchor Ice Waves and their Impact on Winter Ice cover Stability. In: 18th CGU-HS Committee on River Ice Processes and the Environment Proc. 18th Workshop on the Hydraulics of Ice Covered Rivers, Quebec City, Quebec, August 18-20, 2015.

Judge, D.G., Lavender, S.T., Carson, R.W., Ismail, S. 1997. Headpond Ice Jams – Where Will They Occur? In: CGU HS Committee on River Ice Processes and the Environment Proc., 9th Workshop on River Ice, September 24-26, 1997, Fredericton, N.B, 73-87.

Kammerer, J.C. 1990. Largest rivers in the United States: U.S. Geological Survey Open-File Report 87-242, 2 pp.

Kerr, D.J., Shen, H.T., Daly, S.F. 2002. Evolution and hydraulic resistance of anchor ice on gravel bed. Journal of Cold Regions Science and Technology. 35 (2): 101-114.

Kesserwani, G., Ghostine, R., Vasquez, J., Mosé, R., Abdallah, M. Ghenaim, A. 2008. Simulation of subcritical flow at open-channel junction. Advances in Water

Kolerski, T., Shen, H.T. 2015. Possible effects of the 1984 St. Clair River ice jam on bed changes. Canadian Journal of Civil Engineering, 42: 696-703.

Kovachis, N. 2011. Patterns of river breakup timing and sequencing, Hay River, NWT. Master's Thesis. University of Alberta, Edmonton, Canada, 459 pp.

Lal, A.M. W., Shen, H. T. 1991. A Mathematical for River Ice Processes, Journal of Hydraulic Engineering, ASCE, 117(7): 851-867.

Larsen, P. 1975. Notes on the stability of floating ice blocks. Proceedings IAHR Third International Symposium on Ice Problems, Hanover, NH, 305-313.

Law, S.W. 1965. Dividing flow in an open channel. Thesis presented to McGill University, Montreal, Quebec, in partial fulfillment of the requirements for the degree of Masters of Engineering, 89 pp.

Lindenschmidt, K.E. 2017. RIVICE - A Non-Proprietary, Open-Source, One-Dimensional River-Ice Model. Water, 9(5), 314: 1-15.

Mackay, J. R. 1963. The Mackenzie Delta Area, N.W.T. Miscellaneous Report 23. Geological Survey of Canada, Ottawa, Ontario, 202 pp.

Malenchak, J. 2011. Numerical modelling of river ice processes on the Lower Nelson River. Ph.D. Thesis, University of Manitoba, Winnipeg, Canada.

Malenchak, J., Clark, S. 2013. Chapter 5: Anchor Ice. In: Beltaos, S. (ed) River Ice Formation. CGU HS Committee on River Ice Processes and the Environment, 135-157.

Marcotte, N., Robert, S. 1986. Elementary mathematical modelling of anchor ice. In: Proceedings of 8th IAHR International Symposium on Ice, Iowa City, Iowa, Iowa Institute of Hydraulic Research, Volume 1: 493-506.

Matousek, V. 1984a. Types of Ice Run and Conditions for their Formation, In: Proceedings of 7th IAHR International Symposium on Ice, Hamburg, Germany. Volume 1: 315-327.

Matousek, V. 1984b. Regularity of the Freezing-up of the Water Surface and Heat Exchange between water body and water surface, In: Proceedings of 7th IAHR International Symposium on Ice, Hamburg, Germany. Volume 1: 187-200.

McFarlane, V., Loewen, M., Hicks, F. 2014. Laboratory measurements of the rise velocity of frazil ice particles. Journal of Cold Regions Science and Technology. 106-107 (2014): 120-130.

McFarlane, V., Loewen, M., Hicks, F. 2015. Measurements of the evolution of frazil ice particle size distributions. Journal of Cold Regions Science and Technology. 120: 45-55.

Michel. B. 1971. Winter regime of rivers and lakes. Cold Regions Science and Engineering Monograph III-B1a. U.S. Army Cold Regions Research and Engineering Lab, Hanover, NH. 131 pp.

Michel, B., Marcotte, N., Fonseca, F., Rivard, G. 1982. Formation of border ice in the Ste. Anne River. Proceedings of the Workshop on Hydraulics of Ice-Covered Rivers, University of Alberta, Edmonton, Alberta, Canada, 38-61.

Miles, T. 1993. A study of border ice growth on the Burntwood River. M. Sc. Thesis, University of Manitoba, Winnipeg, Canada.

Morley, J. 2012. Observations of flow distributions and river breakup in the Mackenzie Delta, NWT. Master's Thesis, University of Alberta, Edmonton, Alberta, 288 pp.

Nafziger, J., Hicks, F., Andrishak, R., Marsh, P., Lesack, L. 2009. Hydraulic Model of River Flow and Storage Effects in the Mackenzie Delta, Canada. 17th International Northern Research Basins Symposium and Workshop, 1-10.

Nafziger, J., Kovachis, N., Emmer, S. 2021. A Tale of Two Basins: The 2020 river ice breakup in northern Alberta, part I: The Athabasca River. In: CGU-HS Committee on River Ice Processes and the Environment Workshop on the Hydraulics of Ice Covered Rivers. August 29-September 1, 2021, Saskatoon, SK.

Nafziger, J., She, Y., Hicks, F. 2019. Dynamic river ice processes in a river delta network. Cold Regions Science and Technology, 158: 275-287.

Nafziger, J., She, Y., Hicks, F., Cunjak, R.A. 2017. Anchor ice formation and release in small regulated and unregulated streams. Journal of Cold Regions Science and Technology. 141: 66-77.

Nash, J. E., Sutcliffe, J. V. 1970. River flow forecasting through conceptual models, Part 1 - a discussion of principles. Journal of Hydrology 10(3): 282-290.

Newbury, R. W. 1968. Nelson River: A study of subarctic river processes. Ph.D. Thesis, Johns Hopkins University, Baltimore, Maryland.

Nezhikhovskiy, R. A. 1964. Coefficients of roughness of bottom surface on slush-ice cover. Soviet Hydrology (American Geophysical Union), 127-150.

Osada, K., Ettema, R., Shimizu, Y., Wakai, A. 2020. ASCE Journal of Cold Regions Engineering, 34(1): 0401917.

Oveisy, A., She, Y. 2017. Modelling Ice Jam Formation in the Hay River Delta during 2009 Breakup. Proceedings on the 19th Workshop on the Hydraulics of Ice Covered Rivers, Whitehorse, Yukon, Canada.

Pan, J., Shen, H.T., Jasek, M. 2020. Anchor ice effects on river hydraulics. Cold Regions Science and Technology, 174 (2020) 103062.

Pandey, A.K., Mohapatra, P.K., Jain, V., Bhatia, U. 2020. Studying subcritical opposing channel flows. Journal of Applied Water Engineering and Research, 8:4, 262-276.

Pariset, E., Hausser, R. 1961. Formation and evolution of ice covers on rivers. Transactions of the Engineering Institute of Canada 5: 41-49.

Pariset, E., Hausser, R., Gagnon, A. 1966. Formation of ice covers and ice jams in rivers. ASCE Journal of the Hydraulics Division 92(HY6): 1-24.

Parkinson, F.E., Holder, G.K. 1982. Liard-Mackenzie winter regime study, final report. LHL 830. Prepared for British Columbia Hydro and Power Authority. Lasalle Hydraulic Laboratory Ltd., Montreal, Quebec.

Peters, D.L., Prowse, T.D., Pietroniro, A. Leconte, R. 2006. Flood hydrology of the Peace-Athabasca Delta, northern Canada. Hydrological Processes. 20: 4073-4096.

Petryk, S., 1995. Chapter 5: Numerical Modeling. In: Beltaos, S. (ed) River Ice Jams. Water Resources Publication, L.L.C. Colorado, USA.

Petryk, S., Panu, U.S., Kartha, V.C., Clement, F., 1981. Numerical Modeling and Predictability of Ice Regime in Rivers. 6th IAHR International Symposium on Ice, Quebec City, Canada, Volume 1: 426-435.

Potok, A.J., Quinn, F.H. 1979. A Hydraulic Transient Model of the Upper St. Lawrence River for Water Resources Research, Water Resources Bulletin, American Water Resources Association, 15(6): 1538-1555.

Ramamurthy, A.S., Qu, J., Vo, D. 2007. Numerical and experimental study of dividing open-channel flows, ASCE Journal of Hydraulic Engineering, 133 (2007): 1135-1144.

Rivière, N., G. Travin, and R. J. Perkins. 2014. Transcritical Flows in Three and Four Branch Open-Channel Intersections. Journal of Hydraulic Engineering 140 (4): 04014003.

Shabayek, S. 2002. Conservation Equations for Subcritical Flow in Open Channel Junctions. PhD. thesis, University of Alberta, Edmonton, AB, 210 pp.

Shabayek, S., Steffler, P., Hicks, F. 2002. Dynamic model for subcritical combining flows in channel junctions. Journal of Hydraulic Engineering. 128(9): 821-828.

She, Y., Hicks. F. 2006. Modeling ice jam release waves with consideration for ice effects. Cold Regions Science and Technology, 45: 137-147.

She, Y., Hicks, F., Steffler, P., Healy, D. 2009. Constitutive Model for Internal Resistance of Moving Ice Accumulations and Eulerian Implementation for River Ice Jam Formation. Journal of Cold Regions Science and Technology 45: 137-147.

Shen, H.T. 2005. CRISSP1D programmer's manual. In CEATI Report No. T012700-0401. Department of Civil Engineering, Clarkson University, Potsdam, N.Y., 188 pp.

Shen, H.T. 2006. A one-dimensional comprehensive river ice model. In: Proceedings of the 18th IAHR International Symposium on Ice, Sapporo, Japan, 61-68.

Shen, H.T. 2010. Mathematical modeling of river ice processes. Cold Regions Science and Technology 62: 3-13.

Shen, H.T. 2016. Chapter 9: River Ice Processes. In: Wang, L.K., Yang, C.T., Wang, M.-H.S. (eds) Advances in Water Resources Management, Springer International Publishing Switzerland, 483-530.

Shen, H.T., Ackermann, N.L. 1980. Wintertime Flow Distribution in River Channels, Journal of the Hydraulics Division, ASCE, 106(HY5): 805-817.

Shen, H.T., Shen, H., Tsai, S.-M. 1990. Dynamic transport of river ice. Journal of Hydraulic Research 28 (6): 659-671.

Shen, H.T., Wang, D.S. 1995. Under Cover Transport and Accumulation of Frazil Granules, Journal of Hydraulic Engineering, ASCE, 121(2): 184-194.

Shen, H.T., Wang, D.S., Lal, A.M. W. 1995. Numerical Simulation of River Ice Processes. Journal of Cold Regions Engineering, ASCE, 9: 107-118.

Sun. Z. C. and Shen, H.T. 1988. A field investigation of frazil ice jam in Yellow River. In: CGU HS Committee on River Ice Processes and the Environment Proc., 5th Workshop River Ice / Ice Jams, Winnipeg, Canada, 157-175.

Taylor, E.H. 1944. Flow characteristics at rectangular open channel junctions. Trans. ASCE, 109: 893-902.

Terroux, A., Sherstone, D., Kent, T., Anderson, J., Bigras, S., & Kriwoken, L. 1981. Ice regime of the Lower Mackenzie River and Mackenzie Delta. The National Hydrology Research Institute, Environment Canada. Hull, Quebec, 115 pp.

Tetra Tech, Ice. 2013. Initial Geomorphic Reach Delineation and Characterization, Middle and Lower Susitna River Segments (FERC No. 14241). Prepared for Alaska Energy Authority, February 2013, 24 pp.

Theriault, I., Sucet, J.-P., Taha, W. 2010. Validation of the Mike-Ice model simulating river flows in presence of ice and forecast of changes to the ice regime of the Romaine River due to hydroelectric project. In: Proceedings of the 20th IAHR International Symposium on Ice, Lahti, Finland.

Timalsina, N., Charmasson, J., Alfredsen, K.T. 2013. Simulation of the ice regime in a Norwegian regulated river. Cold Regions Science and Technology, 94: 61–73.

Tsang, G. 1988. Development of mathematical modelling for prediction of river cooling and frazil and anchor ice formation. In: CGU HS Committee on River Ice Processes and the Environment Proc., 5th Workshop River Ice / Ice Jams, Winnipeg, Canada, 393-416.

Tsang, G. 1970. Change of Velocity Distribution in a Cross-Section of a Freezing River and the Effect of Frazil Ice Loading on Velocity Distribution. In: Proceedings of the

1st International Symposium on Ice, Reykjavik, Iceland. International Association of Hydro-Environment Engineering and Research, 1-11.

Turcotte, B., Morse, B. 2013. Ice jam mitigation at the St. Félicien Zoo. In: 17th CGU HS Committee on River Ice Processes and the Environment Proc., 17th Workshop on Hydraulics of Ice Covered Rivers, Edmonton, Alberta, July 21-24, 2013.

Uzuner, M.S. 1975. The composite roughness of ice covered streams. Journal of Hydraulic Research 13: 79-102.

Uzuner, M.S. and Kennedy, J.F. 1972. Stability of Floating Ice Blocks. ASCE Journal of the Hydraulics Division 98 (HY12): 2117-2133.

Uzuner, M.S., Kennedy, J.F. 1976. Theoretical Model of River Ice Jams. ASCE Journal of the Hydraulics Division 102 (HY9): 1365-1383.

van der Sanden, J. J., Drouin, H. 2011. Spring 2008 Ice Cover Condition, Mackenzie River Delta, Northwest Territories, Canada. Remote sensing map set. Ottawa, ON.

Waddle, T. 2010. Field evaluation of a two-dimensional hydrologic model near boulders for habitat calculation. River Research and Applications, 26: 730-741.

Weber, L.J., Schumate, E.D., Mawer, N. 2001. Experiments on Flows at a 90° Open-Channel Junction. Journal of Hydraulic Engineering, 127(5): 340-350.

Yuan, S., Zhou, J., Hu, D., Zhu, S. 2020. An integral 1-D Eulerian-Lagrangian Method and Its Application to a Hydrodynamic River Network. Water 12, 542, 16 pp.

Wang, D.S., Shen, H.T. 1993. Frazil and anchor ice evolution in rivers. Report 93-09, Department of Civil and Environmental Engineering, Clarkson University, Potsdam, New York.

Wang, D.S., Shen, H.T., Crissman, R.D. 1995. Simulation and Analysis of Upper Niagara River Ice-Jam Conditions. Journal of Cold Regions Engineering, 9(3): 119-134.

Wuebben, J.L. 1984. The rise pattern and velocity of frazil ice. In: CGU HS Committee on River Ice Processes and the Environment Proc., 3rd Workshop on the Hydraulics of Ice Covered Rivers, Fredericton, New Brunswick, Canada, 297-316.

Ye, S.Q., Doering, J. 2004. Simulation of the supercooling process and frazil evolution in turbulent flows. Canadian Journal of Civil Engineering, 31: 915-926.

Ye, S.Q., Doering, J., Shen, H.T. 2004. A laboratory study of frazil evolution in a counter-rotating flume. Canadian Journal of Civil Engineering, 31: 899-914.

Zhang, F., Mosaffa, M. Chu, T., Lindenschmidt, K-E. 2017. Using Remote Sensing Data to Parameterize Ice Jam Modeling for a Northern Inland Delta. Water, 9, 306.